Università degli Studi di Napoli Federico II
Dipartimento di Scienze Fisiche

Tesi di Dottorato in Fisica Fondamentale ed Applicata

A statistical mechanical approach to the study of gels and colloidal systems

Tiziana Abete

Tutor:
Chiar.mo Prof. A. Coniglio

Coordinatore:
Chiar.mo Prof. G. Miele

XIX ciclo 2003-2006

Contents

Introduction

Important issues of fundamental physics and the numerous industrial applications as well as the connections with biology have attracted the interest of the scientific world on "complex systems" of soft matter, such as colloidal suspensions, gels, biopolymers, glasses and granular media. Although these systems are very different from each other they display several common features, as the slowing down of the dynamics at high densities. In particular, gelling systems occupy a relevant role in our everyday life (polymers, colloids, proteins,..) but the features which characterize the transition from a liquid-like system to a disordered elastic solid are not yet well understood. The burst of research activity on gels in the 80s was mainly aimed to describe the formation of the gel structure in terms of percolation models [1, 2, 3] and produced a satisfying and coherent characterization of a large number of polymeric materials. Such an investigation effort was in prevalence concentrated on the characterization of the percolation transition but did not really lead to a comprehensive understanding of the gel dynamics. In particular, some analogies between the complex dynamics in polymer gels, glasses and spin glasses are observed and suggested in the literature [4, 5], but never conclusively interpreted. A necessary step to build a complete theory on such complex systems would be therefore to deeper understand the microscopic mechanisms underlying the analogies among these different systems. In order to contribute to this issue, we attack the problem from two different sides. On one hand we investigate by means of Monte Carlo simulations two specific problems within an international collaboration with experimental groups. On the other hand, we investigate the gel dynamics and its relations to structural properties proposing a general model for irreversible gelation, whose properties are analyzed by means of molecular dynamics simulations.

Among polymer gels, biopolymers play an important role for their numerous application in food and pharmaceutical industries. Particularly interesting is the case of gelatin, one of the main constituent of biological tissues, which is extracted from collagen. If the temperature is sufficiently low, gelatin chains in solution may form a physical gel, i.e. a reversible gel, due to the formation of triple helix structures among gelatin chains. The gel is thermoreversible, i.e. by raising the temperature the sol state is recovered. Biodiversity due to chemical composition of the native collagen, molecular weight distribution, solution prop-

erties such as concentration or pH, influences the temperature of helix formation in the physical gel [6]. When the temperature is higher than the denaturation temperature, gelatin chains behave as linear polymers in solution. In this case, helices do not form, but a chemical gel, i.e. a permanent gel, may form due to the reaction between amine groups along the gelatin chain and cross-linking molecules, which in the following we will refer to as reactant agent, added to the solution. Indeed, varying opportunely the parameters which characterize gelatin solutions, the kinetics of reaction between chains and reactant may be tuned and gels with a wide range of different structural and mechanical properties may be obtained. In addition, gelatin solutions show an even richer phenomenology since a combination of chemical and physical gelation can be observed. As a consequence several structures may form, influencing the mechanical response and the transport properties of the gel phase. Recently, the case of chemical gelation has been investigated on gelatin solution with bisvinylsulphonemethyl (BVSM) reactant agent [7], in which the reaction between gelatin chains and reactant has been monitored. The kinetics of cross-link formation was found to follow a double exponential decay with two characteristic times, which could not be explained. In the experiments the direct measurements of microscopic cross-link kinetics is not possible and therefore alternative investigations are required to achieve a deeper comprehension of cross-link formation. In particular the primary question is to understand how the two time scales controlling the kinetics depend on the formation of single-bonds between cross-linkers and chains, bonds leading to a bridge between two gelatin chains or else to loops within the chains. Moreover it would be crucial to understand how these time scales are related to the properties of the gelatin solution (concentration, pH...) and of the cross-linking molecules (concentration, reactivity...). By means of Monte Carlo simulations on the lattice, we provide new insights into the main features of the kinetics of bond formation in chemical gelation of gelatin chains. Our model consists in a solution of chains diffusing on a cubic lattice: each chain is composed of effective units, represented by elementary cells of the lattice, diffusing via bond fluctuation dynamics [8]. A fixed fraction of units in each chain is tetra-functional, representing active sites which may link to reactant. The role of concentration, reactivity of cross-linking molecules and rigidity of formed bonds on the kinetics is investigated in simulations, complementing the experimental findings [9]. Within this approach we follow the kinetics of the gel formation varying the gelatin concentration, the cross-linker concentration and its bonding probability (i.e. reactivity). Our data reproduce extremely well the experimental findings about kinetics as they are characterized by two time scales. The simulations moreover show that the two time scales detected in the experiments correspond respectively to the average time of forming single bonds "reactant-chain" and bridges "chain-chain" via cross-linker. We give evidence that the ratio of these two characteristic times controls the kinetics of the bond formation: variations of the concentration and the cross-linker reactivity strongly affect this ratio and therefore the kinetics of

the gelation process.

Gelatin gels play an important role also in a completely different phenomenon based on degradation processes. In these processes a reverse gelation transition may occur due to the breaking of chemical bonds as a consequence of enzyme activity, the end result being a transition from a gel to a sol phase. Such reverse gelation transition assumes a particularly important role in biology as the process of dissemination of tumors in human body involves the degradation of the extracellular matrix (ECM), a gel made of various proteins, including gelatin, connected to form an elastic network that extends macroscopically. This gel is normally impermeable to cell passage, and ensures organ integrity by insulating organs and preventing cell dissemination. However, during specific processes the ECM can be degraded by a variety of proteolytic enzymes, that catalyze the hydrolysis of the cross-links between peptide chains constituting the ECM, increasing its permeability to the cell passage. At some point this degradation process can solubilize the gel, realizing a "gel-sol" transition, and bringing the ECM to a liquid state, in which cells are no longer confined and can freely diffuse. In this view, beyond the biochemical processes involved at molecular level, the understanding of the physical mechanisms of the ECM degradation is of great importance. Recently, a series of interesting experiments have been realized to study the *in vitro* degradation of protein gels by exogenous proteinases [10, 11]. By scattering measurements, the gel fraction has been monitored: as expected, it is zero below the transition threshold and grows above it following a power law behavior $\sim \epsilon^\beta$, where ϵ is the distance from the threshold. With various gel-enzyme combinations, and different enzyme concentrations, it was found that the gel fraction power law behavior is governed by an exponent $\beta \simeq 1$. This result is quite unexpected, because the sol-gel transition is usually well described by random percolation, which is obtained when each bond between two monomers is present with probability p, and there is no correlation between different bonds. According to random percolation theory the gel fraction, i.e. the density of the infinite cluster, which is zero below the transition threshold p_c, grows as $(p-p_c)^\beta$ for $p > p_c$, with $\beta = 0.41$ in three dimensions quite different from the one measured in the gel degradation experiments. In order to explain the change in the universality class with respect to random percolation, we introduce a very simple model, which we call "pacman percolation model", in which the protein gel is schematized as a cubic lattice of $N = L^3$ sites, where each site represents an (hexavalent) monomer. At time $t = 0$ all the bonds between nearest neighbor monomers are present. One or more enzymes are introduced in the system in random initial positions. At each step, every enzyme moves from one site to a nearest neighbor site, chosen randomly between the six possible neighbors, and hydrolyzes (deletes) the corresponding bond if not yet hydrolyzed. Our results indicate that, in the limit of zero density of enzymes, the model undergoes a (reverse) percolation transition, which falls in a universality class different from random percolation. In particular we measure a gel fraction critical exponent

$\beta = 1.0 \pm 0.1$, in excellent agreement with experiments on the real system. We show that the deviation from the random percolation universality class is due to the presence of long range correlations between bonds. If density of enzymes is sufficiently high, the system falls into the random percolation universality class. This is expected because, for very high density of enzymes, each bond is cut by a different enzyme, so that there are no correlations between bonds.
In order to have information on the mechanical response of the system, we should investigate the behavior of the viscosity and the elastic modulus. The theory of critical phenomena, which can be used to describe the sol-gel transition, predicts that, near the transition, the macroscopic quantities describing the system are related to the distance from the transition $(p-p_c)$ by power laws. Hence, the viscosity diverges as $(p-p_c)^{-k}$ below the transition $p < p_c$, and stays infinite above it, while the elastic modulus, that is zero below the transition, grows above it as $(p-p_c)^f$. Following the analogies proposed by de Gennes [12, 13], the exponents f of the elastic modulus and k of the viscosity should be equal respectively to the critical exponents t and s of the conductivity in the random resistor and random super-conducting networks. In order to compute the conductivity and therefore t, a present bond of the model is substituted with a resistor of unitary conductance, and an absent bonds is substituted with a resistor of zero conductance. The total conductivity Σ of the model is measured as a function of bond density. We obtain that it is zero for $p < p_c$, while it grows as $(p-p_c)^t$ for $p > p_c$ with $t = 3.5 \pm 0.1$. In order to compute s, a present bond of the model is substituted with a superconductor of infinite conductance, and an absent bonds is substituted with a resistor of unitary conductance. In this case the total conductivity Σ diverges as $(p-p_c)^s$ for $p < p_c$ with $s = 1.1 \pm 0.1$ as p approaches p_c from below, and is infinite for $p > p_c$. These findings have stimulated more experiments and interestingly enough preliminary results show a good agreement with the predicted critical exponent t.

To summarize this part related to biological problems, we study by means of computer simulations of lattice models both gelation reactions and degradation processes of a common biopolymer, the gelatin, which has been extensively investigated experimentally. In both cases our results, obtained by Monte Carlo simulations of simple lattice models, are directly compared to the measurements made on these systems giving new insight into the processes involved in the considered reactions. Not only we interpret the experimental findings, but we also obtain new predictions about physical quantities some of which have not been directly measured yet. Therefore our models, introduced to investigate gelation and degradation processes, represent a powerful tool to describe the specific systems investigated experimentally.

Nevertheless the gelation transition is relevant for a wide class of different systems. Thus in order to investigate the typical features of gelation transition, in the framework of transitions to a disordered out of equilibrium solid state, we introduce a general model for gelling systems. Our aim is to analyze in details

the analogy between gelation transition and percolation transition, obtaining a relation between thermodynamical observable and percolative properties. Furthermore, a deeper investigation of gelation transition is proposed, in order to clearly comprehend the analogies/differences among transitions involving structural arrest and slow dynamics, such as gelation, glass and jamming transitions.

By means of a $3d$ model, we analyze the analogies between gels and other complex systems undergoing slow dynamics, such as supercooled liquids or spin glasses by a molecular dynamics study of static and dynamical properties of the system. We consider a system made of interacting soft spheres, using a truncated Lennard-Jones potential in order to have only the repulsive part. At a certain time quenched bonds are formed among particles whose distance is lower than a certain fixed value R_0, so that permanent clusters of particles are formed. The bond interaction is represented by a finite elongation non-hookean spring (FENE) potential [14], which has been widely used to study linear polymer chains. As the particle density increases, a spanning cluster made of linked particles appears. Due to the percolation of permanent bonds between neighboring particles, the system undergoes a gelation transition in the universality class of random percolation. In fact we analyze the structural properties of the system within the percolation approach. The viscoelastic response as the the gelation threshold is approached, is investigated. The obtained results about the critical behavior of viscosity and elasticity are compared to experimental findings and to the predictions of different models. The dynamical behavior is studied measuring the self intermediate scattering function, which measures the correlations between the positions of a given particle at two instant of time. We analyze its behavior varying the density of the system and the wave number k. For the first time we analyze the dynamical heterogeneities in gels, by means of fluctuations of the self intermediate scattering function, representing a dynamical susceptibility. In the sol phase close to the percolation threshold, we find that this dynamical susceptibility is an increasing function of time, growing until it reaches a plateau. Approaching the gelation threshold the asymptotic value of the susceptibility diverges with the same exponent γ as the mean cluster size. Moreover, we demonstrate that the asymptotic value of the susceptibility is equal to the mean cluster size. These findings suggest an alternative way of measuring critical exponents in a system undergoing chemical gelation, the self intermediate scattering function being related to the scattered intensity in light scattering experiments. Usually the study of dynamic heterogeneity is extremely powerful to unravel the local dynamics and its role in slow relaxation phenomena. In particular the presence of dynamic heterogeneities is considered as a peculiar feature of structural glasses and this tool is firstly tested on polymer gels in our investigation. When the glass transition is approached in the supercooled regime, there is no significantly growing static correlation length. In spite of this, a dynamical correlation length [15], which is related to the size of correlated domains and diverges approaching the transition threshold, is observed. In our model for chemical gelation we observe a behavior

very different from the one observed in glassy systems: no peak is present in the susceptibility, which is instead a increasing function of time, growing until it reaches a plateau. In the case of irreversible gels, our study elucidates the static nature of the observed dynamical heterogeneities. Furthermore, we note that the monotonic behavior of the dynamical susceptibility is similar to the one observed in a spin glass model with quenched interactions, suggesting a possible common description of the phase transition involved.

The thesis is organized as follows: In chapter 1 we define gels, making the distinction among chemical gels, physical gels and colloidal gels. Furthermore, we discuss a simple model for gelation: the percolation theory. In chapter 2 we we review the fundamental aspects of the phenomenology of gelling systems and the results of experimental investigations. As one of the most common biopolymer gels is the gelatin, in chapter 3 we present the basic features of gelatin gels and we present recent experimental results obtained from the study of both gelation and degradation processes. In chapter 4 we introduce the model for chemical gelation of gelatin chains and present our results about the kinetics of the reaction between chains and reactant. The model for the degradation process of extracellular matrix is described in chapter 5, where we analyze the non trivial relation between the gelation transition and the reverse gelation transition. In chapter 6 we introduce the model for irreversible gelation and discuss the results for the structural and dynamical properties. The presence of heterogeneities in irreversible gelling systems is discussed in chapter 7, stressing their static nature, differently from structural glasses, and noting the analogy with spin glasses. Finally we make conclusive remarks and indicate the possible developments of this work in the conclusive section.

Chapter 1

Sol-Gel transition and critical phenomena

Gelling systems occupy a relevant role in our everyday life (polymers, colloids, proteins, etc.), from pharmaceutical applications to food industries. The sol-gel transition is characterized by the passage from a viscous regime to an elastic one. The change in the viscoelastic response of the system is determined by the formation of a spanning interconnected network which can be due to chemical bonds (chemical gels) or inter-particle interactions (physical gels and colloidal gels). Within this picture, the formation of the gel structure may be described in terms of percolation models and the macroscopic quantities describing the system are related to the distance from the transition threshold by power laws. Several measurements have been performed in order to determine the critical exponents of such power laws, producing a satisfying and coherent characterization of a large number of polymeric materials.
In this chapter we discuss the sol-gel transition, reviewing the nature of gels and their microscopic structure. We make the distinction among chemical gels, physical gels and colloidal gels, presenting an overview of theoretical and experimental results. We describe the main features of percolation theory and analyze some experimental methods generally used to measure percolative properties.

1.1 Sol-gel transition and percolation theory

The gelation transition transforms a viscous liquid into an elastic disordered solid. In general this process is due to the formation of a macroscopic molecule which makes the system able to bear stresses. As the transition threshold is approached, the liquid viscosity progressively increases with a power law behavior, until it diverges. At the onset of the gel phase, an elastic modulus appears which increases near the gelation threshold following a power law behavior.
The chemical reaction may be induced in different ways [16, 17], for example by

irradiating the system, by lowering the temperature or by introducing catalysts in the solutions. In polymer systems, this is due to the polymerization process during which chemical bonds form between monomers in solution.
The extent of the gelation process may be measured by the fraction p of bonds which have been formed between monomers, i.e. the ratio of the actual number of formed bonds to the maximum number of formable bonds. Also monomer concentration ϕ, temperature T or the elapsed time t from the solution preparation time may be used to measure the polymerization extent. Nevertheless, in general the polymerization extent p is used as the control parameter also in the experimental characterization of the sol-gel transition, with the assumption that the other parameters, like temperature T, concentration ϕ, or time parameters, are proportional to it.

The gelation transition is a connectivity transition, hence the simplest way to describe the gelation transition is to represent it as a percolation transition [18]. As first suggested by Flory, the percolation model is considered as the basic model for the gelation transition due to formation of chemical bonds between monomers: finite clusters of linked particles represent groups of linked monomers, and the spanning cluster which form at the percolation threshold represents the macromolecule constituting the gel phase. We denote the number of monomers in a molecule by s and then call this molecule an s-cluster. An isolated monomer is a 1-cluster. Within this approach, the sol phase corresponds to a solution of finite clusters, and the gel phase is represented by the percolating cluster [19, 20]. In real systems it is observed that the gel usually coexists with the sol. Also in percolating systems usually finite clusters are trapped in the interior of the percolating cluster. As a consequence, in gelation there is no phase separation. Indeed, in experiments the gel phase cannot be easily separated from the sol phase, affecting the experimental determination of several quantities.
If the fraction p of formed bonds with respect to all the possible ones is $p = 0$, no bonds have been formed and all monomers are isolated 1-clusters, whereas for $p = 1$ all bonds have been formed and thus all monomers are linked into one "infinite"[1] network. For a particular critical value $p = p_c$ an infinite cluster starts to appear: for p below p_c only finite clusters are present in solution, whereas above p_c there is an infinite cluster. Hence p_c is the percolation threshold. Approaching p_c clusters of all sizes s form. In fact the percolation theory states that the number of s-cluster per site n_s, i.e. the fraction of s-clusters, follows a power law behavior at the percolation threshold: $n_s \propto s^{-\tau}$ for $s \to \infty$ at the transition threshold $p = p_c$. The exponent τ is the Fisher exponent and in a $3d$ random percolation model $\tau \simeq 2.2$ [18]. In general for $p \to p_c$, the behavior of the cluster size distribution n_s is characterized by both the exponent τ and σ: $n_s = s^{-\tau} f\left[(p - p_c)s^{\sigma}\right]$. The exponent σ governs the behavior of the cutoff size

[1]The thermodynamical limit implies infinite systems, hence the percolating cluster which spans the whole system is infinite.

$s_\xi \propto |p - p_c|^{-1/\sigma}$ which marks the crossover behavior of $f(z)$. The function $f(z)$ turns out to approach a constant value for $|z| \ll 1$, i.e. $s \ll s_\xi$, and to decay faster than any power law for $|z| \gg 1$, i.e $s \gg s_\xi$.
According to the theory of critical phenomena [21], near the transition threshold the macroscopic quantities describing the system are related to the distance from the transition threshold $p - p_c$ by power laws. In particular, according to the percolation theory the density of the percolating cluster P_∞, which is the order parameter of the transition, is zero below the transition and grows above it as $(p - p_c)^\beta$. The density P_∞ corresponds to the experimental parameter X_{gel}, that is the gel fraction, which measures the fraction of monomers forming the macroscopic stress bearing molecule. Another interesting quantity which characterizes a percolating system is the connectedness length ξ, defined as follows:

$$\xi = \frac{\sum_s R_g(s) n_s s^2}{\sum_s n_s s^2}, \tag{1.1}$$

where the sum is considered over all finite clusters, n_s is the fraction of s-clusters and $R_s(s)$ is the gyration radius of s-clusters. Approaching the transition threshold, the connectedness length ξ diverges as $|p - p_c|^{-\nu}$. From its definition, such length ξ is the average cluster diameter. Setting the molecular weight of monomers to unity in the theoretical approach, s represents also the weight of a s-cluster. Hence $\chi = \sum_s n_s s^2$, where the sum is considered over finite clusters, is the mean cluster size. It diverges approaching the percolation threshold following a power law behavior $|p - p_c|^{-\gamma}$. The mean cluster size corresponds to the experimental parameter M_w, that is the weight average mass. In the percolation theory, the mean cluster size plays the role of a static susceptibility, as it can be shown that it behaves as the fluctuations of the order parameter P_∞ [21].
It is important to point out that exponents ν, β, γ, etc... are universal, that is they do not depend on the microscopic details of the system, but only on global characteristics like the dimensionality of the system, or whether or not there are long range correlations between particles and bonds. Systems with the same values of such exponents are said to belong to the same *universality class* [21]. Finally, we point out that not all the critical exponents are independent variables, but they are related each others by several relations. For example ν, β and γ must satisfy the relation $2\beta + \gamma = d\nu$ [18, 21], where d is the Euclidean dimension of the embedding space. By means of computer simulations, the percolation threshold and critical exponents of percolating quantities may be easily measured [22] and accurately determined, for example using standard finite size scaling analysis [18], so that the universality class of the model under investigation may be clearly identified. Nevertheless, in experiments some difficulties in the determination of critical exponents may arise, as we discuss in Sect.1.4.

1.2 Percolation and thermal phase transitions

Percolation transition is a purely geometrical transition and as a consequence the percolation theory focuses on geometrical properties of formed structures. Nevertheless percolative quantities, such as the mean cluster size or the number of clusters, may be put in correspondence with thermodynamical quantities characterizing thermal phase transitions. In fact, percolation theory may be obtained in the framework of a general spin model, the Potts model [23], which was introduced to study magnetic systems. The Potts model describes an ensamble of interacting spin variables, each of them having q possible states $\sigma = 1, 2, ..., q$. When $q = 2$ we recover the Ising model [21]. The Potts model is defined by the following Hamiltonian:

$$H = -J \sum_{<ij>} \left(\delta_{\sigma_i \sigma_j} - 1\right) - h \sum_i \left(\delta_{\sigma_i 1} - 1\right), \tag{1.2}$$

where σ_i is the spin variable of site i, J is the interaction energy and h is an external magnetic field which favors alignment of all the spins in the state $\sigma = 1$. The percolation quantities may be obtained from the Potts model Hamiltonian in the limit $q \to 1$ [24]. For every value of the spin variable σ_i we can write:

$$e^{J(\delta_{\sigma_i \sigma_j} - 1)} = e^{-J} + (1 - e^{-J})\delta_{\sigma_i \sigma_j}$$
$$e^{h(\delta_{\sigma_i \sigma_j} - 1)} = e^{-h} + (1 - e^{-h})\delta_{\sigma_i 1}.$$

Hence, the partition function may be written as:

$$Z = Tr_{\{\sigma_i\}} \sum_{C \subseteq E} p^{|C|}(1-p)^{|D|} \prod_{<ij> \in C} \left[e^{-h} + (1 - e^{-h})\delta_{\sigma_i 1}\right], \tag{1.3}$$

where E is the set of all the configurations of bonds in the lattice, C is a subset of E, $D = E - C$ with $|C|$ and $|D|$ being the number of bonds respectively in the subset C and D, and p is defined as $p = 1 - e^{J/k_B T}$. In order to calculate the partition function, we note that the trace over $\prod_{<ij> \in C}$ is equal to 1 when all the spins in the cluster C are aligned, otherwise is zero. In addition, the quantity in square brackets is equal to 1 if $\sigma_i = 1$, and this case occurs only once, otherwise it is equal to e^{-h}, and this case occurs $q - 1$ times. Thus for the partition function we obtain:

$$Z = \sum_{C \subseteq E} p^{|C|}(1-p)^{|D|} \prod_r \left[(q-1)e^{-h s_r / k_B T} + 1\right], \tag{1.4}$$

where s_r is the number of sites belonging to the r-th cluster in the configuration C. Hence, introducing the brackets $< ... >$ to indicate the configurational average, we may write:

$$Z \mid_{h=0} = < q^{N_C} >, \tag{1.5}$$

where N_C is the number of clusters. Starting from the expression of the partition function in Eq. 1.4, we calculate the free energy defined as:

$$F = k_B T \lim_{N\to\infty} \frac{1}{N} \frac{d}{dq} \ln Z, \tag{1.6}$$

where N is the number of sites in the lattice. Hence we obtain:

$$F \mid_{h=0} = N_C \tag{1.7}$$

$$\frac{d^k F}{dq^k} = (-1)^k \sum{}' s^k n_s, \tag{1.8}$$

where the sum $\sum'$ is performed over finite clusters. There relations indicate that using the Potts model, a connection between percolative properties, such as the number of clusters, and thermodynamical variables, such as the free energy, may be provided. In fact, the free energy may put in correspondence with the number of clusters in percolating model, while the k-th derivative of the free energy may be put in correspondence with the k-th momentum of cluster size distribution.

1.3 Chemical and physical gels

According to the nature of bonds between molecules, gels divide into two categories: *chemical* or *strong gels* and *physical* or *weak gels*.
Chemical gels are obtained when covalent bonds form between the molecules: they may be produced by a rapid quench of the system or by irradiating it with light. Formed bonds between particles cannot break anymore and the system remains in the gel phase raising the temperature.
In physical gels, instead, bonds between particles are reversible, in the sense that raising the temperature bonds between particles break and the sol phase is recovered. Furthermore, in physical gels bonds between particles in solution form and break continuously by the action of fluctuations of thermal energy. In physical gels, gelation may be due to the formation of hydrogen bonds between molecules, which easily break if the temperature increases.
While in the case of chemical gels we expect to have an evident transition from a viscous regime to an elastic one, in the case of physical gels, in which bonds continuously form and break, there is not a real transition from a regime to the other one. On sufficiently long time scales, the system behaves as a liquid. The differences between these two kinds of gels are evident when investigating the behavior of the free energy approaching the transition threshold [25].

Let us investigate the case of a system made of identical particles, with functionality ζ, that may link each other with probability p, distributed on the sites of a lattice.
In physical gels bonds are not permanent and they can form and break in thermal equilibrium. Let be E_b and S_b the energy and the entropy respectively of

the bound state, and E_n and S_n the same quantities for the unbound state. The probability p to form a bond at temperature T is given by:

$$p = \frac{\exp\left[(TS_b - E_b)/k_BT\right]}{\exp\left[(TS_b - E_b)/k_BT\right] + \exp\left[(TS_n - E_n)/k_BT\right]}. \tag{1.9}$$

We may write the free energy in terms of the partition function, obtaining:

$$F = -k_BT \ln\left\{p \exp\left[(TS_b - E_b)/k_BT\right] + (1-p)\exp\left[(TS_n - E_n)/k_BT\right]\right\}. \tag{1.10}$$

From the previous equation it is evident that the free energy does not present any singularity at the transition threshold p_c. Therefore there is not any phase transition in the ordinary sense at percolation threshold in physical gelation processes. The presence of the percolating cluster does not necessarily produce a sharp change in the viscoelastic properties of the system, so that the physical gel is similar to a highly viscous liquid.

The presence of the percolating cluster strongly influences the properties of the system if bonds are permanent, i.e. in chemical gels. In this case bonds between molecules cannot be broken and may be treated as quenched variables. Any realization of bonds generates a distribution of different species of molecules, characterized by the number of monomers s and by the topology t. In the following we shall indicate the distribution with $n \equiv \{n_{st}\}$, a set of numbers indicating the number of molecules belonging to the species s and t. The free energy of a given realization $\{C\}$ of bonds is given by:

$$F\{C\} = \ln Z\{n\} \tag{1.11}$$

where $Z\{n\}$ is the number of configurations compatible with the distribution of molecules n generated by the realization $\{C\}$. If w is the degeneracy of a finite molecule, the partition function $Z\{n\}$ is given by:

$$Z\{n\} = w^{N_C}, \tag{1.12}$$

where N_C is the number of molecules. The free energy $\overline{F}$ of the quenched system is obtained averaging over the realizations $\{C\}$:

$$\overline{F} = < \ln Z\{n\} > \tag{1.13}$$

where the brackets indicate the average over the bond realizations. In the case of randomly distributed bonds, the probability $P\{C\}$ for a given realization C can be written as follows:

$$P\{C\} = p^n(1-p)^{N-n}, \tag{1.14}$$

where n is the number of bonds in the configuration $\{C\}$ and N the total number of bonds in the lattice. Using this probability distribution and the results of Eq. 1.12, we obtain for the free energy of the quenched system:

$$\overline{F} = < N_C > \ln w. \tag{1.15}$$

Hence the free energy of the quenched system is proportional to the number of clusters. It follows that it has the same critical behavior of the average number of clusters in the usual random percolation [18]:

$$\overline{F} \propto \epsilon^{2-\alpha} \tag{1.16}$$

where $\epsilon = |p - p_c|/p_c$. It is worth to notice that approaching the transition threshold the number of clusters N_c and hence the free energy $\overline{F}$ do not diverge, but the second derivative is discontinuous. The presence of this singular behavior of the free energy in chemical gels indicates that there is a transition in an ordinary sense at the percolation threshold. As a consequence, in chemical gelling systems, the appearance of a permanent percolating cluster crucially affects its properties causing a sharp passage from a viscous regime to an elastic ones.

1.4 Experimental methods

Within the percolation approach to the gelation transition, the first step in the investigation of gelling systems is to determine the universality class to which the system belongs. To correctly determine the critical exponents, an accurate measurement of the critical threshold is needed. The gelation threshold may be measured by rheology experiments, as the intersection point of the loss modulus $G'(\omega)$, which is related to the viscosity coefficient η, and the storage modulus $G''(\omega)$, which is related to the elastic response [26], where ω is the frequency of the applied stress. In this case, the gelation threshold is measured as the point that marks the passage from a dominant viscous regime to an elastic one. However, the results obtained by this method may be not sufficiently accurate to correctly determine the value of critical exponents. Moreover, the measurement of critical exponents of percolating quantities, such as the mean cluster size or the gel fraction, may request the manipulation of the gel itself, representing another font of error. Manipulation of gel, as dilution or separation of gel and sol phases, may cause not controllable modification of the formed structures or in some case the breakage of clusters, strongly affecting experimental results.

Even if several difficulties arise in experimental determination of critical exponents, a coherent and complete characterization of a large number of polymeric materials has been provided [1, 2, 3]. As a matter of fact, several experiments, performed on PDMS [27], polyester gels [28, 29], diisocynate/triol gel [30], polyurethane [31], indicate that the percolation model well describes the geometrical properties of gels, such as the molecule size distribution (Fig. 1.1).

In usual approaches, to determine percolating quantities as the weight average mass, which corresponds to the mean cluster size in percolation approach, or the average cluster diameter, which corresponds to the connectedness length, light scattering measurements may be performed. In such measurements, the sample needs to be dissolved in a known quantity of solvent in such a way that

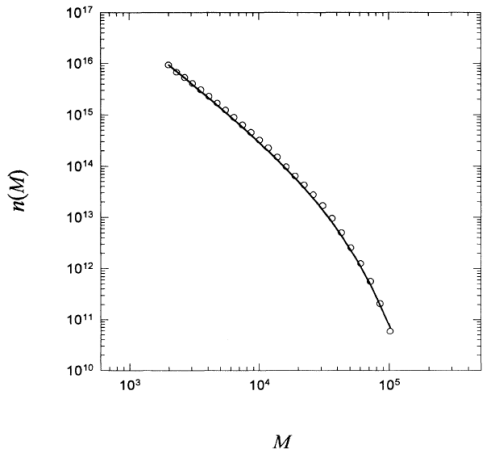

Figure 1.1: Data obtained by size exclusion chromotography experiments performed on hydroxy terminated polyester gels [28]. From the fit $\tau = 2.20 \pm 0.05$ and $\sigma = 0.452 \pm 0.011$ are obtained, in good agreement with random percolation results [18].

each cluster is separated from the others. Furthermore, both the experimental determination of the density of the percolating cluster and the measurement of the weight average mass can be performed by weighting the macromolecule. In order to perform such measurement, the gel fraction must be separated by the sol phase. Beyond the gelation threshold finite clusters, which are trapped in the holes of the macromolecule, must be extracted from the gel phase. Such separation of the sol and gel is very difficult to achieve experimentally, and clusters in this process tend to break [20].

Let us discuss in detail light scattering technique generally used to measure the weight average mass M_w. Assuming monodisperse molecules with radius of gyration R_g and molecular weight M, the intensity of the scattered light I satisfies the following relation:

$$cI_{c\to 0}^{-1} \propto \frac{1}{M}\left(1 + \frac{k^2 R_g^2}{3}\right) \quad \text{for} \quad k^2 R_g^2 \leq 1, \tag{1.17}$$

where c is the concentration of the solution and $k = 4\pi \sin(\theta/2)/\lambda$ is the momentum transfer, with λ being the wavelength of the incident light and θ the scattering angle. For a polydisperse system it can be shown [32] that if $k^2 R_g^2 \leq 1$, the curve $cI^{-1} = f(k^2)$ has a slope proportional to ξ/M_w and an intercept in $k = 0$ proportional to $1/M_w$. It is worth to notice that light scattering experiments must be performed in dilute solutions. Since the size of clusters may increase during the dissolution due to swelling, it is possible that the measurement of gyration radius may be corrupted. These experiments have been performed with several kinds of gelling system, as polycondensates of decamethylene glycol/benzene-1,3,5-triacetic acid (DMG/BTA) [33], in copolymer of methyl methacrylate with other methacrylates [1], and other copolymers [2]. For these systems, using the

described method, the value of the exponent γ cannot be determined, because within the studied range Δp the weight average mass cannot be expressed by any simple power law. This may be due to high inaccuracy in the determination of p_c. Actually, the precision of p_c must be much higher than the range Δp on which measurements are performed. One way to overcome the inaccuracy in the determination of the transition threshold is to compare the different quantities ξ, M_w and X_{gel}, respectively the average cluster diameter, the weight average mass and the gel fraction, and to measure the ratio ν/β and γ/β. These ratio may be obtained plotting ξ and M_w versus X_{gel} as $\xi \propto X_{gel}^{-\nu/\beta}$ and $M_w \propto X_{gel}^{-\gamma/\beta}$. However, one has to take into account that the gel extraction, which has to be done in order to perform such measurements, may be achieved only incompletely, as finite clusters may be trapped into the gel phase. Moreover, the cluster radius may increase by dissolution of the sample. These effects may increase the experimental values of the ratio ν/β and γ/β. Finally, in high molecular weight polydisperse samples, the choice of the fitting curve may be crucial for a correct determination of the critical exponents.

1.5 Colloidal gelation

In colloidal suspensions mesoscopic particles are dispersed in another substance. These systems, as also polymer solutions, possess structures at a mesoscopic level that determine their macroscopic physical properties. In attractive colloidal suspensions at low concentrations [34, 35] a structural arrest, called *colloidal gelation*, is observed. Here the slowing down of dynamics is associated to the formation of long-living compact structures with the change of viscoelastic properties.

Colloidal systems present a complex phase diagram [35, 36, 37] that may be described using as parameters the volume fraction ϕ and the inverse of attraction energy $(U/k_BT)^{-1}$ (Fig. 1.2). At low volume fraction and high strength of attraction, the system behaves as a chemical gel, since bonds formed between particles may be considered permanent compared to observation time scales. As the volume fraction increases and the attraction between particles decreases, the viscoelastic behavior of the system resembles that of gels as it is characterized by power laws. Nevertheless the rich phenomenology characterizing the behavior of the system in this region of the phase diagram is not at all comprehended and actually it is one of the most appealing subjects of investigation. If the volume fraction increases further, particles become more crowded and a glassy dynamics appears [38]: the system behaves as an attractive glass [39]. At higher temperature, where $k_BT/U \gg 1$, the attractive interaction no longer affects the dynamics, and the system behaves as a repulsive glass. Particles are trapped into cages made of neighboring particles and the dynamics is characterized by two times: the first one is the typical time of diffusion inside the cage, whereas the second one is the typical time for the cage to break and for particles to diffuse

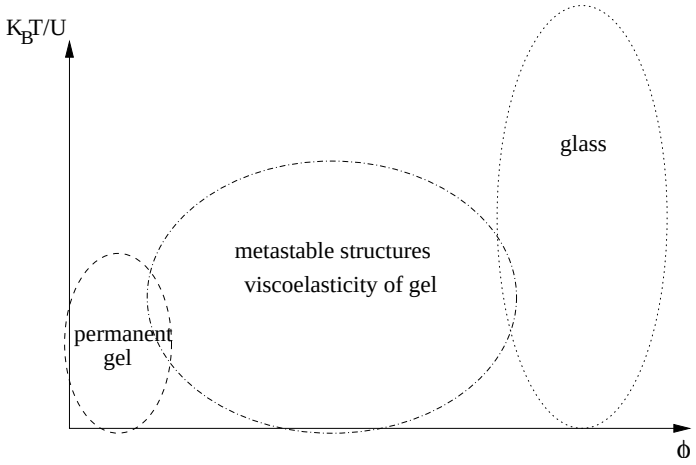

Figure 1.2: A schematic representation of the phase diagram of a colloidal suspension with attractive interaction between particles.

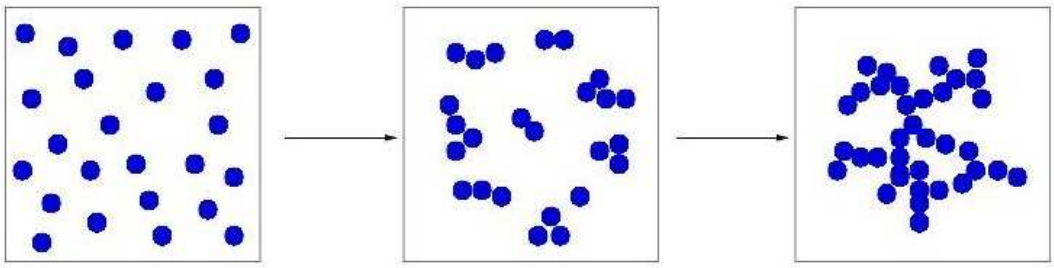

Figure 1.3: A schematic representation of the aggregation process of particles in solution.

outside it.

For colloidal suspensions at low volume fractions and strong attractions between particles (i.e. the dashed region of the phase diagram in Fig. 1.2), the kinetics of the gelation process may be characterized by diffusion and aggregation of particles [40, 41] (Fig. 1.3): particles in solution diffuse until they touch and react getting bonded. As particles stick together to become clusters, the clusters themselves continue to diffuse, collide and aggregate. The kinetics of diffusion and aggregation of molecules may be different passing from a system to the other one. Two limiting regimes of kinetics have been identified among the various processes observed in different systems: rapid, diffusion-limited cluster aggregation (DLCA) and slow, reaction-limited aggregation (RLCA). Each regime exhibits distinct behaviors, characterized by different fractal dimension of

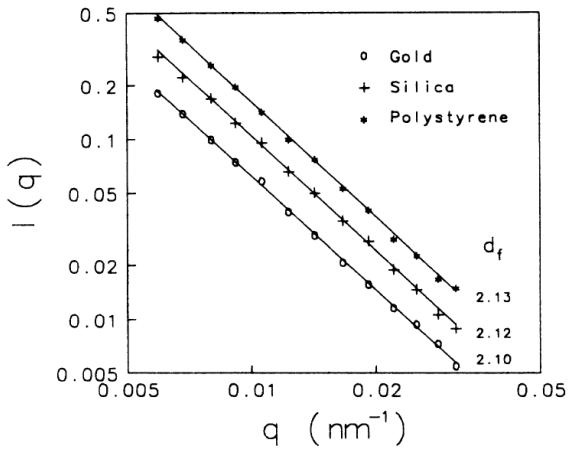

Figure 1.4: Static light scattering from RLCA aggregates of gold ($\circ$), silica ($+$) and polystyrene ($*$) [42]. The measured fractal dimensions are respectively $D = 2.10$, $D = 2.12$ and $D = 2.13$.

the clusters, different shape of the cluster mass distribution, and different kinetics of aggregation. It is worth to notice that this behavior does not depend on the detailed nature of the colloid, provided that the essential physical interactions are the same. Since in RLCA the sticking probability is very low, two approaching clusters can, on statistical basis, sample all possible mutual configurations before they finally stick together. Thus the smallest clusters in the polydisperse distribution have a high probability of interpenetrating the large ones. This effect leads to less tenuous clusters respect to DLCA. As a consequence the fractal dimension in RLCA results higher than the one of DLCA [42]. The fractal dimension of the macromolecule formed by diffusion aggregation processes may be measured by light scattering experiments, investigating the behavior of the static structure factor $S(k)$ as a function of the wave number k [43]. This experimental technique is discussed in detail in App. A. Aggregates formed by RLCA from silica, polystyrene latex, and gold have been studied with different methods, including light scattering, small-angle x-ray scattering, transmission electron microscopy (TEM), giving $D \approx 2.1$ [42] (Fig. 1.4). Also aggregates formed by DLCA from fluorinated polymer particles [44] have been investigated with different methods, obtaining $D \simeq 1.8$ (Fig. 1.5).
When gel formation is due to DLCA or RLCA processes, the gelation process corresponds to the formation of an interconnected network which evolves dynamically, but the same approach as the chemical gelation holds within the appropriate observation time scale. The gelation transition may again be described in terms of percolation theory.

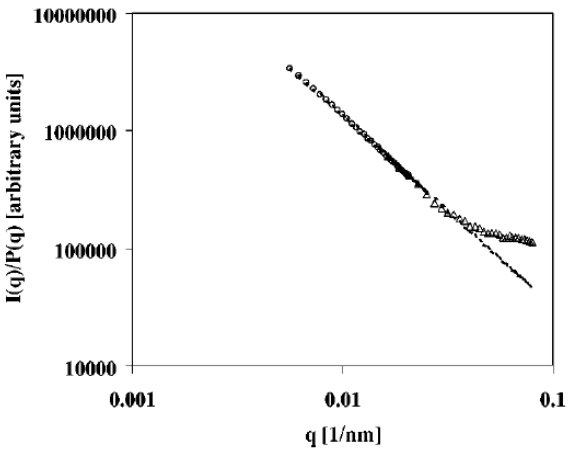

Figure 1.5: Static light scattering and small-amgle neutron scattering intensities for DLCA aggregates in 18 mm cuvette (circles) and 0.1 mm cuvette (triangles) [44]. The measured fractal dimension is $D \simeq= 1.8$.

1.6 Conclusion

In this chapter we have reviewed the fundamental properties of gelling systems. We have discussed the main features of percolation theory, stressing that it represents a good description of structural properties of gelling systems. The gelation transition may be interpreted as a connectivity transition both in chemical gels and in physical ones, the latter being characterized by non permanent bonds among monomers. An overview of experimental methods and results has been presented, in order to describe the phenomenology involved in gelation transition. In the next chapter we present an overview of experimental results on the dynamics of gelling systems, describing the main features of models used to interpret and comprehend the rich phenomenology involved in gelation transition.

Chapter 2

Gel: an elastic disordered solid

From an experimental point of view, the sol phase can be characterized by finite viscosity, whereas the gel phase exhibits elastic behavior, due to the presence of a macroscopic interconnected stress-bearing molecule. The formation and the presence of such macromolecule strongly influence the relaxation functions of gelling systems which exhibit a complex non exponential behavior.
In this chapter we present an overview of theoretical and experimental results concerning the dynamics of gelling system, focusing on widely used models to describe the viscoelastic response.

2.1 Viscoelasticity of gelling systems

In the previous chapter, using the percolation theory approach, we have described the gelation transition analyzing the behavior of static properties, as the mean cluster size, the size distribution and the fractal dimension of the formed structures. Even if the percolation theory provides a coherent characterization of different gelling materials, it cannot be used to describe the dynamical evolution of gels and the changes in mechanical response due to the formation of the spanning macromolecule. In fact it describes a purely static transition corresponding to topological changes of the system. Experimental findings reveal that the macroscopic quantities characterizing the system follow power law behavior as the transition threshold is approached, in agreement with the prediction of the theory of critical phenomena. In particular, the viscoelastic response of chemical gelling systems is characterized by power law behavior: the viscosity $\eta \propto (p_c - p)^{-k}$, where p is the control parameter of the transition and p_c is its value at the threshold, and the Young elastic modulus $E \sim (p - p_c)^f$.

In experiments, approaching the transition threshold, the divergence of the viscosity is observed. The critical exponent k is not unique but the obtained values may be grouped into two families: $k \sim 0.8$ (Fig. 2.1) observed in gelatin gels [45, 46], in some silica gels (TEOS) [47], in pectin biopolymer gels [48],

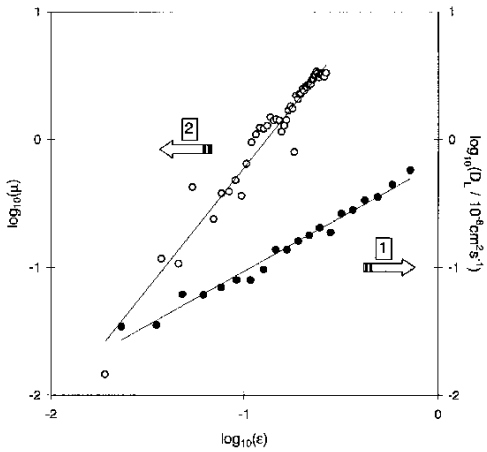

Figure 2.1: The divergence of the viscosity and the growth of elasticity for a gelatin solution. ϵ is the distance from the gelation threshold. Black symbols: diffusion coefficient of probe particles in the sol phase, fitted by a power law $\sim \epsilon^{0.85}$. Void symbols: shear elastic modulus in the gel phase, fitted by $\sim \epsilon^{1.9}$ [45].

and $k \sim 1.3$ (Fig. 2.2) observed in PDMS [27], in polyester gels [28, 29], in polyurethane gels [31], in some kind of end-linking gels [49], in tetramethoxysilicon (TMOS) silica gels [50], in epoxy resins [51].

Also when studying the elastic response of gels, experiments give a wide range of values of the critical exponent f that may be grouped into different families: $f \sim 2$ observed in gelatin gels [45, 46], in some silica gels (TEOS) [47], in agarose gels [52], $f \sim 3$ observed in polyester gels [28, 29], in epoxy resins [51], in some branched polymer gels [53], or $f \sim 4$ typically observed in colloidal gels [35, 36, 37, 54].

The different values of critical exponents k and f may be recovered within different theoretical models. In particular within the Rouse model approximation [16, 55], in which hydrodynamic interactions and excluded volume repulsion among monomers in a polymeric molecule are neglected, the viscosity critical exponent $k \simeq 2\nu - \beta$, where ν characterizes the critical behavior of the connectedness length and β is the critical exponent of the gel fraction. Using the random percolation critical exponents for a $3d$ system, the previous relation gives $k \sim 1.3$. On the other hand, the de Gennes analogy between gelation problem and electrical percolation network models, which is descried in Sect. 2.2, predicts that the viscosity diverges at the gelation threshold as the conductivity in a random superconducting network [13]. The conductivity of a random superconducting network diverges as $(p - p_c)^{-s}$ approaching the transition threshold for $p < p_c$ with $s \sim 0.7$ in $3d$, and stays infinite above it. Thus, within this analogy, $k \sim 0.7$. Following this electrical analogy, the elastic modulus in the gel phase grows above the gelation threshold as the conductivity in a random resistor network [12]. In this case, the conductivity, that is zero below the transition, grows above it as

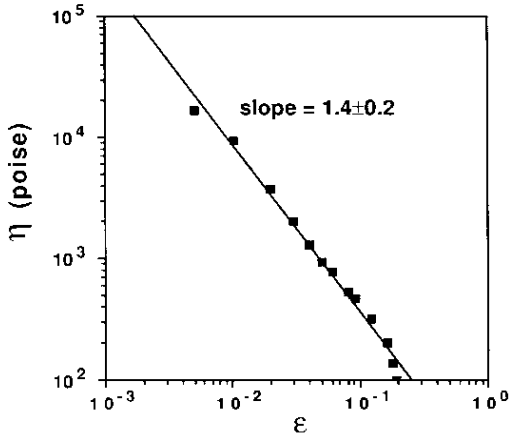

Figure 2.2: The divergence of the viscosity for epoxy resins. $\epsilon = (t_{gel} - t)/t_{gel}$ is the distance from the gelation threshold measured as function of time [51].

$(p-p_c)^t$ with $t \sim 1.9$ in $3d$. Hence, in the limit of validity of this analogy, $f \sim 1.9$. By evaluating the entropic contribution of the percolating cluster in the gel [25], it is obtained that the elasticity critical exponent $f = d\nu$, which in the case of random percolation in $3d$ gives $f \simeq 2.7$. Higher values of f are obtained using vulcanization models [16, 17, 56], which gives $f \sim 3.5$ in $3d$, or considering the energy variation due to bond-bending [57]. In this case $f \sim 4$.

2.2 The analogy between viscoelasticity and conductivity

Elastic percolating networks may be described by the Born Hamiltonian for a regular lattice of elastic elements [58]:

$$\mathcal{H} = \frac{1}{2} \sum_{ij} k_{ij} \left[a(\vec{r}_i - \vec{r}_j)_{\parallel}^2 + b(\vec{r}_i - \vec{r}_j)_{\perp}^2 \right], \tag{2.1}$$

where the sum is performed over the couples i, j of nearest neighbor particles. The coefficients a and b of the two elastic terms weigh respectively the relative displacement along the direction of the bond connecting i and j and the one orthogonal to the direction of the bond. If they are equal, the Hamiltonian in Eq. 2.1 describes a purely scalar problem, as the elastic energy depends only on the modulus of the relative displacements. The equilibrium condition at each site may be written as:

$$\sum_j k_{ij}(|\vec{r}_i - \vec{r}_j|) = 0. \tag{2.2}$$

Suppose to substitute each spring k_{ij} with a resistor with conductivity σ_{ij}. Using the analogy between Eq. 2.2 and the Kirchoff law for the current conservation at

each site

$$\sum_j I_{ij} = \sum_j \sigma_{ij}(V_i - V_j) = 0, \tag{2.3}$$

de Gennes first proposed the analogy between the macroscopic elastic constant of the spring network and the macroscopic conductivity of the resistor network [12]. Both the macroscopic conductivity and the macroscopic elasticity are due to the percolating cluster. The macroscopic conductivity does not grow above the transition threshold as the mass of the percolating cluster, as there are dangling ends that contribute to the mass but do not contribute to the conductivity. de Gennes noticed as this is also true for the macroscopic elastic modulus of the percolating cluster of a spring network. This analogy states a correspondence between the elastic constants k_{ij} with the conductances σ_{ij} of the resistors, and the position $\vec{r}_i$ with the voltage V_i of each site. Hence according to this analogy, the critical exponent f which governs the growing of the macroscopic elastic modulus should be equal to the critical exponent t of the macroscopic conductivity. Nevertheless, it is worth to notice that the elastic problems has a vectorial nature, and in many cases the elastic response is determined by more than one elastic constant. In $3d$ random percolating systems $t \simeq 1.9$: the conductivity critical exponent $f \simeq 1.9$ has been obtained for several gelling systems, such as gelatine gels [45, 46] and agarose gels [52].

Pushing further the analogy with an electrical network, de Gennes suggested the analogy between the viscosity and the conductivity of a super-conducting network [13]. He considered a network in which bonds are substituted with a super-conducting junction, whereas absent bonds are substituted with resistor of finite conductance. At the percolation threshold of super-conducting bonds an infinite macroscopic conductivity is observed. According de Gennes analogy, conductive bonds with a non-zero end-to-end voltage difference correspond to couples of particles with a finite mobility, which have non-zero relative velocity. Super-conducting bonds, instead, correspond to couples of blocked particles. The percolating cluster of blocked particles would produce a macroscopic infinite viscosity. Then the critical exponent k of the viscosity should be equal to the critical exponent s of the macroscopic conductivity in the super-conducting network. In a $3d$ random percolating system $s \sim 0.7$ [59]. Within this approach, the divergence of the viscosity is seen in terms of a progressive solidification of the sol, corresponding to the blocking of the monomer movements, instead of the idea of the divergence of relaxation time. In fact, the transformation in an elastic solid does not necessarily implies the arrest of monomer movements. On the other hand, the value of the critical exponent for the viscosity predicted by this analogy is observed in several systems and in numerical studies [60].

2.3 Entropic elasticity

Any deformation of solid systems usually produces a change in the internal energy. At temperature $T \geq 0$ a deformation produces topological constraints corresponding to an entropy reduction, which may be not negligible compared to internal energy variation. As a consequence, the entropic contribution to the free energy variation $\Delta F = \Delta E - T\Delta S$ is dominant, thus the elastic response has also a not negligible entropic origin. This is the case of the Gaussian chain, where the length of each bond constituting the chain has a Gaussian distribution of mean value b. The probability distribution function for the end-to-end distance r of a Gaussian chain made of N of such bonds is given by:

$$\Psi(\vec{r}) = \left(\frac{3}{2}\pi b^2\right)^{3/2} \exp\left(-\frac{3r^2}{2Nb^2}\right), \tag{2.4}$$

hence its free energy can be written as follows:

$$F = -k_B T \ln \Psi(\vec{r}) \sim k_B T \frac{3r^2}{2Nb^2}. \tag{2.5}$$

When the chain is stretched and its end-to-end distance increases, the free energy increases and a restoring force arises. As a consequence the chain has an elastic behavior, due to the entropic contribution to the free energy. Accordingly an entropic elastic constant $K = 3k_B T/Nb^2$ can be defined.

Let us consider the case of gelation. The gelation transition may be described using the percolation theory so that the gelation threshold corresponds to the percolation threshold, where the connectedness length ξ, defined in percolation theory [18], diverges following a power law behavior $\xi \sim |p - p_c|^{-\nu}$. The elastic free energy per unit volume can be written as

$$F_{el} = \sum_{nodes} K(\vec{R}_i - \vec{R}_j)^2, \tag{2.6}$$

where the sum is restricted to nodes, which constitute the gel network, in the unit volume and K is the elastic constant of the chain connecting i to j. The percolating cluster may be seen as a macrolink of length ξ, hence $|\vec{R}_i - \vec{R}_j| = \xi$ is the distance between two nearest-neighbor nodes and in a volume ξ^d there is only one node. As a consequence the elastic free energy per unit volume is

$$F_{el} \sim \xi^{-d} K \xi^2 \sim (p - p_c)^f \tag{2.7}$$

where f is the elasticity exponent. As $K \sim (p - p_c)^\zeta$, we obtain $f = (d - 2)\nu + \zeta$. Assuming that $K \sim \xi^{-2}$, as it has been obtained in a Gaussian chain, we obtain $f = (d - 2)\nu + 2\nu = d\nu$. The same result may be obtained with an heuristic reasoning. Near the percolation threshold, the characteristic length scale ξ_{den} of density fluctuations may be neglected with respect the connectedness

diverging length ξ. The incipient spanning cluster may be described as a macro-link whose end-to-end distance fluctuates under the effect of temperature, having a certain distribution length scale which is presumably equal to the percolation connectedness length ξ. Under a small shear deformation, each chain is slightly stretched or compressed, thus contributing k_BT to the elastic modulus. As there are roughly ξ^{-d} effective chains per unit volume, the elastic modulus should scale as $k_BT\xi^{-d} \sim (p-p_c)^{d\nu}$ near the transition threshold.

Summing all the contributions to the free energy, we have $F \sim A(p-p_c)^{2-\alpha} + B(p-p_c)^f$, the first term being the usual one for percolation [18]. When the entropic contribution is dominant, $f = d\nu$, which using scaling relations [18] may be written as $d\nu = 2-\alpha$, then $f = 2-\alpha$ in any dimension. On the other hand, the analogy proposed by de Gennes, discussed in the previous paragraph, predicts $f \simeq 1.9$ in $d = 3$, hence the elastic term of the free energy will be dominant compared with $2 - \alpha \simeq 2.6$.

Interestingly, a renormalization group approach to the study of the critical behavior of the elastic modulus [61] has demonstrated that, if excluded volume interactions can be neglected, the critical exponent f is equal to that of the random resistor network conductivity, as predicted by de Gennes. In contrast, when excluded volume effects are relevant, the exponent should cross over to $d\nu$, provided that the percolation connectedness length is much larger than the density fluctuation length.

2.4 Decay of density fluctuations

The fundamental object that is used in the study of the dynamical behavior of liquids is the time-dependent generalization of the equilibrium pair distribution function, the so called *van Hove function* [62]. Given a system composed by N particles in a volume V, in which the position of the α-th particle at time t is $\mathbf{r}_\alpha(t)$, the density operator is given by [63]

$$\rho(\mathbf{r},t) = \sum_{\alpha=1}^{N} \delta^3(\mathbf{r} - \mathbf{r}_\alpha(t)), \tag{2.8}$$

whose mean value is $< \rho(\mathbf{r},t) >= \rho = N/V$. The van Hove function is the autocorrelation function of $\rho(\mathbf{r},t)$ in space and in time, and is defined as

$$G(\mathbf{r},t) = \frac{1}{\rho} < \rho(\mathbf{r},t)\rho(0,0) >= \frac{V}{N} \sum_{\alpha,\beta=1}^{N} < \delta^3(\mathbf{r}_\alpha(0))\delta^3(\mathbf{r} - \mathbf{r}_\beta(t)) > . \tag{2.9}$$

It describes the probability of finding a particle around $\mathbf{r}$ at time t, given that there is a particle in the origin at time $t = 0$. It separates naturally into two terms, usually called the *self* part $G_s(\mathbf{r},t)$ and the *distinct* part $G_d(\mathbf{r},t)$, given respectively by the sum over the diagonal terms $\alpha = \beta$, and by the sum over the

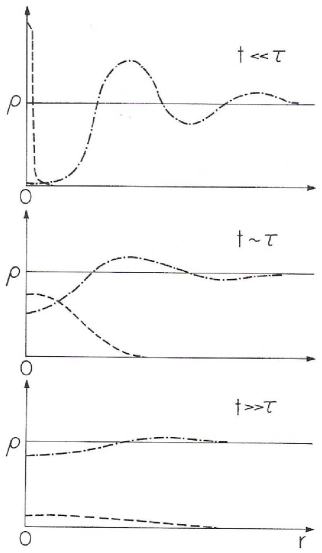

Figure 2.3: Typical van Hove function for a simple liquid, in the three time regimes $t \ll \tau$, $t \simeq \tau$, and $t \gg \tau$, where τ is the structural relaxation time of the liquid [62]. The dashed curve is $G_s(\mathbf{r}, t)$ and the dot-dash curve is $G_d(\mathbf{r}, t)$.

off-diagonal terms $\alpha \neq \beta$. They describe respectively the probability that the particle in $(\mathbf{r}, t)$ is the same that was in $(0, 0)$, or a different one. For $t = 0$ one has $G_s(\mathbf{r}, 0) = \delta^3(\mathbf{r})$ and $G_d(\mathbf{r}, 0) = \rho g(\mathbf{r})$, where $g(\mathbf{r})$ is the static pair correlation function. For $t \to \infty$ or $\mathbf{r} \to \infty$ one has

$$\lim_{\mathbf{r}\to\infty} G_s(\mathbf{r}, t) = \lim_{t\to\infty} G_s(\mathbf{r}, t) = \frac{1}{V} \simeq 0, \tag{2.10}$$

$$\lim_{\mathbf{r}\to\infty} G_d(\mathbf{r}, t) = \lim_{t\to\infty} G_d(\mathbf{r}, t) = \frac{N-1}{V} \simeq \rho. \tag{2.11}$$

The typical behavior of $G_s(\mathbf{r}, t)$ and $G_d(\mathbf{r}, t)$ in the time regimes $t \ll \tau_s$, $t \simeq \tau_s$, and $t \gg \tau_s$, is shown in Fig. 2.3, τ_s being the structural relaxation time of the liquid.

The space Fourier transform of $\rho(\mathbf{r}, t)$ is the density fluctuation of wave number $\mathbf{k}$,

$$\rho_{\mathbf{k}}(t) = \int d^3\mathbf{r} e^{-i\mathbf{kr}}\, \rho(\mathbf{r}, t), \tag{2.12}$$

whose mean square value is called *static structure factor*,

$$S(\mathbf{k}) = \frac{1}{N} < |\rho_{\mathbf{k}}|^2 > = \int d^3\mathbf{r} e^{-i\mathbf{kr}}\, G(\mathbf{r}, 0) = 1 + \rho \int d^3\mathbf{r} e^{-i\mathbf{kr}}\, g(\mathbf{r}). \tag{2.13}$$

The corresponding transform of $G(\mathbf{r}, t)$ gives the autocorrelation function of density fluctuations, also called *intermediate scattering function* or *coherent scattering function*,

$$F(\mathbf{k}, t) = \frac{< \rho_{\mathbf{k}}(t)\rho_{-\mathbf{k}}(0) >}{< |\rho_{\mathbf{k}}|^2 >} = \frac{1}{S(\mathbf{k})} \int d^3\mathbf{r} e^{-i\mathbf{kr}}\, G(\mathbf{r}, t). \tag{2.14}$$

If we consider only the self part of the van Hove function, we obtain the *self intermediate scattering function* or *incoherent scattering function*,

$$F_s(\mathbf{k},t) = \int d^3\mathbf{r} e^{-i\mathbf{kr}}\, G_s(\mathbf{r},t) = \frac{1}{N}\sum_{\alpha=1}^{N} < \exp^{i\mathbf{k}(\mathbf{r}_\alpha(0)-\mathbf{r}_\alpha(t))} > . \tag{2.15}$$

Finally, Fourier transforming over time we obtain the *coherent dynamical structure factor*

$$S(\mathbf{k},\omega) = \frac{S(\mathbf{k})}{\pi} F(\mathbf{k},\omega) = \frac{S(\mathbf{k})}{2\pi}\int_{-\infty}^{\infty} e^{i\omega t}\, F(\mathbf{k},t) = \frac{1}{2\pi}\int_{-\infty}^{\infty} e^{i\omega t}\int d^3\mathbf{r} e^{-i\mathbf{kr}}\, G(\mathbf{r},t), \tag{2.16}$$

and the *self* or *incoherent dynamical structure factor*

$$S_s(\mathbf{k},\omega) = \frac{1}{\pi} F_s(\mathbf{k},\omega) = \frac{1}{2\pi}\int_{-\infty}^{\infty} e^{i\omega t}\, F_s(\mathbf{k},t) = \frac{1}{2\pi}\int_{-\infty}^{\infty} e^{i\omega t}\int d^3\mathbf{r} e^{-i\mathbf{kr}}\, G_s(\mathbf{r},t), \tag{2.17}$$

that are (for classical systems) even functions of both $\mathbf{k}$ and ω.

The static and dynamic structure factors provide the most useful link between theory and experiment, being proportional to the cross section for the elastic and anelastic scattering of radiation from the system. The most used radiation in this sense are slow neutrons [64], which for energies comparable with k_BT at 300 K have a wavelength of the order of 2 Å, that is approximately the distance between neighboring particles. In this case the cross-section for the scattering of a neutron, with momentum transfer $\hbar\mathbf{k}$ and energy transfer $\hbar\omega$, is proportional to the coherent dynamical structure factor $S(\mathbf{k},\omega)$. By varying the isotopic composition of the nuclei in the liquid, or by using polarized neutrons, it is possible to measure separately the coherent and incoherent cross-sections, and thus to separate the contribution due to $S_s(\mathbf{k},\omega)$.

The scattering of light is also used to investigate the properties of liquids, but there are two differences with the case of slow neutrons. First, the light scattering is entirely coherent, so that no information on $S_s(\mathbf{k},\omega)$ can be gained. Second, the wavelengths of light are of order $4000 - 8000$ Å, so that one can apply the phenomenological equations of hydrodynamics [65, 66] to calculate the spectral distribution of scattered light. Thus scattering of light is not useful if one is interested in the dynamics of the system outside the hydrodynamic region [1], that is for wavelengths comparable with the inter-particle distance.

The static structure factor $S(\mathbf{k})$ can be measured experimentally by scattering of X-rays, electrons, or fast neutrons, that have energies much greater than k_BT for the wavelengths of interest. In this case the scattering can be treated, to a

[1]The hydrodynamic region corresponds to wave number $k \simeq 10^{-3}$ Å^{-1}, where the density fluctuations vary very slowly in space compared with typical near-neighbor separations.

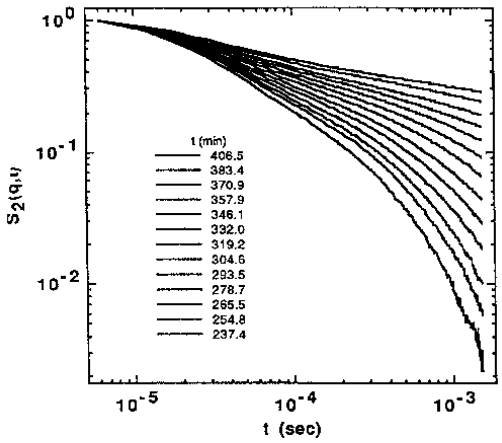

Figure 2.4: Dynamic scattering function in silica gel (TMOS) [69]. As the gel point is approached a stretched exponential slowing down is observed, with $\beta = 0.65 \pm 0.05$. At the gel point a power law decay becomes evident.

very good approximation, as being elastic, and the cross-section is proportional to

$$\int_{-\infty}^{\infty} d\omega \, S(\mathbf{k}, \omega) = S(\mathbf{k}). \tag{2.18}$$

This relation is called *elastic sum rule*, and suggests a useful way of normalizing $S(\mathbf{k}, \omega)$. Interesting results have been obtained by dynamic light scattering experiments in gelling systems [67, 68, 69, 70] showing a non-exponential behavior of the intermediate scattering function $F(\mathbf{k}, t)$ approaching the transition threshold. In general $F(k, t)$ is well fitted by a stretched exponential decay (Fig. 2.4)

$$F(k, t) \sim \exp\left[(t/\tau)^{\beta}\right]. \tag{2.19}$$

The values of the exponent β [2] may depend on the wave vector k considered and on the particular system under investigation, for example in tetramethoxysilicon (TMOS) silica gels $\beta \sim 0.65$ [67], and in an interacting polymer gel $\beta \sim 0.4$ [68]. The stretched exponential behavior of the intermediate scattering function is a consequence of the widening of the molecule size distribution towards the percolation regime. Therefore over sufficiently large length scales the behavior of the intermediate scattering function is due to the contribution of different relaxation processes characterized by different relaxation times, whose superposition produces a detectable deviation from an exponential law. It is worth to notice that in fact the relaxation process is controlled by the growth of the connectivity inside the system. Approaching the transition threshold, the mean molecule size

[2] This exponent must not be confused with the critical exponent of the order parameter in percolation theory, i.e. the density of the infinite cluster.

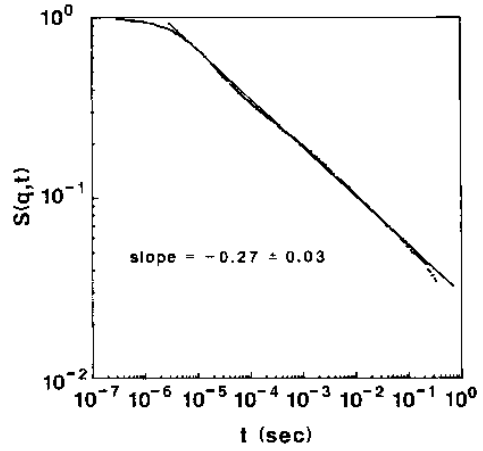

Figure 2.5: At the gel point the scattering function shows a power law behavior in silica gels (TMOS) [67].

critically grows. As a consequence the onset of a power law decay (Fig. 2.5) of the intermediate scattering function is observed [4, 67], indicating that the relaxation is controlled by the formation of the percolating cluster, with associated relaxation times critically growing. In the gel phase the relaxation behavior can be different, displaying complex behavior depending on the type of considered gel.

These features of the dynamics are well reproduced by Monte Carlo simulations of a lattice model [71] and by molecular dynamics simulations in continuum space [72], which are discussed in detail in Chap. 6.

2.5 Conclusion

In this chapter we have presented an overview of experimental results on viscoelastic behavior of gelling system, reporting the most common observed values of critical exponents of viscosity coefficient and of elastic modulus. We have focused on two different models for elastic response of gels: We have described the analogy proposed by de Gennes between an elastic network and a random resistor network, and we have discussed the role of entropy in the elastic response. Furthermore, we have discussed the non trivial relaxation of gelling system, due to the widening of size distribution of formed molecules in different gel types.
In the next chapter we discuss in detail gelatin gels, which have been deeply investigated by means of experiments as they represent one of the most common biopolymer gels. We present experimental results regarding two specific processes, the first one is a gelation process and the latter is a degradation process. Interestingly, experiments give new results, whose deeper comprehension requires more extensive investigations.

Chapter 3

Recent experimental results on gelation and degradation processes

Polymer gels have received great attention not only for their numerous technological and biological applications but also because they exhibit common features with other complex systems, such as supercooled liquids, colloidal gels, and so on. An important role is occupied by biological polymers, in particular gelatin, as it is one of the main constituent of human tissues. Gelatin gels have been widely investigated since 80's, but recently new interesting results have been obtained. In fact, while the main effort was devoted to investigate the physical gelation process and the percolation properties of the gel phase, recently an increasing interest on kinetics and on degradation processes has come out. Moreover, introducing molecules in solution, able to bind to gelatin amine groups, chemical bonds may form between gelatin chains and reactant, leading to the formation of chemical gels. The mechanical properties of the formed gel strongly depend on the parameters characterizing the reaction and may be finely tuned. Gelatin degradation is also an interesting phenomenon to be investigated, as it occurs in several biological processes. In fact, in tumor dissemination the degradation of the extracellular matrix, a gelatin gel, is involved.
In this chapter we briefly describe gelatin. We present recent experimental results on the chemical gelation process by the action of reactant molecules, analyzing the kinetics of the reaction. Moreover, we discuss interesting results obtained by the investigation of a degradation process due to the action of cutting molecules.

3.1 A bipolymer gel: the gelatin

Among physical gels, gelatin gels have been widely studied since 80's [45] because of their presence in collagen from various sources (fish or mammalian) and their

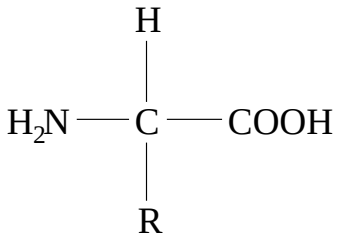

Figure 3.1: The chemical structure of the amine group in the collagen chain.

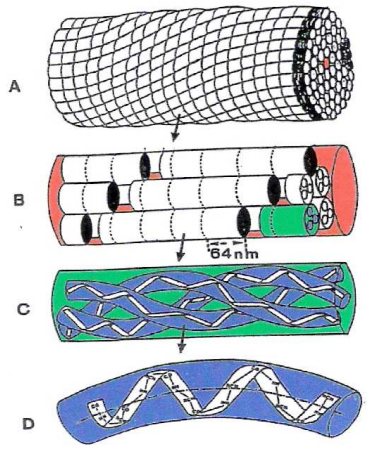

Figure 3.2: The structure of the fibers of collagen at differen length scales: A) Fibers of collagen; B) structure of one fiber; C) triple helix of collagen; D) conformation of a left handed helix [74].

numerous applications in pharmaceutical, photographic and food industries. Gelatin is denatured collagen: It is a linear chain of polypeptides, whose basic unit is the amine acid (Fig. 3.1). The amine group is made of a central carbon atom, to which an hydrogen atom H, a $COOH$ group, a H_2N and a radical group R are linked. The sequence of acids in the chain determines its physical and chemical properties, in addition to the structural ones. The radical group R of the amine group may be hydrophobic, polarized not charged, which may form hydrogen bonds with water, or polarized charged (NH_2^+, NH_3^+, COO^-). The effective charge of the latter type of groups depends on the pH of the solution.

In the native state, the collagen is in the form of a fiber [73] (Fig. 3.2 A), made of rods of length about 2800 Å and diameter 15.3 Å (Fig. 3.2 B). Each rod is constituted by a triple helix (Fig.3.2 C), in which each chain is a left handed helix (Fig.3.2 D). The triple helix is right handed and its step is equal to 86 Å, ten times the step of the chain helix, which is made of 1052 residues. The triple helix is stabilized by hydrogen bonds [75], which are also responsible for its rigidity.

The formation of helices in gelatin solutions takes place when the temperature is lowered below the denaturation temperature. The process of helix formation

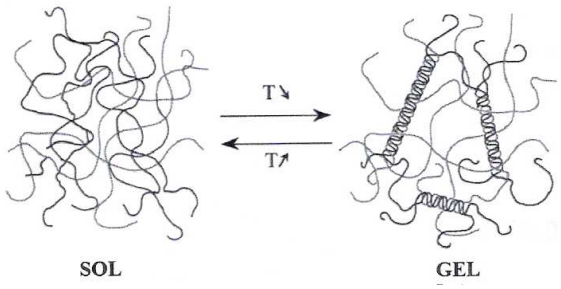

Figure 3.3: Formation of helices in gelatin solution [74].

begins in the region rich in proline and hydroproline. A given gelatin chain may contribute to the formation of different helices, as it is shown schematically in Fig. 3.3. The gel resulting from the formation of triple-helix structures is a physical gel: hydrogen bonds, which are reversible, stabilize the helices and break when the temperature rises.

If the temperature increases above the denaturation temperature, about 36^oC, the hydrogen bonds are completely broken and the triple helices do not persist in the system[1]. As a consequence, at higher temperature gelatin chains behave as linear polymers in solution. Three different regime may be considered, depending on the concentration of gelatin in solution, respectively a dilute regime concentration, the overlap concentration C^*, defined as the concentration for which polymer coils touch each other, and higher density regime concentration. In the dilute regime, where the concentration is sufficiently low ($C < C^*$), the gelatin in solution form independent coils. The radius of gyration R_g of coils may be measured by light scattering measurements [76]: for gelatin of molar mass $M_w = 19 \cdot 10^4\ g \cdot mol^{-1}$ in aqueous solution, $R_g = 350$ Å. At the concentration C^* of gelatin chains, the coils start to touch each other. For gelatin with $M_w = 19 \cdot 10^4\ g \cdot mol^{-1}$ in aqueous solution it has been obtained $C^* \approx 0.5\%$ [77]. If the concentration increases further ($C > C^*$), the gelatin chains in solutions are entangled and the motion is dominated by reptation, i.e. the chain moves back and forth along itself.

Along the gelatin chain there are some chemical units that can react with particular molecules forming covalent bonds. If these type of molecules, which in the following we will refer to as *cross-linkers*, are present in solution, chemical bonds between them and these chain units may form. As a consequence different chains may be permanently linked together, so that as the concentration of bonds between different chains increases the sol-gel transition takes place. The resulting gel is a chemical gel. In particular in the next section we consider gelatin solutions with the addition of bisvynilsulphonemethyl (BVSM) reactant [7], able to form

[1]The temperature at which triple helices disappear strongly depends on the acid composition of the chains. Here we refer to the collagen of mammalian.

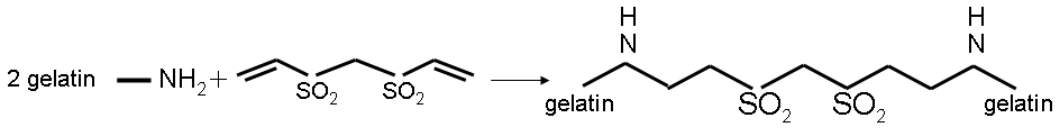

Figure 3.4: Reaction of bond formation between gelatin chains and cross-linkers.

bonds with the lysine, the hydroxylysine, the histidine, and possibly with other amine groups of gelatin chains (Fig. 3.4).

3.2 Microcalorimetry measurements and chemical gelation

Physical gels made of gelatin helices have been widely investigated [6, 45, 46] and a complete characterization of their viscoelastic properties has been provided. Nevertheless the chemical gel obtained by bond formation between gelatin chains and reactant molecules provides a new appealing system to be investigated in order to analyze the relation between structure and mechanical response. The influence of various parameters, such as gelatin or reagent concentration and solution pH, on bond formation was investigated [7]. In experiments, the kinetics of the reaction between amine groups of gelatin chains and BVSM has been monitored by microcalorimetry measurements. The gelatin sample is a photographic grade of gelatin extracted from lime processed ossein with an average molecular weight $M_w \sim 165300 g/mole$, an index of polydispersity $I_p = 2.06$ and an isoelectric point $pI = 4.9$. The granules contain approximately 10% humidity and the concentrations are corrected accordingly. The size of BVSM molecule in the considered solution is ≈ 9.5 Å. The BVSM can create covalent $C - N$ bonds with amine groups of gelatin chains, so that a permanent network is formed at $T \geq 40^oC$, where the triple helix structure of gelatin gels does not form. The influence of system parameters on kinetics of the reaction and elastic properties was analyzed [7]. Microcalorimetry measurements are able to monitor the development of the chemical reaction in time by detecting the enthalpy change during the exothermal formation of $C - N$ bonds. If the pressure and the temperature are kept constant, the enthalpy change corresponds to the heat flux which is interchanged between a reference system and the sample in which the chemical reaction takes place. Hence, using a differential calorimeter, the heat flux as a function of time can be measured and the reaction extent can be easily monitored. Several experiments have been performed at temperature $T = 40^oC$, using solutions with different concentrations of gelatin and reactant, for different values of pH. In Fig. 3.5 the released heat $Q(t)$ is plotted as a function of time for a solution with gelatin concentration $C_{gel} = 12\% g/cm^3$, BVSM concentration $C_{BVSM} = 0.15\% g/cm^3$ and $pH = 6.7$. Normalizing the released heat by

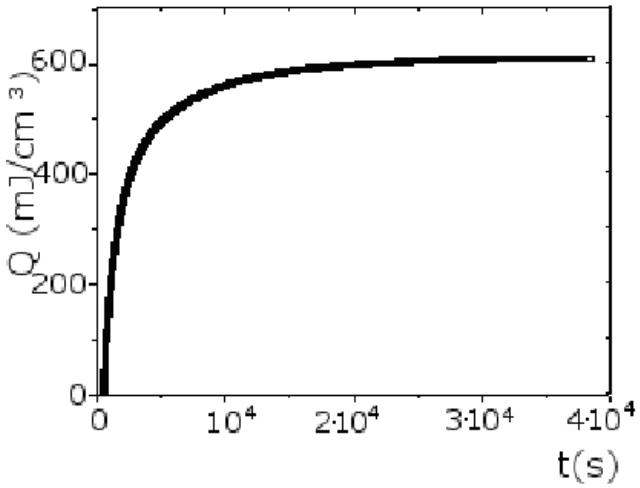

Figure 3.5: Released heat during the chemical reaction between gelatin and reactant, for a solution with $C_{gel} = 12\%$, $C_{BVSM} = 0.15\%$, $pH = 6.7$ and $T = 40^oC$.

the enthalpy change $\Delta H = -40kJ/mol$ due to the formation of a single $C - N$ bond, the curve represents at any time the total number of bonds formed between gelatin chains and BVSM. By writing $Q(t) = A(1 - f(t))$, where A is a dimensional coefficient proportional to ΔH, we introduce the function $f(t)$ which represents the fraction of bonds that remain to form at time t. In Fig. 3.6 $f(t)$ is plotted as a function of time. Data are fitted with the sum of two exponentials:

$$f(t) = A_1 \exp(-t/\tau_1^m) + A_2 \exp(-t/\tau_2^m) \tag{3.1}$$

with $\tau_1^m = 520s$, $\tau_2^m = 9000s$ so that $\tau_2^m/\tau_1^m = 17.31$ (the apex "m" is an abbreviation for "microcalorimetry").

It is worth to notice that, when counting the number of cross-links binding BVSM and gelatin, the method can not discriminate between bonds established by free reactants with a chain and bonds leading to a bridge between two gelatin chains, nor else bonds leading to a loop within a chain. This lack of information on the kinetics leading to the gel formation crucially affects the characterization of the gel structure and therefore its mechanical properties. Finally it may reflect onto the location of the gelation threshold and the determination of the critical exponent of the elastic modulus. In fact, the critical behavior of the shear modulus was measured at low frequency, giving a critical exponent $f = 3.4 \pm 0.3$ [7], close to the expected value for the vulcanization of long chains. As a consequence, a deeper comprehension of the bond formation kinetics is essential, requiring alternative investigations. In particular the primary question is to understand how the two time scales controlling the kinetics depend on the formation of single-bonds and bridges between the cross-linkers and the chains, or else to loops within the chains. Moreover it would be crucial to understand how these

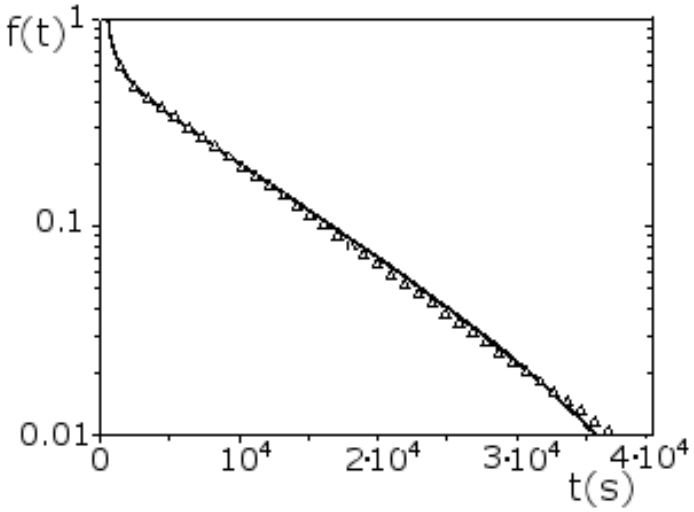

Figure 3.6: The fraction of bonds of the BVSM that remain to form as a function of time, for a solution with $C_{gel} = 12\%$, $C_{BVSM} = 0.15$, $pH = 6.7$ and $T = 40^oC$. The continuous line is the fit with Eq. 3.1.

time scales are related to the properties of the gelatin solution (concentration, pH...) and of the cross-linking molecules (concentration, reactivity...). In the next chapter we analyze the role of concentration and reactivity of cross-linking molecules in the kinetics of bond formation, by complementing the experimental observations with a numerical study.

3.3 The extracellular matrix and its degradation

The extracellular matrix (ECM) is a dense network made of various proteins including collagen. In mammals it forms the basement of membranes, preventing the cell dissemination and ensuring organ integrity. It is the support of cell adhesion and thus regulates cell proliferation, differentiation and locomotion. During specific processes some cells acquire the ability to traverse the ECM, disseminating into distant organs. In such processes, the ECM may be degraded by a variety of proteolytic enzymes, especially metalloproteinases, that catalyze the hydrolysis of the cross-links between peptide chains increasing its permeability. The solubilizing process is due to a change of the environment of the ECM, with an increase of its mesh size and a subsequent increase of its permeability. Moreover, ECM proteolysis[2] modifies not only the biochemistry of the cell environment,

[2]The proteolysis is the process of hydrolysis of proteins into peptides and amino acids by cleavage of their peptide bonds.

but also its mechanic characteristics, like porosity, stiffness and rigidity. These mechanical properties in turn crucially influence cell adhesion, protein expression or locomotion. This solubilizing transition is especially connected with tumor invasiveness, in which some cells access the lymphatic and blood circulation, and disseminate to distant organs (metastasis). Several studies indicate that invasive cells produce proteolysis in the ECM, or induce proteinase[3] secretion from surrounding host cells. Nevertheless, the mechanisms whereby proteinase activity permits tumor invasion through the matrix, are still unclear. To this extent, interesting studies have been performed and the kinetics of gel proteolysis has been investigated. The proteolysis was induced by the action of enzymes that catalyze the hydrolysis of bonds leading to the solubilization of the ECM. In recent experiments [10] the kinetics of gel solubilization has been monitored with a spectrophotometric assay that measures the appearance of solubilized hydrolysis products during the reaction. ECM and fibronectin gels were used, and three types of enzymes were considered, thermolysin, trypsin and proteinase K. The ECM is a gel formed by weak, non-covalent interactions, as attested by gelation reversibility with temperature. Fibronectin is a large protein whose molar mass is $5.5\ 10^5\ g\ mol^{-1}$, which is present in the ECM, mediating cell adhesion. By the addition of glutaraldehyde to concentrated fibronectin solution, a chemical gel may be obtained.

The experimental system comprises two distinct areas (Fig. 3.7): the gel phase is on the bottom of the cuvette, referred as the "matrix area". Above it there are proteinases in solution; this area is referred to as "liquid area". As the reaction begins some enzyme molecules diffuse from the liquid area to the matrix area, catalyzing the formation of hydrolysis products in the matrix area. The solubilized proteolysis products constituting the sol phase diffuse from the matrix area to the liquid area. By light absorbance measurements, the fraction of solubilized product in the liquid area $X_{sol}(t)$ has been determined. The gel fraction X_{gel} has been obtained using the relation $X_{gel}(t) = 1 - X_{sol}(t)$. Measurements on different samples confirm that enzymes are homogeneously distributed into the matrix area before the reaction has proceeded to a notable extent. Hence the hydrolysis proceeds through volume degradation rather than surface degradation of the matrix area. As the reaction proceeds, the gel is decomposed into small groups of molecules, until the macromolecule constituting the matrix area disappears and the sol phase is recovered. The gel-sol transition is reached at some time t_c, when $X_{sol}(t)$ becomes equal to one, or when the gel fraction $X_{gel}(t) = 1 - X_{sol}(t)$ becomes zero. With various gel-enzyme combinations, and different enzyme concentrations, it was found that $X_{gel} \propto |t - t_c|^{\beta}$, with $\beta \simeq 1$, for $t < t_c$ (Fig. 3.8). In particular, for ECM gel and trypsin for example $\beta = 1.01 \pm 0.03$ [10]. These results indicate that the exponent β does not depend on enzyme speci-

[3]The proteinase is any enzyme that catalyzes the splitting of proteins into smaller peptide fractions and amino acids by proteolysis process.

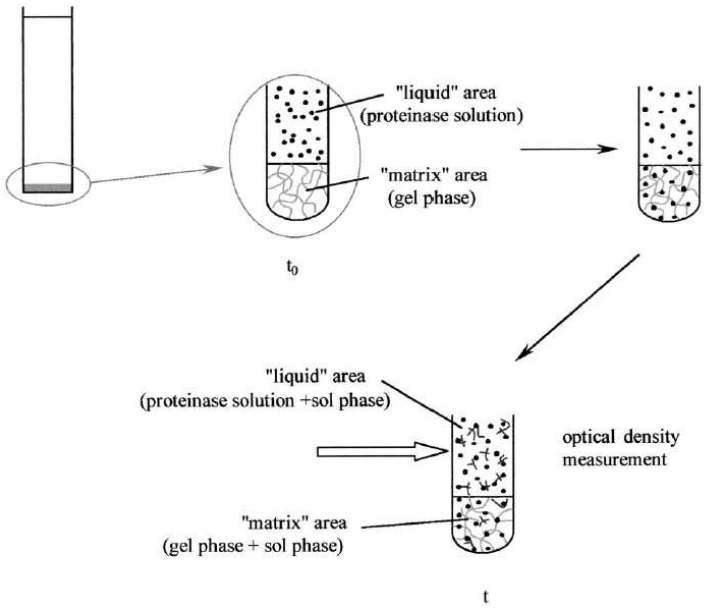

Figure 3.7: Schematic representation of the experimental system for ECM gel proteolysis [10]. The matrix area is 20 times less than the liquid area (upper, left). The development of the reaction process is represented at three different points: initial conditions of the sample (t_0, upper left), diffusion of enzymes in the matrix area (upper right), diffusion of proteolysis products in the liquid area (t, bottom).

ficity or on gel type, but it is related only to the degradation mechanism. As the critical exponents are extracted from the behavior of the system near the transition, and being the density of bonds p a regular function of time around t_c, we can make a Taylor expansion and take only the first order term, obtaining $(p - p_c) \propto (t - t_c)$ near the transition. Therefore $X_{gel} \propto |p - p_c|^\beta$, with $\beta \simeq 1$, for $p > p_c$. This result is quite unexpected, because sol-gel transition is usually well described by random percolation [17], which is obtained when each bond between two monomers is present with probability p, and there is no correlation between different bonds. Random percolation in three dimensions gives a critical exponent $\beta = 0.41$ [18], very different from the one measured in the gel degradation experiments. This deviation from the random percolation universality class may be due to the presence of a long range correlation in the distribution of non-hydrolyzed bonds [11]. In order to verify this hypothesis and to deeper investigate the influence of proteolysis on mechanical properties of ECM, further characterizations of the degradation process are required. In chapter 5 we present a $3d$ lattice model, investigated by means of Monte Carlo simulation, which gives new insight into degradation processes.

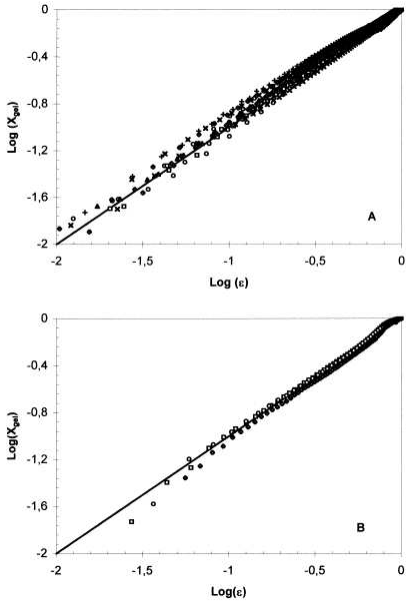

Figure 3.8: Gel fraction X_{gel} as a function of the distance $\epsilon = |t - t_c|/t_c$ from the transition threshold for thermolysin-degraded fibronectin (A) and trypsin-degraded ECM (B) [10]. The different symbols refer to different concentrations of enzymes. The full line is the fitting curve $X_{gel} \propto \epsilon^{\beta}$ with $\beta = 1$.

3.4 Conclusion

In this chapter we have described the main features of gelatin, one of the most studied biopolymers. We have described the main results obtained by microcalorimetry experiments performed on a gelatin solution in which reactant agent were added. Such experiments give information on the kinetics of bond formation, stressing the relevance of two characteristic times in bond formation. To deeper comprehend the nature of these two times, further investigations are needed. In the next chapter we introduce our model for bond formation between gelatin chains and reactant agents, which reveals to be a powerful tool to describe kinetics of bond formation. Furthermore, we have described the interesting results obtained from light scattering experiments on a gelatin gel degraded by enzymes. In chapter 5 we introduce our model for gel degradation process which is able to interpret experimental results and give predictions about quantities which have not measured yet.

Chapter 4

Kinetics of chemical gelation

In gelling systems numerical approaches to the study of rheological and dynamical properties have revealed to be extremely useful for a better understanding of experimental data [71, 78, 79]. Both Monte Carlo and molecular dynamics simulation techniques (described in App. B) have been applied in the last years to the study of different chemical gelation processes [79, 80, 81]. Here we use Monte Carlo simulations on the cubic lattice of a simple model to analyze the kinetics of bond formation in chemical cross-linking of a gelatin solution, considering solutions of polymer chains at different concentrations. Reactant monomers can diffuse in the solution forming bonds with the active sites along the chains and producing the cross-linking. Within this approach we follow the kinetics of the gel formation varying the gelatin concentration, the cross-linker concentration and its bonding probability (i.e. reactivity). Our data reproduce extremely well the experimental findings. They show that the two time scales detected in the experiments correspond respectively to the average time of forming single bond reactant-chain and bridge chain-chain via cross-linker. The ratio of these two characteristic times controls the kinetics of the bond formation: varying the concentration and the cross-linker reactivity strongly affects this ratio and therefore the kinetics of the gelation process.

In Sect. 4.1 the numerical study is described and the results on bond formation are discussed. In Sect. 4.2 the kinetics of bond formation is analyzed and in Sect. 4.4 the dependence of "loops" on solution parameters is investigated. Finally concluding remarks are given in Sect. 4.5.

4.1 Model and numerical study

We perform Monte Carlo simulations on a cubic lattice of a system made of bifunctional monomers, i.e. the reactant, and linear chains, which are represented by a sequence of $n = 10$ linked monomers. One monomer of the chain models a Kuhn segment [82], which is defined as the length over which correlations in the

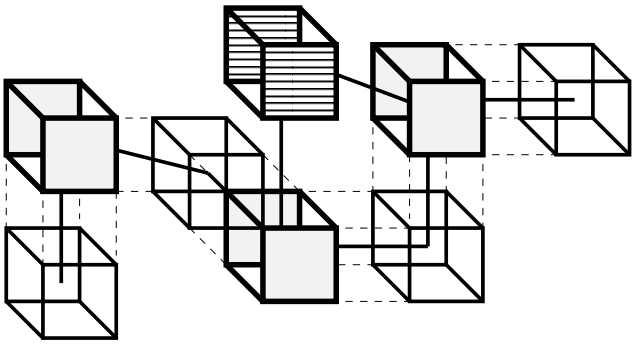

Figure 4.1: A schematic representation of a chain with active sites (filled cubes) and a reactant monomer (stripes filled cubes) linked to them.

direction of the chain tangent are lost. Hence a polymer chain may be modeled as a sequence of Kuhn segments, i.e. freely joined segments. Therefore one monomer of our chain represents more molecular units of the polymer. Using light scattering and small-angle neutron scattering techniques, the length of a Kuhn segment in a gelatin chain has been measured to be of the order of 20 Å [83], corresponding to about 10 amino-acids along the polymer. As compared to the experiments (described in Sect. 3.2), where gelatin chains containing 1000 amino-acids were used, our chains correspond to shorter gelatin chains, containing only about 100 amino-acids. Each monomer occupies simultaneously the eight sites of the lattice elementary cell and, to take into account the excluded volume interaction, two occupied cells cannot have any site in common. Some monomers along the chain are active sites which may bind to the reactant in order to compose complex clusters of chains leading to the formation of a gel. The active sites are tetra-functional: two bonds are formed with the neighbors along the chain and two are not saturated at the beginning of the simulation. Active sites correspond to amine groups along the chain able to react with cross-linking agents. The number of active sites per chain, n_{as}, corresponds to a fixed pH of the solution. In fact, in experiments the increasing of the pH activates more amine groups able to react with the BVSM along the chain, therefore in simulations n_{as} could be varied to study the effect of the pH. Although the number of amine groups in a gelatin chain actually linked to reactant cannot be measured experimentally, it is estimated that at most a fraction of about 20% can react. Therefore we perform most of the simulations for $n_{as} = 5$, which corresponds to a fraction of 10% of active amino-acids in our chain.

Topological constraints play an important role in polymer conformation, strongly influencing the entropy of the system in high density solutions. In such systems, a crucial role is played by entanglement effects, arising from the fact that polymer chains cannot cross each other. To take into account entanglements between chains, de Gennes [16] proposed to model the polymer chain motion as confined into a tube made of the other surrounding chains. He named this kind of motion

"reptation", from the Latin *reptare*, which means *to creep*. As it has been shown in Ref. [84], for the explored density regime, reptating chains reach equilibrium faster than chains moving with local movements. In our simulations, chains are randomly distributed on the lattice and diffuse towards equilibrium reptating, according the slithering-snake algorithm rules and the bond-fluctuation dynamics [8], which are described in App. B.2 and App. B.3. The excluded volume interaction and the self avoiding walk condition for polymer clusters restrict the possibility of monomer movements: to satisfy these two requirements the bond lengths vary into a set of permitted values according to bond-fluctuation dynamics [8]. On a cubic lattice the allowed bond lengths are $l = 2, \sqrt{5}, \sqrt{6}, 3, \sqrt{10}$. At each Monte Carlo step the time is increased by $\delta t = 1$ and one random movement is selected on average for each chain: the move is executed only if it satisfies the the bond-fluctuation dynamics rules and excluded volume conditions.

After chains have diffused and reached equilibrium, we add the reactant to the system and let the solution diffuse towards the stationary state. Chains and reactants diffuse via random local movements. At each Monte Carlo step the time one random move is selected on average for each monomer: if the move satisfies the bond-fluctuation dynamics and excluded volume conditions, it is executed, otherwise it is rejected. These simple laws for local movements [8] give rise to a dynamics which takes into account the main features of the real dynamics of polymer molecules. Due to the diffusion of cross-linkers and chains, when a reactant finds a nearest neighbor unsaturated active site, a bond may form. The process goes on until all the possible bonds are formed.

The bond formation may request to overcome a free energy barrier, depending on the nature of the solution, the active sites and the reactant. In particular, it may depend on some specific local orientation of the molecules, some restriction on the value of the angle between two bonds, due to the rigidity of the $C-N$ link, or else may be affected by variations of the effective reactivity of the cross-linker. In our model we take into account these effects in the following way: the first bond of a reactant monomer is formed along lattice directions as soon as there is a neighboring active site. The second bond is formed with probability $p_b \leq 1$, since a reactant monomer is expected to have less chance to react when is already bonded to a chain, compared to when it is free. In the same spirit of reaction limited aggregation models [41], p_b is an independent parameter which influences the time of formation of bridges between gelatin active sites. The value of p_b should be determined by the features of cross-linking reagent. Moreover, although varying the bridge probability p_b does not affect the gelation transition, it has a crucial effect on the velocity of the reaction, which can be easily enlightened in the numerical simulation as discussed later.

We perform numerical simulations of the model for different lattice sizes ($L = 50, 100, 200$), where the unit length is the lattice spacing $a = 1$, with periodic boundary conditions. The chain concentration C and the cross-linker concentration C_r are defined as the ratio between the number of monomers/reactant

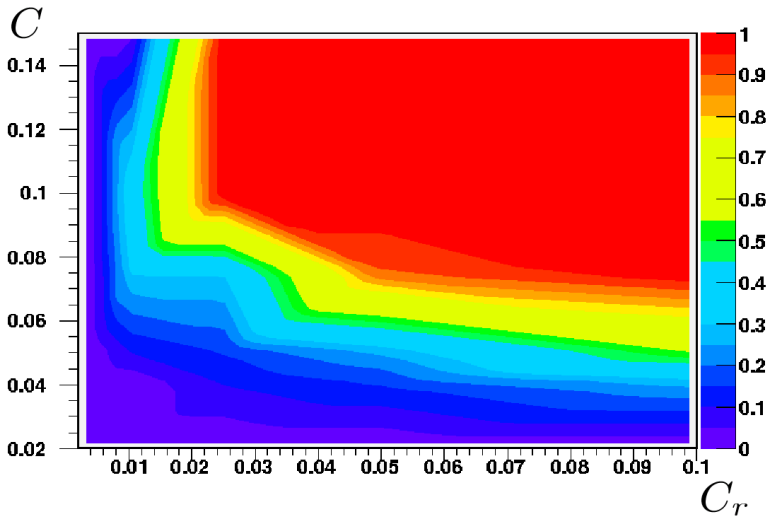

Figure 4.2: The phase diagram, obtained plotting the percolation probability Π as a function of chain and reactant concentration C and C_r respectively, using a color scale. The spanning probability has been averaged over 30 independent initial configurations of a sample of size $L = 100$. The number of active sites per chain $n_{as} = 5$ is kept constant and $p_b = 1$. The red region corresponds to $\Pi = 1$, the purple ones to $\Pi = 0$. The percolation line can be identified with the locus $\Pi = 0.5$ which corresponds to the green region.

and the maximum number of monomers $N_{max} = L^3/8$ in the system. Using the percolation approach we identify the gel phase as the state in which there is a percolating cluster, which spans the whole system [16, 17]. For a fixed set of parameters we generate a number of configurations of the system and monitor the reaction. In order to locate the gelation transition we analyze the percolation probability Π, defined as the fraction of configurations leading to a percolating cluster, and we identify the transition with the line $\Pi = 0.5$ [18]. We determine a qualitative phase diagram, shown in Fig. 4.2, by varying the chain and cross-linker concentrations, C and C_r respectively, for a fixed $n_{as} = 5$.

In experiments the total amount of reactant has been consumed at the end of the reaction process, i.e. the amount of reactant is much lower than the amount of active sites. The reaction stops when all the reactant is linked to amine groups and the system is in the gel phase. Moreover the experimental system [7] is investigated at gelatin concentrations C_{gel} above the overlap concentration $C^*_{gel} = 0.005\ g/cm^{-3}$, defined as the concentration for which polymer coils touch each other. In order to reproduce the experimental conditions the cross-linker concentration has been fixed at $C = 0.025$, which corresponds to $C_r \ll C$ at the sol-gel transition. Under this condition, in simulations the gel phase is located at concentrations C above the overlap concentration which in our system is $C^* \simeq 0.017$. This choice of parameters guarantees that at the end of the reaction the

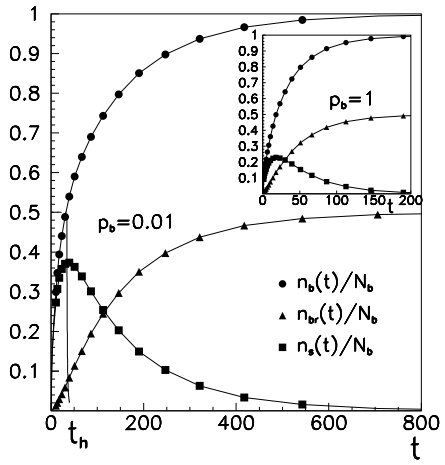

Figure 4.3: Total number of bonds, number of bridges and number of single-bonds normalized by the total number of possible bonds N_b as a function of time for $C = 0.3$, $C_r = 0.025$, $n_{sa} = 5$ and $p_b = 0.01$. Inset: The same quantities for $p_b = 1$. t_h indicates the time corresponding to half of the reaction.

system is in the gel phase.

With finite size scaling analysis we obtain the percolation threshold, that for the case $C_r = 0.025$ is $C_c = 0.10 \pm 0.05$, the critical exponents $\nu = 0.9 \pm 0.1$ for the percolation connectedness length ξ ($\propto |C - C_c|^{-\nu}$) and $\gamma = 1.78 \pm 0.10$ for the mean cluster size χ ($\propto |C - C_c|^{-\gamma}$). These results are in good agreement with the random percolation critical exponents [18]. The random percolating cluster is characterized by a fractal structure: its mass M, i.e. the number of monomers, scales with its linear dimension ξ with a power law behavior ξ^D, where $D \simeq 2.5$ [18]. The structure of the formed network may depend on model parameters and may influence the rheological response of the system.

4.2 Kinetics of bond formation

In simulations we investigate the behavior of the number of bonds formed during the reaction process and we distinguish between:
1. Bonds between a free reactant and an active site (we will refer to the latter type of bond as *single-bonds*);
2. Bonds between a linked reactant and an active site of another chain;
3. Bonds between a reactant and two active sites of the same chain (which in the following we will call *loops*).
We analyze the kinetics of bond formation for a system of size $L = 100$, with $C_r = 0.025$ and $n_{as} = 5$ varying the chain concentration C and the probability

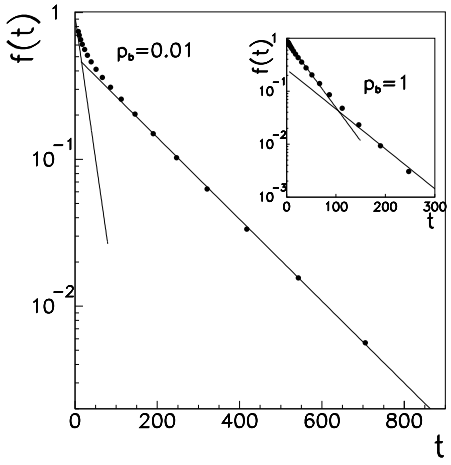

Figure 4.4: Function $f(t) = 1 - n_b(t)/N_b$ as a function of time, where N_b is the total number of possible bonds, for $C = 0.3$, $C_r = 0.025$, $n_{as} = 5$ and $p_b = 0.01$. The full lines are the fitting curves $\sim \exp(-t/\tau_1)$ with $\tau_1 = 20$, and $\sim \exp(-t/\tau_2)$ with $\tau_2 = 166$. Inset: $f(t)$ with $p_b = 1$. The full lines are the fitting curves $\sim \exp(-t/\tau_1)$ with $\tau_1 = 34.4$ and $\sim \exp(-t/\tau_2)$ with $\tau_2 = 57.8$.

p_b of bridge formation. The time is measured in Monte Carlo unit time δt.

Since $C_r \ll C$, the total number of bonds at the end of reaction is equal to twice the number of cross-linkers: $N_b = 2C_rL^3/8$. In Fig. 4.3 the total number of bonds $n_b(t)$ is plotted as a function of the time together with the number of single-bonds $n_s(t)$ (bonds of type 1) and bridges $n_{br}(t)$ (i.e. bonds of type 2 or 3) in the case $p_b = 0.01$. The number of bonds has been normalized by N_b. As the reaction begins, single-bonds form rapidly, then bridges start to form and the degree of connectivity between chains increases. The behavior of the total number of bonds versus time closely resembles the released heat experimentally measured during the reaction reported in Fig. 3.5. The velocity of the reaction is related to the probability p_b of bridge formation. It governs the mean time of bond formation between different chains and strongly influences the duration of the reaction process. In the inset of Fig. 4.3 $n_b(t)$, $n_s(t)$ and $n_{br}(t)$ are plotted as a function of the time for $p_b = 1$, showing that both single-bonds and bridges form more rapidly as compared to the $p_b = 0.01$ case.

The total number of bonds $n_b(t) = n_s(t)+2n_{br}(t)$, and its time dependence can be written as $n_b(t) = N_b(1 - f(t))$. In Fig. 4.4, the function $f(t) = 1 - n_b(t)/N_b$, representing the fraction of bonds that remain to form, is plotted in a semi-logarithmic plot for the case $p_b = 0.01$. The data reproduce extremely well the behavior observed experimentally (Fig. 3.6) and are well fitted by a sum of two exponentials

$$f(t) = a_1 \cdot e^{(-t/\tau_1)} + a_2 \cdot e^{(-t/\tau_2)} \tag{4.1}$$

Table 4.1: Values of τ_1 and τ_s obtained from direct measure for different values of p_b in systems with $C = 0.3$, $C_r = 0.025$. In the last column we report the ratio τ_2/τ_1 obtained by the fit of the function $f(t)$ with Eq.(4.1).

p_b	τ_1	τ_2	τ_2/τ_1	τ_2/τ_1 (fit)
0.002	19.0 ± 0.1	658 ± 3	34.6 ± 0.3	20.8 ± 0.9
0.003	19.0 ± 0.1	459 ± 2	24.2 ± 0.2	18 ± 1
0.005	19.0 ± 0.1	299.5 ± 1.2	15.8 ± 0.1	10.7 ± 0.8
0.01	19.0 ± 0.1	175.6 ± 0.7	9.24 ± 0.06	6.6 ± 0.8
0.02	19.0 ± 0.1	110.6 ± 0.5	5.82 ± 0.04	5.2 ± 0.6
0.03	19.0 ± 0.1	87.8 ± 0.4	4.62 ± 0.03	$4.3 \pm 0.6\pm$
0.05	19.0 ± 0.1	68.9 ± 0.3	3.63 ± 0.02	3.2 ± 0.7
0.08	19.1 ± 0.1	58.0 ± 0.3	3.04 ± 0.02	2.5 ± 0.9
0.1	19.2 ± 0.1	54.2 ± 0.2	2.89 ± 0.02	3.2 ± 1.2
0.2	19.0 ± 0.1	47.1 ± 0.2	2.48 ± 0.02	2.4 ± 0.2
0.3	19.3 ± 0.1	45.1 ± 0.2	2.34 ± 0.02	1.7 ± 0.2
0.5	19.0 ± 0.1	43.3 ± 0.2	2.28 ± 0.2	1.6 ± 0.1
0.8	19.0 ± 0.1	43.6 ± 0.2	2.29 ± 0.2	1.6 ± 0.1
0.9	19.2 ± 0.1	43.8 ± 0.2	2.28 ± 0.02	1.6 ± 0.1

in agreement with the microcalorimetry measurements (Eq. 3.1). From the fit we obtain $\tau_1 = 20 \pm 2$ and $\tau_2 = 166 \pm 5$, for $p_b = 0.01$ and $C = 0.3$, providing $\tau_2/\tau_1 = 8.3 \pm 0.9$.

If the bridge probability p_b varies, the mean time of bridge formation τ_2 changes, and so does the ratio τ_2/τ_1. In the inset of Fig. 4.4 $f(t)$ is plotted for $p_b = 1$. From the fit we obtain $\tau_1 = 34.4 \pm 1.5$, $\tau_2 = 57.8 \pm 1.5$, and hence $\tau_2/\tau_1 = 1.68 \pm 0.08$.

In order to give a microscopic interpretation for these two characteristic times, we directly compute the average time of formation of single bonds and bridges respectively, which cannot be done by microcalorimetry measurements. These two times are in agreement with the fitting parameters τ_1 and τ_2 within error bars. In Tab. 4.1 we report the measured values of τ_1 and τ_2, their ratio and the ratio of the values obtained from the fit with Eq. 4.1.

Next, we analyze the mean square displacement of the reactant monomers when they are free (1) and when they have formed one single bond (2). In Fig. 4.5 we plot the mean square displacements of free reactant and reactant which have formed one single bond for a solution with $C = 0.3$ and $p_b = 0.01$. We note that for $t \simeq 100$ all the reactant monomers have formed one single bond, in fact no free reactants are present in the system. For reactants which have formed one single bond, the mean square displacement increases linearly in time

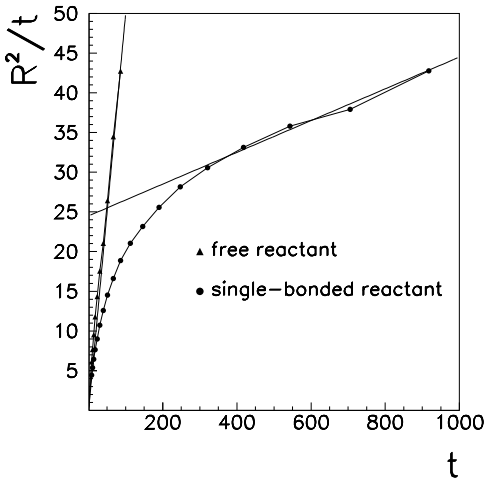

Figure 4.5: Mean square displacement of free reactant monomers (triangles) and reactant which have formed one single-bond (circles) for a system with $C = 0.3$, $C_r = 0.025$, $p_b = 0.01$ and $n_{as} = 5$. The full line are the fitting curves $R^2 \propto D_{1(2)}t$.

only after all the possible bonds have formed ($t \geq 500$ for data plotted in Fig. 4.5). Indeed, bond formation influences the mobility of single-bonded reactant: as bridges between chains form, the mash size of the forming network decreases, hindering chain diffusion so reducing the diffusion coefficient of single-bonded reactant, which are forced to move together with the chain to which it is linked. We have extrapolated the diffusion coefficient D_1 and D_2, obtaining $D_1/D_2 \simeq 10$, which is consistent with the ratio τ_2/τ_1 (see Tab. 4.1). Interestingly we observe that the ratio between the corresponding diffusion coefficients D_1/D_2 is of the order of the ratio τ_2/τ_1 for all the analyzed concentrations of chains and cross-linkers. This result suggests that τ_1 and τ_2 are related to the characteristic times for diffusion of the free reactant and of the reactant linked to a gelatin chain, respectively.

In agreement with this microscopic interpretation, our data (Fig. 4.3 and Fig. 4.4) show that, for the concentrations C and C_r explored, single-bonds form more rapidly than bridges. This different velocity of formation is due, apart from p_b, to the different mobility of free cross-linkers with respect to linked ones, which are forced to move together with the chains to which they are permanently bonded. As a consequence $\tau_1 \leq \tau_2$, i.e. the average time of formation of a single-bond, is generally smaller than the average time of formation of bridges even for $p_b = 1$.

4.3 Time scales and solution parameters

It is interesting to notice that in simulations we can easily vary the bridge probability p_b, to see how the features of the cross-linking reagent could possibly affect the kinetics of the bond formation. Remarkably, we find that this effect can be crucial. Indeed, as p_b governs the bridges formation, it influences the average time

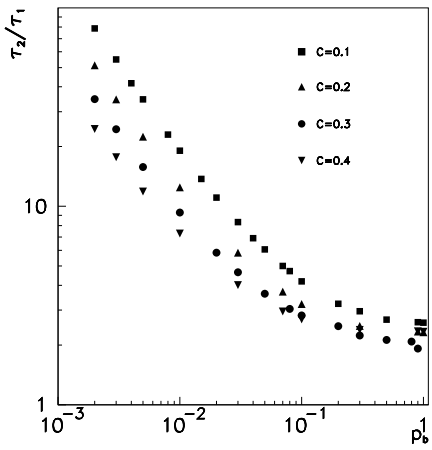

Figure 4.6: The ratio τ_2/τ_1 between the average time of formation of bridges and the average time of formation of single-bonds as a function of bridge probability p_b for different concentrations C of chains, for $C_r = 0.025$ and $n_{as} = 5$.

τ_2: as p_b decreases, the reaction slows down and τ_2 increases. We systematically analyze the behavior of τ_2/τ_1, as a function of bridge probability p_b. In Fig. 4.6 we plot the obtained data: when the bridge probability p_b increases, the average time of bridge formation decreases, and so does the ratio τ_2/τ_1. For $p_b \geq 0.3$ we find that the ratio decreases more slowly apparently tending to a plateau. In this regime, the bridge probability p_b does not influence the kinetics of bond formation, which is completely governed by the diffusion of the monomers and by their concentration. The value of the ratio between the two characteristic times obtained in the experiments at $pH = 6.7$ (see Fig. 3.6) corresponds to a reactant with $0.005 \leq p_b \leq 0.01$ in our simulations.

The experimental findings show that the solution pH also affects the kinetics of bond formation, i.e. the ratio τ_2^m/τ_1^m decreases as the pH decreases. This is in agreement with the chemistry of reaction, where the non protoned form of the amine is reactive. In fact, one could expect different regimes depending on the chain concentration. Indeed, if a decrease of the number of active sites will in general correspond to an increase of τ_1, the effect of this variation on τ_2 is likely to strongly depend on chain concentration. At high concentration of chains, if the number of active sites per chain decreases below a certain level, we expect that these will be surrounded by many other sites of the same chain which are not active. As a consequence, due to excluded volume effects, they will hardly be reached by partially linked cross-linkers, i.e. τ_2 will increase as the number of active sites decreases and so will the ratio τ_2/τ_1. On the other hand, τ_2 strongly depends on the chain mobility and on the formation of loops. Therefore, decreasing the pH at low concentrations leads to an increase of τ_1 that may be

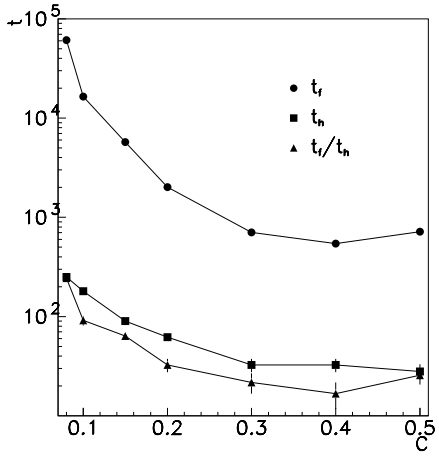

Figure 4.7: The time of reaction end t_f (dots), time of half reaction t_h (squares) and their ratio (triangles) as a function of chain concentration C for $C_r = 0.0025$, $n_{as} = 5$ and $p_b = 0.01$.

balanced by a not so dramatic increase of τ_2, due to the eventual formation of loops. As a consequence one can observe a net decrease of the ratio τ_2/τ_1. We would like to stress that, although the investigation of the role of pH could be in principle done with this model by varying n_{as}, one should use long enough chains to be able to detect the different concentration regimes.
Conversely, when the number active sites increases up to $n_{as} = 10$, in the analyzed concentration range the average time τ_1 does not change appreciably, while τ_2 decreases due to the formation of loops. For bridge probability p_b sufficiently high ($p_b \geq 0.8$), the mean time of bridge formation becomes less than or equal to the mean time of formation of single-bonds: in these cases, the number of bonds $n_b(t)$ may be fitted by a single exponential with the characteristic time τ_1.

To complete our study of the kinetics of bond formation, we measure the time t_h of formation of half of the total bonds, and the duration of the reaction t_f, i.e. the average time needed to form all possible bonds. The data are presented in Fig. 4.7 and show that the ratio t_f/t_h decreases as the concentration increases, tending to a plateau value for $C \geq 0.3$. This behavior is in agreement with the experimental findings: for $C_{BVSM} = 0.3\%\ g/cm^3$ and C_{gel} ranging from 3% to 6%, the ratio t_f/t_h decreases from $t_f/t_h \sim 27$ to $t_f/t_h \sim 15$. For $C_{gel} \geq 6\%$ the ratio remains constant with the concentration. Comparing the experimental results with simulations, we conclude that the regime of concentration $C \sim 0.3$ for the lattice model corresponds to $C_{gel} \sim 6\%$ of the experiments [7]. This correspondence is coherent with the behavior shown in Fig. 4.3, Fig. 4.4, Fig. 4.6 and support the suggested interpretation. It is worth to notice that $t_f/t_h \gg 1$ for the explored range of parameters: this is a consequence of the fact that in the

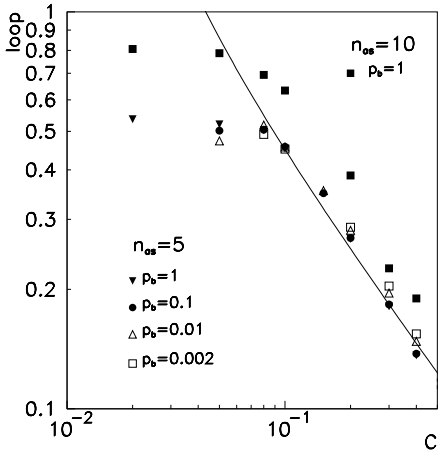

Figure 4.8: Number of loops normalized by the maximum number of bridges $N_b/2$, as a function of gelatin concentration C for $p_b = 0.002, 0.01, 0.1, 1$ for $n_{as} = 5$ and for $p_b = 1$ with $n_{as} = 10$, for $C_r = 0.025$. The full line is the power law fitting curve $\sim C^{-l}$ with $l = 0.75$.

first half of the reaction most of formed bonds are single-bonds. In the second half, bridges between active sites are established, requiring a longer time to form.

4.4 "Loop" formation

We analyze the number of loops which are formed during the cross-linking reaction and which may play a crucial role in the mechanical response of the gel. Loops are not detectable in experimental measurements, but can be easily monitored in simulations. Previous numerical simulations of polymerization process in hexamethylene diisocynate-based polyurethane [85] indicate that the number of loops plays different roles in the various concentration regimes. Indeed the loss of elasticity due to loops may be outweighed by the increase of topological entanglements, depending on the concentration.

At the end of the reaction we count the number of loops, normalized by the maximum number of bridges $N_b/2$, and investigated its behavior as a function of C. Data plotted in Fig. 4.8 refer to chain with $n_{as} = 5$ and $n_{as} = 10$. Our results indicate that the number of loops decreases as the chain density C increases. In the range of concentration explored the number of loops decreases following a power law behavior $\sim C^{-l}$ characterized by an exponent $l = 0.75 \pm 0.05$. The behavior appears to be independent of the bridge probability p_b: this result confirms that the bridge probability only influences the kinetics of bond formation but does not strongly affect the morphology of the system. By opportunely tuning

p_b, i.e. changing the reactant, the velocity of the reaction may be adjusted and the formation of single-bonds and bridges may be tuned in time, but the final geometrical properties of the structure should not be modified. On the other hand, the connectedness of the system may be influenced by the number of active sites per chain n_{as}. In particular, when n_{as} increases, the number of loops formed in the system increases and hence the degree of connectedness of the system decreases (Fig. 4.8). Moreover, in the limit of very diluted solutions of chains where all sites are active ($n_{as} = 10$), loops represent about 80% of the total number of bonds and, as a consequence, the viscoelastic properties can be sensibly modified [85].

4.5 Conclusion

In conclusion, experimental results show that two different timescales affect the kinetics of bond formation in our cross-linked gelatin solution. The numerical data reproduce well the experimental ones and clarify the mechanisms involved in bond formation. Our study shows that the two time scales detected in experiments correspond to the average time of forming single bonds reactant-chain and bridges chain-chain via cross-linker. These two times are related to the characteristic times of diffusion of free reactants and reactants which have already formed one bond. Their ratio controls the kinetics of the bond formation. Concentration variations, the cross-linker reactivity and the pH strongly affect this ratio and therefore the kinetics of the gelation process. Our findings also show that the probability p_b to form a bridge between two active sites allows to finely tune the kinetics of the reaction via the ratio of the two characteristic times. A variation of p_b in our interpretation corresponds to a variation of the free energy barrier to be overcome in order to form the bond, or to different orientations of bonds vectors. Hence to vary p_b corresponds to change the reactant agent in the gelatin solution. Moreover, our data indicate that the number of loops formed between two active sites of the same chain, which has an important effect of the viscoelastic properties of the system, increases when the pH of the solution increases. This model represents a useful tool to investigate rheological behavior of gelatin solutions and the relation between the kinetics of gel formation and gel structures.

In conclusion, in this chapter we have investigated a gelation process. Also degradation phenomena are relevant in polymer physics, hence in the next chapter we analyze an interesting degradation process.

Chapter 5

A degradation process

In the previous chapter we have introduced a lattice model to describe the kinetics of bond formation in a gelation process. Now we analyze the degradation process described in Sect. 3.3 and introduce a lattice model to study the solubilization of extracellular matrix (ECM), a biological gel made essentially of collagen, due to the action of enzymes. Enzymes diffuse in solution and catalyze the hydrolysis of bonds between monomers constituting the extracellular matrix. The gel is schematized as a cubic lattice, and the enzyme as a random walker, that cuts the bonds over which it passes. The model undergoes a (reverse) percolation transition, which for low density of enzymes falls in a universality class different from the random percolation one.

In Sect. 5.1 we introduce and describe our model, investigating its properties within the percolation approach. In Sect. 5.2 the presence of long range correlation between bonds is investigated. The critical behavior of mechanical properties is studied in Sect. 5.3. In Sect. 5.4 the case of uniform density of enzymes is discussed, and final remarks are presented in Sect. 5.5.

5.1 A lattice model

In Sect. 3.3 we have described recent experiments performed on extracellular matrix degraded by enzymes present in solution. Unexpected results have been obtained [10], which indicate that the system does not belong to the random percolation universality class. Hence further investigations are required in order to deeper comprehend the mechanisms involved in the degradation process. We introduce a very simple model, which we call "pacman percolation model" [86], in which the protein gel is schematized as a cubic lattice of $N = L^3$ sites, where each site represents an (hexavalent) monomer. At time $t = 0$ all the bonds between nearest neighbor monomers are present. One or more enzymes are then introduced in the system in random initial positions. At each step, every enzyme moves from one site to a nearest neighbor site, chosen randomly between the

	pacman percolation	experiment	random percolation
p_c	0.139 ± 0.001		0.2488
ν	1.8 ± 0.1		0.88
β	1.0 ± 0.1	1.0 ± 0.1	0.41
γ	3.4 ± 0.2		1.80
t	3.5 ± 0.1		2.0
s	1.1 ± 0.1		0.73
τ	2.3 ± 0.1		2.2
D	2.4 ± 0.1		2.5

Table 5.1: Percolation density and critical exponents in the pacman percolation model and in random percolation in three dimensions.

six nearest neighbors, and hydrolyzes (deletes) the corresponding bond if not yet hydrolyzed [1]. Periodic boundary conditions are chosen. In Fig. 5.1a it is shown the two-dimensional version of the model, with only one enzyme in the system, after the enzyme has walked around for some time. It is evident how the remaining non-hydrolyzed bonds are spatially correlated, with respect to a random percolation model (Fig. 5.1b). At each time step, there will be a distribution of clusters, where two sites belong to the same cluster if there is a path of non-hydrolyzed bond between them. We measure as a function of the bond density p: a boolean variable equal to one if there is a percolating cluster, to zero otherwise; the size of the percolating cluster, if any; the mean cluster size, that is $\frac{1}{N}\sum_s n_s s^2$, where n_s is the number of clusters of size s per site, and the percolating cluster is excluded from the sum. We perform the simulation many times, with different initial positions of the enzymes and random number sequences, and average over all the runs the above mentioned quantities. In this way, we obtain the percolating probability $\Pi(p, L)$, the percolating cluster density $\rho(p, L)$ and the mean cluster size $\chi(p, L)$ as a function of the bond density p and of the size L of the lattice. From these quantities, it is possible to evaluate the percolation density p_c and the critical exponents ν, β and γ [18]. Plotting the percolating probability $\Pi(p, L)$ as a function of p for different lattice sizes L, it is possible to measure the percolation threshold density p_c as the point in which the different curves intersect, for $L \to \infty$. Plotting then $\Pi(p, L)$ as a function of $(p - p_c)L^{1/\nu}$, one can measure the correlation length exponent ν as the value that gives the best collapse of the curves. The error on the exponent can be defined by looking for the largest interval of ν, such that the curves collapse within the error bars. In the same way, plotting $\rho(p, L)L^{\beta/\nu}$ and $\chi(p, L)L^{-\gamma/\nu}$

[1] A complementary model, in which bonds are created rather than deleted by random walkers, has been studied in Ref. [87].

a)

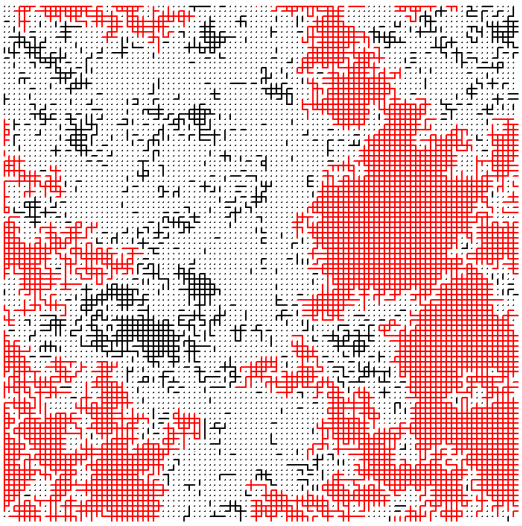

b)

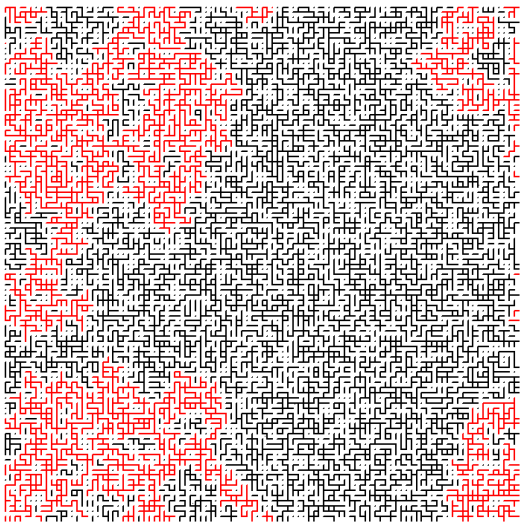

Figure 5.1: a) Pacman percolation model on a square lattice of size $L = 64$, with a single enzyme and after 12000 steps, when the density of non-hydrolyzed bonds is $p = 0.42$. b) The random percolation model with the same bond density. The percolating cluster is the red one.

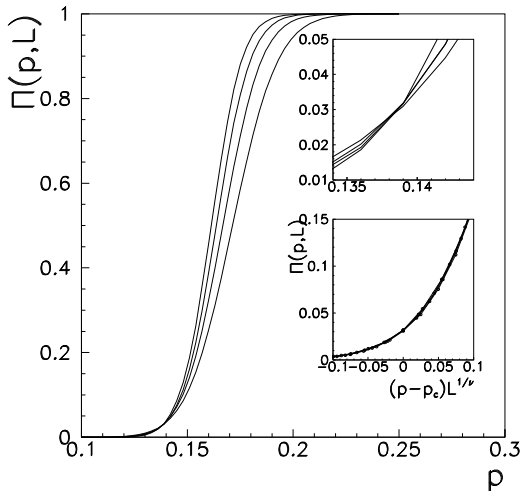

Figure 5.2: Percolation probability $\Pi(p, L)$ as a function of the bond density p, with a single enzyme and for cubic lattices of size $L = 30$, 40, 50, 60. Upper inset: the point of intersection of the curves. Lower inset: data collapse obtained plotting $\Pi(p, L)$ versus $(p - p_c)L^{1/\nu}$, with $\nu = 1.8$ and $p_c = 0.139$.

as a function of $(p - p_c)L^{1/\nu}$, one can measure the exponents β and γ. We first study the "single enzyme" version of the model on the cubic lattice. In Fig. 5.2, Fig. 5.3 and Fig. 5.4 we show the results for lattices of size $L = 30, 40, 50, 60$. We find $p_c = 0.139 \pm 0.001$, $\nu = 1.8 \pm 0.1$, $\beta = 1.0 \pm 0.1$ and $\gamma = 3.5 \pm 0.2$. The obtained value of the critical exponent β, controlling the behavior of the percolating cluster density, is in excellent agreement with the experimental results described in Sect. 3.3 [10], according to which $\beta = 1.0 \pm 0.1$. In Tab. 5.1 the found critical exponents are compared with those of random percolation. These results show that the single enzyme version of the pacman percolation model falls in another universality class with respect to random percolation, which we call "pacman percolation universality class".

To completely characterize the structural properties of our model, we measure the Fisher exponent τ which governs the power law decay of the cluster size distribution n_s at the percolation threshold: $n_s \sim s^{-\tau}$ for $p = p_c$. In Fig. 5.5 we plot the data for a lattice of size $L = 100$, obtaining $\tau = 2.3 \pm 0.1$. This value is consistent with the $3d$ random percolation $\tau \simeq 2.2$. Furthermore, using the scaling relation $D = d - \beta/\nu$, we obtain from our data $D = 2.4 \pm 0.1$, which is consistent within the error bars with the random percolation fractal dimension $D \simeq 2.5$ [18]. Actually, both τ and the fractal dimension D only depend on the ratio β/ν and γ/ν, as $\tau = d/(d - \beta/\nu) + 1$. In Ref. [88] it has been argued that systems belonging to different universality classes, may indeed belong to the same "weak" universality class, in the sense that the ratio β/ν and γ/ν are

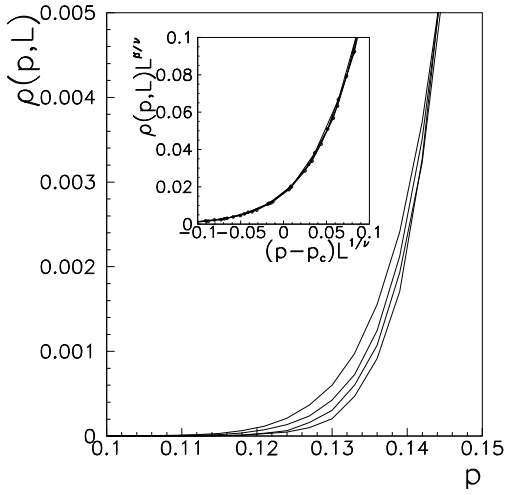

Figure 5.3: Density $\rho(p, L)$ of the percolating cluster as a function of the bond density p, with a single enzyme and for the same lattice sizes of Fig. 5.2. Inset: data collapse obtained plotting $\rho(p, L)L^{\beta/\nu}$ versus $(p - p_c)L^{1/\nu}$, with $\nu = 1.8$ and $\beta = 1.0$ and $p_c = 0.139$.

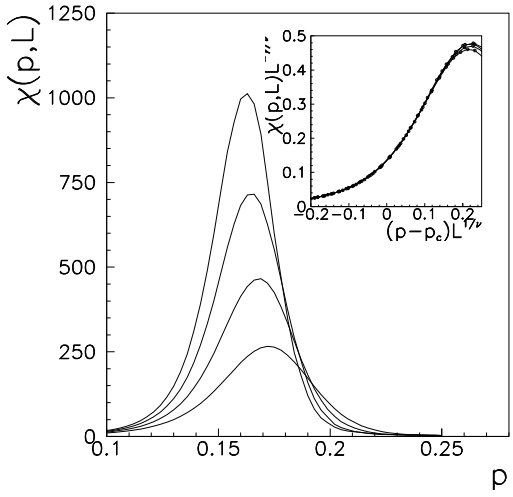

Figure 5.4: Mean cluster size $\chi(p, L)$ as a function of the bond density p, with a single enzyme and for the same lattice sizes of Fig. 5.2. Inset: data collapse obtained plotting $\chi(p, L)L^{-\gamma/\nu}$ versus $(p - p_c)L^{1/\nu}$, with $\nu = 1.8$, $\beta = 3.4$ and $p_c = 0.139$.

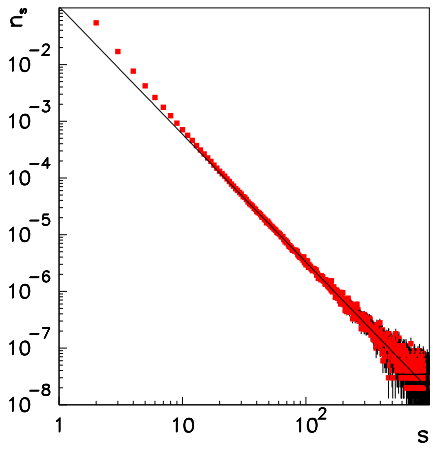

Figure 5.5: Cluster size distribution as a function of cluster size for a system with a single enzyme on a cubic lattice of size $L = 100$, near the percolation threshold $p \simeq 0.14$. The full line is the fitting curve with $\tau = 2.3$.

conserved. As a consequence, if the scaling and hyper-scaling relations between critical exponents hold [18], all the critical exponents which depend on the ratio β/ν and γ/ν (such as $\tau = d/(d - \beta/\nu) + 1$ and $D = d - \beta/\nu$) are equal for systems in the same weak universality class. Accordingly, our model belongs to the random percolation universality class only in the weak sense.

5.2 Long range correlations

In order to explain the change in the universality class with respect to random percolation, we investigate the presence of a long range correlation in the distribution of non-hydrolyzed bonds. The correlation function is defined as $G(|\mathbf{r}|) = \langle \rho(\mathbf{r}')\rho(\mathbf{r}' + \mathbf{r}) \rangle - \langle \rho(\mathbf{r}') \rangle^2$, where $\rho(\mathbf{r})$ is the density of bonds, and the average $\langle \ldots \rangle$ is done over the reference position $\mathbf{r}'$. It was shown by Weinrib and Halperin [89] that if the correlation obeys a power law $G(r) \simeq r^{-a}$ at long distances with $a < d$ (where d is the Euclidean dimension of the system), then the percolation transition falls in a universality class different from the random percolation, in particular with a correlation length exponent $\nu = 2/a$.

We have also verified the relation predicted by Weinrib and Halperin [89] between the exponent ν and the power law governing the decay of correlations, in the single enzyme model. We compute the correlation in the occupation of the bonds i and j $G(|i - j|) = \langle n_i n_j \rangle - \langle n_i \rangle \langle n_j \rangle$, where $|i - j|$ is the distance between the centers of the bonds, and n_i is an occupation variable, equal to 1 if the bond is present, 0 otherwise. In Fig. 5.6 $G(|i-j|)$ is shown for a system of size

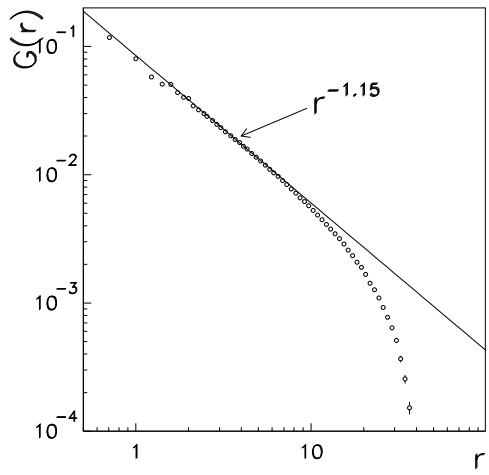

Figure 5.6: Spatial correlation $G(r)$ in the occupation of the bonds, with a single enzyme on a cubic lattice of size $L = 100$, near the percolation threshold $p \simeq 0.14$.

$L = 100$ at the percolation threshold $p = 0.139$. We note that results are averaged over many starting points of the enzyme, so that the system is translationally invariant. The correlations obeys a power law $G(r) \sim r^{-a}$ with $a = 1.15 \pm 0.05$, with an exponential cut-off, presumably due to finite size effects, at distances larger than $r \simeq 30$. The relation $\nu = 2/a$ predicted by Weinrib and Halperin, is quite well verified within the errors. It has been recently argued [11] that for such a model the correlations between bonds should decay as $1/r$, implying $a = 1$ and $\nu = 2$. The prediction, however, is valid only if some conditions are verified, such as long times and large distances. The discrepancy between this prediction and our results may be due to the fact that these asymptotic regimes are not reached in our simulations.

5.3 Viscoelastic response

Our model describes the degradation process due to the action of enzymes within the percolation approach. The percolation theory is a purely static model, which focuses on geometrical properties of structures. Hence, to study the mechanical response of the system with our percolation model, we have to use an analogy between static properties and the dynamical ones under investigation. In particular, we use the analogy proposed by de Gennes between an elastic network and a resistor network, and a viscous fluid and a super-conducting network, described in Sect. 2.2. We analyze the critical exponent t and s of the conductivity in the random resistor and conductor-superconductor networks, that should be in correspondence respectively with the exponents f of the elastic modulus, and

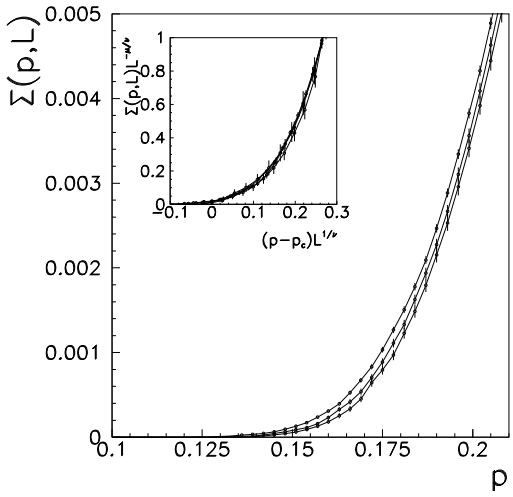

Figure 5.7: Conductivity $\Sigma(p, L)$ of the random-resistor network as a function of the bond density p, with a single enzyme and for the same lattice sizes of Fig. 5.2. Inset: data collapse obtained plotting $\Sigma(p, L)L^{t/\nu}$ versus $(p - p_c)L^{1/\nu}$, with $t = 3.5$, $\nu = 1.8$ and $p_c = 0.139$.

k of the viscosity [12, 13]. In the first case, each present bond of the model is substituted with a resistor of unitary conductance, while absent bonds have zero conductance. The total conductivity Σ of the model is then measured as a function of bond density, and it is zero for $p < p_c$, while it grows as $(p - p_c)^t$ for $p > p_c$. Using finite size scaling as usual we find $t = 3.5 \pm 0.1$; data are plotted in Fig. 5.7. In the second case each present bond of the model is substituted with a superconductor, which has infinite conductance, while absent bonds are substituted with resistors of unitary conductance. In this case the total conductivity Σ diverges as $(p - p_c)^s$ for $p < p_c$, and stays infinite for $p > p_c$. In this case we find $s = 1.1 \pm 0.1$ (see Fig. 5.8). Our results about the viscoelastic response stimulated further measurements on the real sample investigated in Ref. [10, 11]: preliminary results on the critical exponent of the elastic modulus give $f \simeq 3.5$, in good agreement with our prediction.

5.4 Constant density of enzymes

To complete our study of the degradation process due to the action of enzymes, we study the model with a uniform density ρ_E of enzymes. $N_E = \rho_E L^3$ enzymes are distributed in random positions on the lattice, and at each step every enzyme makes one random move. Critical exponents are extracted as described before, performing finite size scaling analysis [18]. We find that, as long as the concentration is $\rho_E \leq 0.5$, the effective critical exponents measured are the same of the

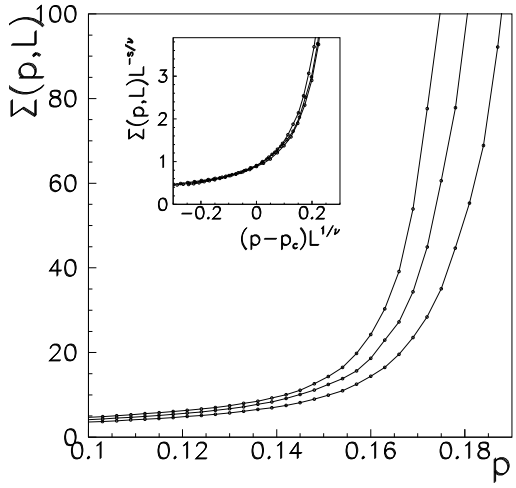

Figure 5.8: Conductivity $\Sigma(p, L)$ of the conductor-superconductor network as a function of the bond density p, with a single enzyme and for the same lattice sizes of Fig. 5.2. Inset: data collapse obtained plotting $\Sigma(p, L)L^{-s/\nu}$ versus $(p-p_c)L^{1/\nu}$, with $s = 1.1$, $\nu = 1.8$ and $p_c = 0.139$.

single enzyme model, that is those of the pacman percolation universality class. For $\rho_E \geq 0.7$ instead we measure exponents in agreement with random percolation. This is expected because, for very high density of enzymes, each bond is cut by a different enzyme, so that there are no correlations between bonds. For intermediate values of ρ_E, intermediate values of the critical exponents are obtained.

From a renormalization point of view, one may expect that the pacman percolation universality class should be relevant only for a density of enzymes vanishing in the thermodynamic limit, such as for the single enzyme model, while for any finite density of enzymes the model should fall in the random percolation universality class. On the other hand, our results indicate that a slow crossover exists, such that for finite but low density of enzymes effective critical exponents are measured in the pacman percolation universality class. This may be true also for the experimental observations.

To compare our numerical results with experiments, one has to express the density of enzymes in the same manner. This can be done expressing the experimental density as $(d_B/d_E)^3$, where d_E is the mean distance between enzymes, and d_B is the mean distance between the cross-links of the network. The latter can be evaluated by $d_B \simeq (k_B T/G)^{1/3}$, where G is the elastic modulus of the gel (before enzyme degradation), and T is the temperature. In experiments of Ref. [10], $G \simeq 40$ Pa and $T \simeq 300$ K, so that $d_B \simeq 40$ nm, whereas d_E is between 70 and 400 nm. The experimental concentration corresponds therefore to an enzyme density between 0.001 and 0.2, in the density region where the effective

critical exponents measured in the simulations are those of the pacman percolation universality class. This confirms the agreement of the value of the exponent β measured in simulations and in experiments.

5.5 Conclusion

In conclusion, we have used a percolation model to study the degradation process of ECM due to the action of enzymes. Our results show that, for low density of enzymes, our model belongs to a different universality class from random percolation. The change in the critical exponents may be due to long range correlations. If the density of enzymes is sufficiently high, the correlation between bonds disappears and there is a crossover to random percolation. Our results about the elastic response of the system stimulated further experimental measurements. Preliminary results are in good agreement with our predictions.

This model, as well as the one presented in Chap. 4, has been introduced to investigate and comprehend the mechanisms involved into specific processes regarding a particular real system. It reveals to be a powerful tool to investigate degradation processes due to the action of enzymes. Nevertheless, it remains strictly related to the particular system investigated in experiments. In order to study the gelation transition from a more general point of view, in the next chapter we introduce a general model for irreversible gels.

Chapter 6

A model for irreversible gelation

In the previous chapters we have described two lattice models (Chap. 4 and Chap. 5) which have been introduced in order to interpret the main features of two typical processes of gel formation and gel degradation. These models provide a powerful tool to investigate such phenomena, in order to clarify the relation between structural and dynamical properties of gels. Nevertheless, our models are intrinsically related to specific samples analyzed by experiments, i.e. gelatin chains linked by reactant agents and gels degraded by the action of enzymes. In order to study the general features of gelation transition, and in particular the dynamical properties of gelling systems approaching the transition, we introduce a more general model for irreversible gelling systems. We consider a system made of interacting spheres, which represent monomers in solution. We study the structure and the dynamics in chemical gels by means of molecular dynamics simulations. In particular, we investigate the structural properties analyzing percolative quantities. The dynamics is investigated analyzing the self intermediate scattering functions. Furthermore we study the viscoelastic response of the model and compare our findings to experimental measurements and to results obtained by different models.

In Sect. 6.1 we introduce the model and give the details of the numerical simulations whereas in Sect. 6.2 percolation properties are discussed. In Sect. 6.3 we investigate the dynamical evolution of the system, analyzing the self intermediate scattering functions. Finally, the viscoelastic response is discussed in Sect. 6.4 and in Sect. 6.5. In Sect. 6.6 concluding remarks are presented.

6.1 Model and numerical simulations

We consider a $3d$ system of N particles interacting via a Lennard-Jones potential, truncated in order to have only the repulsive part:

$$U_{ij}^{LJ} = \begin{cases} 4\epsilon[(\sigma/r_{ij})^{12} - (\sigma/r_{ij})^{6} + \frac{1}{4}], & r_{ij} < 2^{1/6}\sigma \\ 0, & r_{ij} \geq 2^{1/6}\sigma \end{cases} \tag{6.1}$$

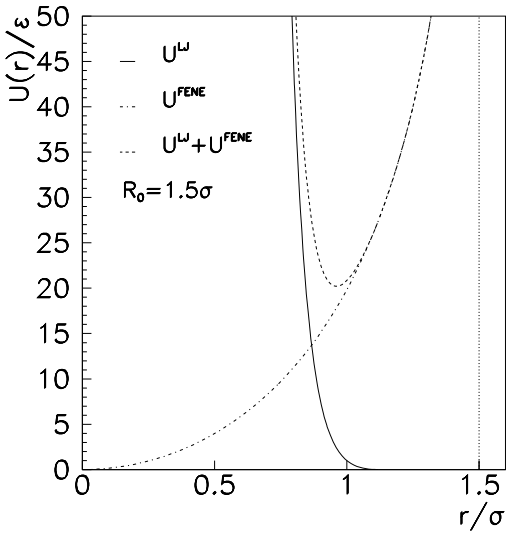

Figure 6.1: The truncated Lennard-Jones potential, the FENE potential and their sum versus the distance r between particles.

where r_{ij} is the distance between the particles i and j.

After the equilibration, we introduce quenched bonds by adding an attractive potential:

$$U_{ij}^{FENE} = \begin{cases} -0.5k_0R_0^2 \ln[1-(r_{ij}/R_0)^2], & r_{ij} < R_0 \\ \infty, & r_{ij} \geq R_0 \end{cases} \tag{6.2}$$

representing a finitely extendable nonlinear elastic (FENE). The introduction of the FENE potential leads to the formation of permanent bonds among all the particles whose distance at that time is lower than R_0. The FENE potential was firstly introduced in Ref. [90] and widely used to study linear polymeric systems [14]. We choose $k_0 = 30\epsilon/\sigma^2$ and $R_0 = 1.5\sigma$ with $\sigma = 1$ as in Ref. [14] in order to avoid any bond crossing and to use an integration time step Δt not too small. In fact, increasing k_0 would reduce the maximum bond extension further but would require a reduction in Δt.

We perform molecular dynamics simulations of this model. The equations of motion are solved in the canonical ensemble (with a Nosé-Hoover thermostat) using the velocity-Verlet algorithm [91, 92], which is described in App. B.4, with a time step $\Delta t = 0.001\delta\tau$, where $\delta\tau = \sigma(m/\epsilon)^{1/2}$ is the standard unit time for a Lennard-Jones fluid and m is the mass of a particle. In the following we will use reduced units where the unit length is σ, the unit energy is ϵ and the Boltzmann constant k_B is set equal to 1. The temperature is fixed at $T = 2$ and the volume fraction $\phi = \pi\sigma^3 N/6L^3$ (where L is the linear size of the simulation box in units

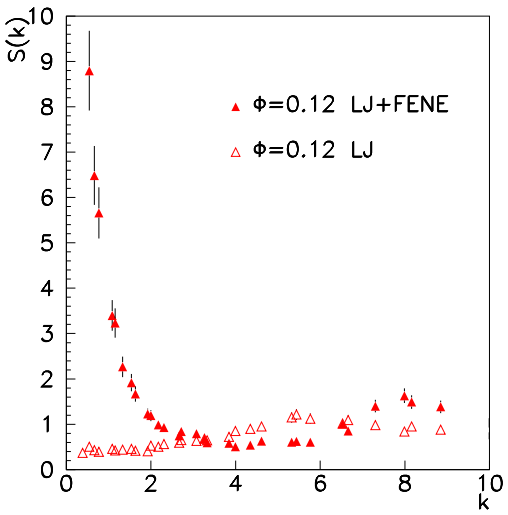

Figure 6.2: Static structure factor $S(k)$ at $\phi = 0.12$ for particles interacting via Lennard-Jones potential (void triangles) and via Lennard-Jones plus FENE potential (full triangles).

of σ) is varied from $\phi = 0.02$ to $\phi = 0.2$. We use periodic boundary conditions and we average all the investigated quantities over 30 independent configurations of the system.

We calculate the static structure factor $S(k) = \frac{1}{N}\sum_{ij}\langle e^{i\vec{k}\cdot(\vec{r}_i-\vec{r}_j)}\rangle$ [63], where the average $\langle\ldots\rangle$ is over independent configurations of the system, at stationarity. In Fig. 6.2 we compare $S(k)$ at the same volume fraction respectively before and after the introduction of the bonds: The appearance of spacial correlations at low wave vectors can be related to an effective attractive interaction due to the presence of the bonds. The intensity of the low wave vector correlations increases with the volume fraction but it is always small as compared to the number of particles and no phase separation is observed. The deep change of the structure factor is a clear evidence that the introduction of permanent bonds strongly influences the static properties of the system, as well as the dynamical ones.

6.2 Gelation transition

In our model the onset of the gel phase corresponds to the formation of a percolating cluster of permanent bonds [16, 17, 20] as typically observed in chemical gelation. Varying the volume fraction ϕ, we calculate in the numerical simula-

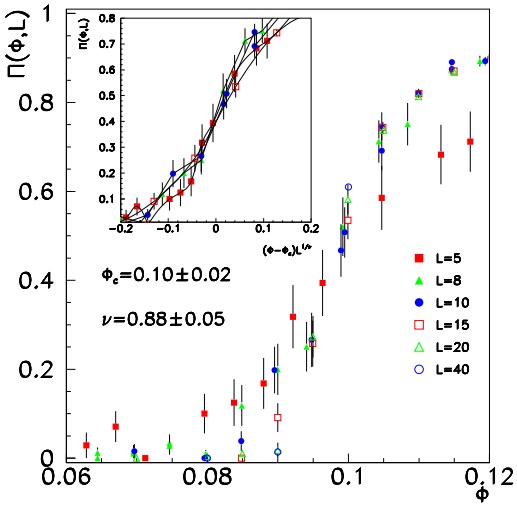

Figure 6.3: Percolation probability $\Pi(\phi, L)$ as a function of the volume fraction ϕ for boxes of size $L = 5, 8, 10, 20, 40$. Inset: Data collapse obtained plotting $\Pi(\phi, L)$ versus $(\phi - \phi_c)L^{1/\nu}$ with $\nu = 0.88$ and $\phi_c = 0.10$.

tions the percolation probability $\Pi(\phi)$ (i.e. the average number of configurations where a percolating cluster is found) and, from the cluster size distribution $n(s)$, the mean cluster size $\chi(\phi) = \sum s^2 n(s) / \sum s n(s)$. For each volume fraction we use simulation boxes of different sizes $L = 5, 8, 10, 15, 20, 40$. From a standard finite size scaling analysis [18], we obtain the percolation threshold ϕ_c, and the critical exponents ν (which governs the power law divergence of the connectedness length $\xi \sim |\phi - \phi_c|^{-\nu}$ as the transition threshold is approached from below) and γ (governing the power law divergence of the mean cluster size $\chi \sim |\phi - \phi_c|^{-\gamma}$).

Data are showed in Fig. 6.3 and in Fig. 6.4 and the obtained results are $\phi_c = 0.10 \pm 0.02$, $\nu = 0.88 \pm 0.05$ and $\gamma = 1.85 \pm 0.05$. The obtained value of the percolation threshold is in good agreement also with the results obtained in Ref. [93], where the percolation of interacting soft sphere has been investigated. In Ref. [93] the authors investigate the shift of the percolation threshold varying the ratio r/R_0, where r is the sphere radius and R_0 is the maximum bond length, and changing the probability p_b of forming bonds between two spheres whose distance is lower than R_0. Our model corresponds to the case $p_b = 1$ and $r/R_0 = 1/3$.

In Fig. 6.5 we plot the cluster size distribution n_s at the percolation threshold for a system with $N = 1000$ particles. We find that at the transition threshold the cluster size distribution follows a power law behavior $n_s \sim s^{-\tau}$ [18] with a Fisher exponent $\tau = 2.23 \pm 0.02$.

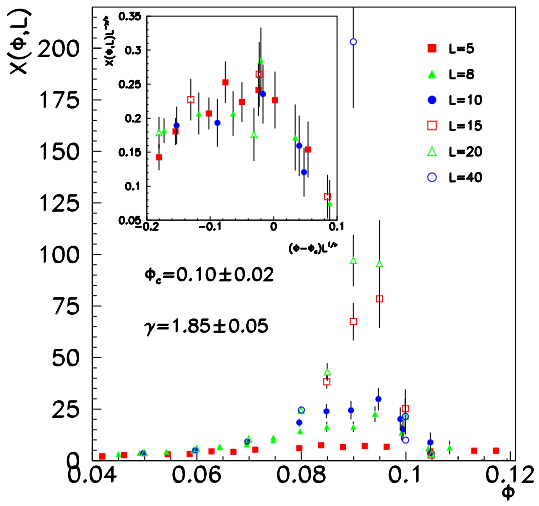

Figure 6.4: Mean cluster size $\chi(\phi, L)$ as a function of the volume fraction ϕ for boxes of the same sizes of Fig. 6.3. Inset: Data collapse obtained plotting $\chi(\phi, L)L^{-\gamma/\nu}$ versus $(\phi - \phi_c)L^{1/\nu}$ with $\nu = 0.88$, $\phi_c = 0.10$ and $\gamma = 1.85$.

Finally in Fig. 6.6 the radius of gyration R_g as a function of the mass s of clusters is plotted for a system with $N = 1000$ particles. The data are well fitted by a power law with exponent $1/d_f = 0.44 \pm 0.03$ (full line in figure) which gives $d_f = 2.3 \pm 0.1$ in agreement with the fractal dimension $d_f \simeq 2.5$ of the random percolation clusters in a three-dimensional system.

The measured values of the critical exponents satisfy the hyper-scaling relations ($2\beta + \gamma = \nu d$, $d_f = d - \beta/\nu$, and $\tau = 2 + (d - d_f)/d_f$ [18]) and are in good agreement with those of the $3d$ random percolation ($\nu = 0.88$, $\gamma = 1.80$ and $\tau = 2.18$ [18]). Hence we conclude that our model belongs to the random percolation universality class, in agreement with several experimental results performed on gelling systems [28]. Thus, the geometrical properties of chemical gels are well described by our model within the percolation theory.

6.3 Dynamical properties: self intermediate scattering functions

We study the dynamics at equilibrium by measuring the self intermediate scattering function $F_s(k, t)$:

$$F_s(k, t) = [\langle \Phi_s(k, t) \rangle] \tag{6.3}$$

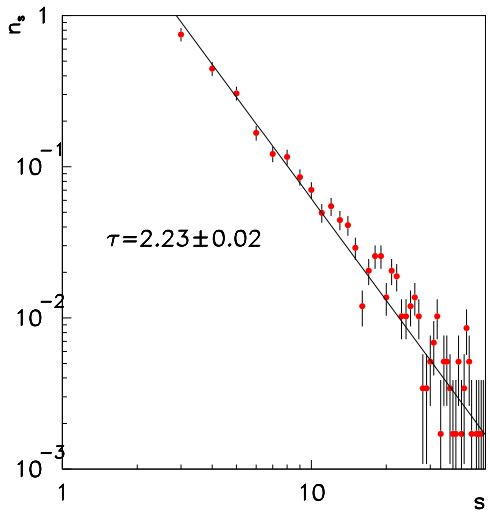

Figure 6.5: Average number (per particle) of clusters with mass s versus s for $N = 1000$ and $\phi = \phi_c = 0.1$. They are fitted with a power law $s^{-\tau}$ with $\tau = 2.23$ (full line).

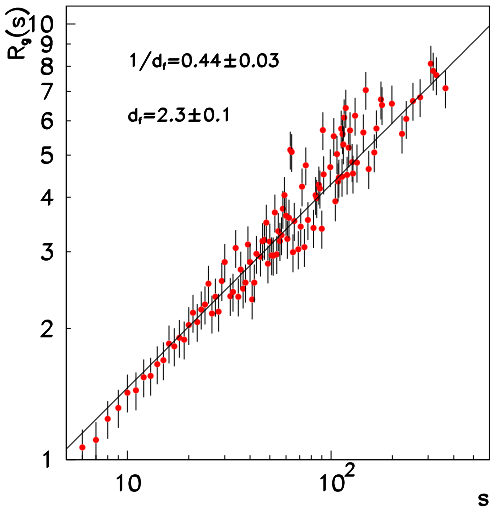

Figure 6.6: Radius of gyration R_g as a function of the mass s of clusters for a system made of $N = 1000$ particles and $\phi = \phi_c = 0.1$. The data are fitted with a power law $R_g \simeq s^{1/d_f}$ with $d_f = 2.3$ (full line).

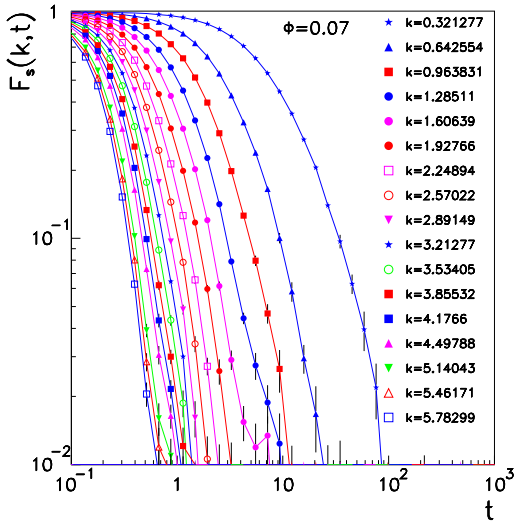

Figure 6.7: Self intermediate scattering for different wave vectors at $\phi = 0.07$ as a function of the time t. For high wave vectors the decay is well fitted by an exponential behavior; for the lowest wave vector $k = 2\pi/L$ a stretched exponential decay appears $\sim e^{-(t/\tau)^\beta}$.

where

$$\Phi_s(k,t) = \frac{1}{N}\sum_{i=1}^{N} e^{i\vec{k}\cdot(\vec{r}_i(t)-\vec{r}_i(0))}, \tag{6.4}$$

and $\langle \ldots \rangle$ is the thermal average for a fixed bond configuration whereas $[\ldots]$ is the average over bond configurations. For very low values of the volume fraction the self intermediate scattering function decays to zero following an exponential behavior for all the wave vectors $|\vec{k}|$ considered. As the volume fraction increases towards the percolation threshold, a significant length scale dependence of the dynamics is observed, which we systematically analyze in the following.

In Fig. 6.7 the self intermediate scattering function $F_s(k,t)$ is plotted as a function of the time for different wave vectors for $\phi = 0.07$, i.e. $\phi < \phi_c$. For high wave vectors $k = |\vec{k}|$ the long time decay is exponential whereas for low wave vectors it starts to follow a stretched exponential behavior $\sim e^{-(t/\tau)^\beta}$, with a stretching exponent $\beta = 0.75 \pm 0.01$. For this volume fraction, the cluster size distribution has already started to widen towards the percolation regime, and therefore over sufficiently large length scales the behavior of $F_s(k,t)$ will be due to the contribution of different relaxation processes, characterized by different relaxation times, whose superposition produces a detectable deviation from an exponential law.

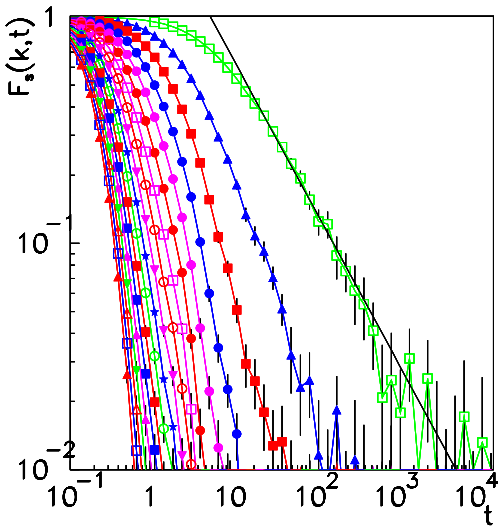

Figure 6.8: $F_s(k,t)$ for different values of the wave vector at $\phi \simeq \phi_c$ as a function of the time t. For the lowest wave vector a power law decay appears $\sim t^{-c}$. The full line corresponds to the power law with the exponent $c = 0.65 \pm 0.03$.

As the volume fraction is increased towards the percolation threshold, the mean cluster size in the system critically grows. In Fig. 6.8 $F_s(k,t)$ is plotted for the percolation threshold ϕ_c as a function of time for different values of the wave vector. For the lowest wave vector $k = 2\pi/L$ the onset of a power law decay is observed, indicating that over these length scales the relaxation is controlled by the formation of the percolating cluster, with an associated relaxation time critically growing. Finally, in Fig. 6.9 the self intermediate scattering function $F_s(k,t)$ for the lowest wave vector $k \simeq 0.35$ is plotted as a function of time for different volume fractions ϕ approaching the percolation threshold, giving the relaxation dynamics over length scales of the order of the system size. At very low values of the volume fraction the self intermediate scattering function decays to zero following an exponential behavior. As the volume fraction is increased above the percolation threshold, we observe the onset of a stretched exponential decay $\sim e^{-(t/\tau)^\beta}$, with β decreasing as a function of the volume fraction (for instance $\beta = 0.75 \pm 0.01$ for $\phi = 0.07$ and $\beta = 0.58 \pm 0.02$ for $\phi = 0.085$). At the transition threshold the long time decay is characterized by a power law behavior $\sim t^{-c}$, with the exponent $c = 0.65 \pm 0.03$. We note that the onset of the power law regime of the self intermediate scattering function for the lowest wave vector is observed for $\phi = 0.09$, which is slightly smaller that the percolation threshold ϕ_c measured performing finite size scaling analysis. This effect is due to the fact

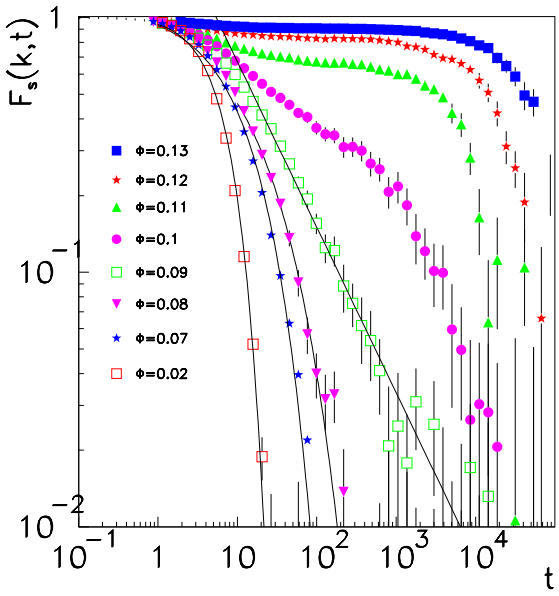

Figure 6.9: Self intermediate scattering function for different volume fractions ϕ and $k \sim 0.35$ as a function of time t. For $\phi << \phi_c$ the decay is well fitted by an exponential behavior; if ϕ approaches to ϕ_c a stretched exponential decay appears $\sim e^{-(t/\tau)^\beta}$ with $\beta = 0.75 \pm 0.01$ for $\phi = 0.07$. At the percolation threshold the decay is well fitted by a power law $\sim t^{-c}$ with $c = 0.65 \pm 0.03$. For $\phi > \phi_c$ the decay become slower and slower. The full lines are the fitting curves.

that the dynamics is studied for a finite system made of $N = 1000$ particles, that is $L \simeq 10$. If the volume fraction increases further, the decay become slower and slower, showing a logarithmic behavior until a two step decay appears. These features of the dynamics well reproduce the experimental observations in different systems [3, 4, 67, 69, 70]. Moreover they agree with previous results obtained via Monte Carlo simulations of a lattice model [94].

6.4 Viscosity critical behavior

As it has been discussed in the previous section, the self intermediate scattering function slowly goes to zero as the percolation threshold is approached for $\phi \leq \phi_c$. In fact, the dynamics of the system critically slows approaching the gel phase. The widening of size distribution approaching the transition threshold reflects into the superposition of different relaxation times, with the subsequent slowing down of the correlations decay. The formation of the percolating cluster influences

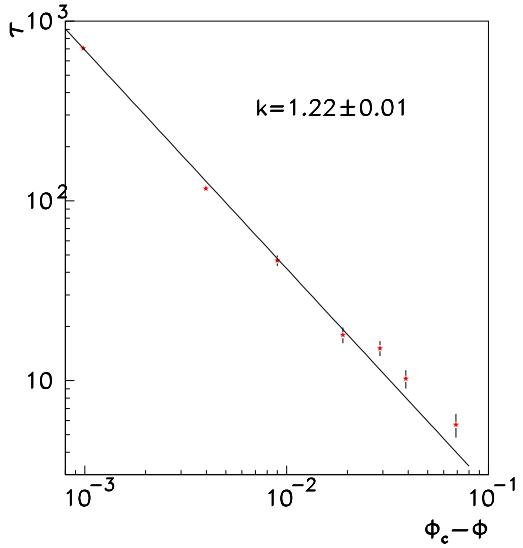

Figure 6.10: The relaxation time τ as a function of the distance from the percolation threshold $\phi_c - \phi$. The full line is the fitting curve $\sim (\phi_c - \phi)^{-k}$ with $\phi_c = 0.09$ and $k = 1.22 \pm 0.01$.

dramatically the relaxation to equilibrium, inhibiting the dynamical evolution and involving longer and longer relaxation times. As a consequence the viscosity of the system increases, diverging as the transition threshold is approached. It can be shown, that the viscosity coefficient η is proportional to the structural relaxation time τ: $\eta \propto \tau$ [26]. Indeed, the relaxation time can be expressed as $\tau \sim \eta/G$, where G is the equilibrium value of the elastic response in the solid-like behavior: $G = \sigma/u_0$, σ being the stress and u_0 the strain. Hence, the relaxation time diverges approaching the gelation threshold following a power law behavior with the same critical exponent of the viscosity coefficient.

We measure the relaxation time, defined as follows:

$$\tau = \left[\left\langle \frac{\int_0^t F_s(k_{min}, t') t' dt'}{\int_0^t F_s(k_{min}, t') dt'} \right\rangle \right] \tag{6.5}$$

where the time t is such that for $t' \geq t$ and $\phi < \phi_c$, $F_s(k, t') = 0$. The triangular brackets $\langle ... \rangle$ indicate thermal average for a fixed bond configuration, whereas the square brackets stand for the average over bond configurations.

Our data, plotted in Fig. 6.10, are fitted with a power law $\tau \propto (\phi_c - \phi)^{-k}$ with $\phi_c = 0.10 \pm 0.02$ and $k = 1.22 \pm 0.01$. The value of the exponent is in good agreement with the ones experimentally measured in PDMS [27], in polyurethan gel [28] and in polyester gels [29]. Furthermore, it is in good agreement with the

result obtained from Monte Carlo simulations on cubic lattice performed in Ref. [71].

6.5 Elastic response

For volume fractions $\phi \geq \phi_c$ the onset of an elastic behavior is observed. The spanning cluster makes the system able to respond to external stress with a restoring force. The elastic constant K may be defined as the ratio between the external force and the deformation. In an elongation experiment where $\delta = l - l_0$ is the linear deformation of the system and the restoring force is a linear function of the displacement δ, the elastic free energy is equal to $F \sim K\delta^2$. Using the Young elastic modulus E, the free energy per unit volume is equal to $F/V \sim E\delta^2/l_0^2$, and hence $K \sim EV/l_0^2$. Then for a cube of size L we obtain $K \sim EL^{d-2}$. The Young elastic modulus has a power law behavior governed by the critical exponent f: $E \propto (\phi - \phi_c)^f \propto \xi^{-\tilde{f}}$, with $\tilde{f} = f/\nu$ and ξ being the connectedness length ($\sim |\phi - \phi_c|^{-\nu}$). As a consequence

$$K \sim L^{d-2}\xi^{-\tilde{f}}. \tag{6.6}$$

Hence, the elastic modulus presents the following scaling behaviors as a function of the system size L and of the distance from the percolation threshold $(\phi - \phi_c)$:

$$\phi > \phi_c \quad (\xi \text{ finite}) \quad K \propto L^{d-2} \tag{6.7}$$

$$\phi = \phi_c \qquad\qquad K \propto L^{-\tilde{z}} \tag{6.8}$$

$$\text{fixed } L \qquad\qquad K \propto \xi^{-\tilde{f}} \propto (\phi - \phi_c)^f \tag{6.9}$$

where $\tilde{z} = z/\nu = \tilde{f} - (d-2)$.
In order to determine the behavior of the elastic modulus K, we assume that in the equilibrium configuration the free energy reaches its minimum, and we perform a series expansion around the equilibrium configuration:

$$F \simeq \frac{1}{2}\sum_{\alpha,i_\alpha} K(\vec{r}_{i_\alpha} - \vec{r}_{i_\alpha}(0))^2 + O(\vec{\Delta}r^2), \tag{6.10}$$

where $\vec{r}_{i_\alpha}(0)$ is the equilibrium position and $\vec{r}_{i_\alpha}$ is the position after the deformation of the i-th particle of the cluster α. In fact, when the system is at equilibrium, the average free energy F is proportional to temperature:

$$[\langle F \rangle] = [\langle \frac{1}{2} K \Delta R^2 \rangle] \sim k_B T \tag{6.11}$$

where ΔR^2 is the fluctuation of the particle positions, and $\langle ... \rangle$ is the thermal average, whereas $[...]$ is the average over bond configurations. Since the elastic modulus K increases following a power law behavior above the transition

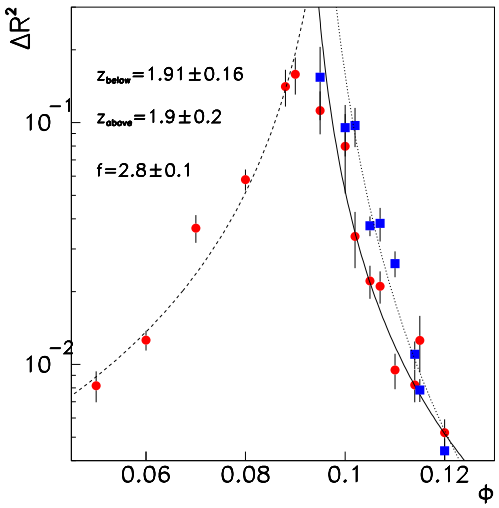

Figure 6.11: Fluctuations ΔR^2 of the radii of gyration of the percolating cluster (squares) and of the finite clusters (circles) above and below the percolation threshold as a function of the volume fraction ϕ; the lines are the curves obtained fitting the data with a power law with exponent respectively f for the percolating cluster, z_{below} and z_{above} for finite clusters.

threshold, also $1/\Delta R^2$ has to behave in the same manner approaching the percolation point from above, in order to keep constant the product $K\Delta R^2$. As a consequence, the critical behavior of ΔR^2 is characterized by the same critical exponent of K, with the opposite sign. Indeed, when the system is in the gel phase, the calculation of the fluctuations ΔR_p^2 of the gyration radius of the percolating cluster, with the subsequent determination of the critical exponent f of the elastic modulus is not an easy task, as the dynamics is very slow. To improve the statistics and in order to obtain independent determination of f and z respectively, we also calculate the fluctuations ΔR_f^2 of the gyration radius of finite clusters, performing a weighted average over the cluster size distribution:

$$\Delta R_f^2 = \frac{\sum_s \Delta {R_s}^2 n_s s^2}{\sum_s n_s s^2} \tag{6.12}$$

As the elastic modulus starts growing from zero at the transition threshold, in order to keep constant the free energy in Eq. 6.11, we expect the fluctuations of the gyration radius to diverge.
In Fig. 6.11 the fluctuations of the gyration radius are plotted as function of volume fraction ϕ: both the fluctuations ΔR_p^2 of the percolating cluster, and that

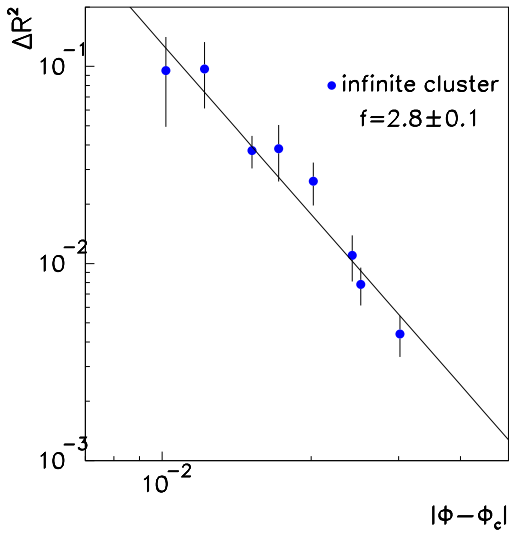

Figure 6.12: Fluctuations of the radius of gyration of the percolating cluster. The full line is the fitting curve $\propto (\phi - \phi_c)^{-f}$ with $f = 2.8$ and $\phi_c = 0.09$.

ΔR_f^2 of the finite clusters diverge as the transition threshold is approached. Data are fitted with power law behavior. For $\phi > \phi_c$, where there is a spanning cluster, we calculate the fluctuations ΔR_p^2 of the gyration radius of the percolating cluster. In Fig. 6.12 ΔR_p^2 is plotted as a function of the distance from the percolation threshold $(\phi - \phi_c)$. We measure the critical exponent f using the scaling relation reported in Eq. 6.9 and fitting our data with a power law behavior, and we gain $f = 2.8 \pm 0.1$. To obtain an independent estimation of z we calculate the fluctuations ΔR_f^2 of the gyration radius of finite clusters. In fact, using the self-similarity properties, the finite clusters may be considered as percolating clusters of a system with size ξ, equal to the gyration radius, at the transition threshold: The scaling relation to be used is Eq. 6.8 where $L = \xi$, i.e. $\Delta R_f^2 \propto \xi^{-\tilde{z}} \propto |\phi - \phi_c|^{-z}$. In Fig. 6.13 we plot ΔR_f^2 as a function of $|\phi - \phi_c|$ for $\phi > \phi_c$ and $\phi < \phi_c$ determining the critical exponent z. By fitting data below and above the transition threshold with the function $A\,|\phi - \phi_c|^{-z}$ we obtain $z_{below} = 1.91 \pm 0.16$ and $z_{above} = 1.9 \pm 0.2$ respectively. The two estimations coincide within error bars: averaging the values obtained above and below the percolation threshold, we obtain $z = 1.9 \pm 0.2$. The consistency of z_{below} and z_{above} reflects the self-similarity of the system at $\phi < \phi_c$ and $\phi > \phi_c$. The power laws fitting data have distinct prefactors, $A_{below} \simeq 3 \cdot 10^{-5}$ and $A_{above} = 5 \cdot 10^{-6}$ respectively. Indeed, even if the critical behavior of the gyration radius fluctuations of finite clusters is the same below and above the critical threshold, the amplitude of the fluctuations varies. In

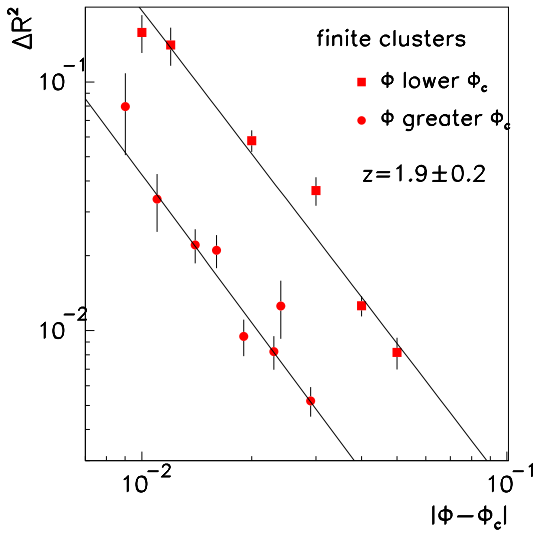

Figure 6.13: Fluctuations ΔR^2 of the radii of gyration of the of the finite clusters above (dots) and below (squares) the percolation threshold fitted with the curve $A|\phi - \phi_c|^{-z}$ with $\phi_c = 0.1$ and $z = 1.91$.

fact, above the percolation threshold, the amplitude of fluctuations is influenced by the presence of the percolating cluster: due to excluded volume effects, the presence of the infinite cluster inhibits fluctuations of gyration radius of finite clusters. Nevertheless, the scaling behavior of fluctuations is not influenced by the presence of the percolating cluster and the critical exponent $z_{above} \simeq z_{below}$. In addition, we note that the measured exponents z and f satisfy the relation $z = f - (d-2)\nu$.

Our results well reproduce experimental findings obtained in several gelling materials, such as polyurethane gels [28] and polyester gels [29]. We observe that the viscosity critical behavior of these system is also in agreement with our results. Furthermore, our findings are in good agreement with the theoretical predictions presented in Ref. [25] and discussed in Sect. 2.3, where on the basis of entropic considerations, $f = d\nu$ has been obtained. In $3d$ random percolating systems $\nu \simeq 0.88$, and hence $f \simeq 2.64$. In a system belonging to the $3d$ Ising model universality class, where $\nu \simeq 0.6$, we expect to have $f \simeq 1.8$. If we consider a system which undergoes phase separation, such as attractive colloids which at low volume fraction and low temperature may form a gel, at the critical point Ising critical exponents are obtained, as a consequence we expect $f \simeq 1.8$. The latter value of f is in agreement with de Gennes prediction on elastic modulus critical behavior [12], obtained using the analogy between a spring network and

a conductive network (Sect. 2.2). Furthermore, recently by means of renormalization group calculations it has been argued that $f = d\nu \simeq 2.7$ in systems where excluded volume effects are relevant, while $f \simeq 1.9$ when excluded volume effects may be neglected [61]. Indeed at the critical point compensation effects between attractive and repulsive interactions, due to excluded volume effects, arise, thus possibly making excluded volume interactions negligible. Actually, the critical behavior of the elastic modulus at the critical point is a subject under investigation.

6.6 Conclusion

In conclusion, we have presented a molecular dynamics study of a model undergoing chemical gelation and we have investigated its structural and dynamical properties. Due to the formation of permanent bonds between particles, the gelation transition corresponds to the percolation threshold (random percolation). We have found that the correlation functions in the sol phase and at the transition threshold behave as observed in the experiments in a number of gelling systems. In chemical gels the onset of a stretched exponential decay is typically associated to the wide cluster size distribution close to the gelation threshold, producing a wide distribution of relaxation times. At the percolation threshold, the longest relaxation time diverges due to the critical growing of the percolation correlation length, producing a long time power law decay. We have measured the critical exponent of the elastic modulus computing the fluctuations of gyration radius of both percolating and finite clusters. Our results are in good agreement with experimental findings and theoretical predictions of different models.
Our model for permanent gels reveals to be a powerful tool to investigate gelling systems, as it well reproduce the most common structural and dynamical properties of such systems. In the next chapter, we present an innovative investigation on gelling system, analyzing the behavior of fluctuations of dynamics and its relations to percolative properties.

Chapter 7

Static and dynamic heterogeneities in irreversible gels

In this chapter we analyze the heterogeneities in the model introduced in the previous chapter, in terms of the fluctuations of the self intermediate scattering functions. For the first time we apply the study of fluctuations of self intermediate scattering function, usually applied in glass investigations, to gels. In the sol phase close to the percolation threshold, we find that fluctuations, which are a dynamical susceptibility, are a monotonically increasing function of time. The asymptotic value of this dynamical susceptibility diverges at the gelation transition as the mean cluster size. We find that the observed behavior of the dynamical susceptibility is due to the static nature of the heterogeneities and it is similar to the one observed in a spin glass with quenched interactions. These findings suggest an alternative way of measuring the mean cluster size in a system undergoing a chemical gelation.

In Sect. 7.1 we analyze heterogeneities in our model for irreversible gelling systems. The analogy between the asymptotic value of the dynamical susceptibility and the percolation correlation function is discussed in Sect. 7.2. In Sect. 7.3 our results about heterogeneities in chemical gels are compared to the results obtained in a dilute spin glass models with quenched interactions. Finally, Sect. 7.4 contains the concluding remarks.

7.1 Dynamical susceptibility

We now analyze and discuss the behavior of the dynamical susceptibility $\chi_4(k,t)$, introduced and generally used in the framework of glass transitions, associated to the fluctuations of the self intermediate scattering function $F_s(k,t) = [\langle \Phi_s(k,t) \rangle]$

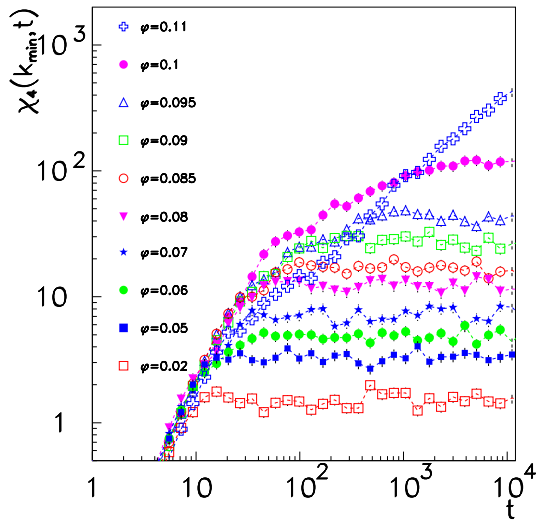

Figure 7.1: $\chi_4(k_{min}, t)$ as a function of t for $\phi = 0.02$, 0.05, 0.06, 0.07, 0.08, 0.085, 0.09, 0.095, 0.10, 0.11 (from bottom to top).

where

$$\Phi_s(k,t) = \frac{1}{N}\sum_{i=1}^{N} e^{i\vec{k}\cdot(\vec{r}_i(t)-\vec{r}_i(0))}, \tag{7.1}$$

and $\langle \ldots \rangle$ is the thermal average for a fixed bond configuration and $[\ldots]$ whereas the average over bond configurations. The dynamical susceptibility is defined as:

$$\chi_4(k,t) = N\left[\langle|\Phi_s(k,t)|^2\rangle - |\langle\Phi_s(k,t)\rangle|^2\right] \tag{7.2}$$

For the first time we perform in a gelling system the analysis of this function, commonly used in the investigation of glassy systems, such as supercooled liquids. In supercooled liquids $F_s(k,t)$ presents a typical two step behavior with a stretched exponential decay at long times due to the cooperative rearrangements of particles. In fact, in supercooled liquids, the motion of a particle depends to some degree on the motion of its neighbors. The first decay of $F_s(k,t)$ is due to the diffusion of the particle inside the cage made of its neighbors. The second step decay, which is slower, is due to the breakage of the cage and to the cooperative rearrangement of particles. The rearranging movement of one particle is only possible if a certain number of particles also move. The average size of such cooperative rearranging regions depends on the spatial extension of correlated thermal fluctuations. Each region rearranges into another configuration independently of its environment. Thus in supercooled liquids dynamical heterogeneities are due to the presence of independent cooperative rearranging regions.

In such systems $\chi_4(k,t)$ grows in time towards a maximum, before decreasing for long times as a consequence of the transient nature of dynamic heterogeneities. The value of the maximum is expected to diverge as the dynamical transition temperature is approached from above [15, 95]. We compute the dynamical susceptibility $\chi_4(k,t)$ in our model for irreversible gels: For the smallest wave vector $k = 2\pi/L \sim 0.35$, the dynamical susceptibility $\chi_4(k,t)$ has the behavior shown in Fig. 7.1. Differently from the behavior typically observed in glassy systems, we find that, for $\phi < \phi_c$, $\chi_4(k,t)$ is a monotonically increasing function of time, tending to a plateau whose value increases with the volume fraction. For $\phi \geq \phi_c$ the system is out of equilibrium and $\chi_4(k,t)$ always increases as a function of time and does not reach any asymptotic value.

Indeed we demonstrate that in the thermodynamic limit, when $k \to 0$ and $t \to \infty$, $\chi_4(k,t)$ tends to the mean cluster size.

Being $\lim_{t\to\infty}\langle\Phi_s(k,t)\rangle = 0$ at $\phi < \phi_c$, we have:

$$\begin{aligned}\lim_{t\to\infty}\chi_4(k,t) &= \lim_{t\to\infty}\frac{1}{N}\sum_{i,j=1}^{N}\left[\langle e^{i\vec{k}\cdot(\vec{r}_i(t)-\vec{r}_i(0))}e^{-i\vec{k}\cdot(\vec{r}_j(t)-\vec{r}_j(0))}\rangle\right] \\ &= \frac{1}{N}\sum_{i,j=1}^{N}\left[\left|\langle e^{-i\vec{k}\cdot(\vec{r}_i-\vec{r}_j)}\rangle\right|^2\right]. \end{aligned} \tag{7.3}$$

In the last passage of Eq. 7.3 we have considered that, for large enough time t, the term $e^{-i\vec{k}\cdot(\vec{r}_i(t)-\vec{r}_j(t))}$ is statistically independent of $e^{-i\vec{k}\cdot(\vec{r}_i(0)-\vec{r}_j(0))}$, being $\vec{r}_i(t) - \vec{r}_j(t)$ independent of $\vec{r}_i(0) - \vec{r}_j(0)$, so that we can factorize the thermal average. In Eq. 7.3, we may now separate the sum over connected pairs ($\gamma_{ij} = 1$, that is pairs belonging to the same cluster), and disconnected ones ($\gamma_{ij} = 0$, that is pairs belonging to different clusters), so that

$$\begin{aligned}\lim_{t\to\infty}\chi_4(k,t) &= \frac{1}{N}\sum_{i,j=1}^{N}\left[\gamma_{ij}\left|\langle e^{-i\vec{k}\cdot(\vec{r}_i-\vec{r}_j)}\rangle\right|^2\right] \\ &+ \frac{1}{N}\sum_{i,j=1}^{N}\left[(1-\gamma_{ij})\left|\langle e^{-i\vec{k}\cdot(\vec{r}_i-\vec{r}_j)}\rangle\right|^2\right] \end{aligned} \tag{7.4}$$

Let us analyze separately the contribution of the disconnected particles, introducing the pair correlation function $h_{ij}(r)$ [63], defined as $h_{ij}(\vec{r}) + 1 = g_{ij}(\vec{r})$, where $(1/V)g_{ij}(\vec{r})$ gives the probability density of finding the particle i in $\vec{r}$, given the particle j in the origin. The pair correlation function can be written as:

$$h_{ij}(\vec{r}) = g_{ij}(\vec{r}) - 1 = V\langle\delta(\vec{r} + \vec{r}_i - \vec{r}_j)\rangle - 1. \tag{7.5}$$

Hence, we can write the delta-function in terms of the pair correlation function $h_{ij}(\vec{r})$, obtaining the following expression:

$$\langle\delta(\vec{r} + \vec{r}_i - \vec{r}_j)\rangle = \frac{1}{N}\rho[h_{ij}(\vec{r}) + 1], \tag{7.6}$$

where $\rho = N/V$. The delta-function can now be used to write the exponential of Eq. 7.4 in an integral form:

$$\langle e^{-i\vec{k}\cdot(\vec{r}_i-\vec{r}_j)}\rangle = \int d^3\vec{r}\, e^{-i\vec{k}\cdot\vec{r}}\, \langle\delta(\vec{r}+\vec{r}_i-\vec{r}_j)\rangle. \tag{7.7}$$

Hence, using Eq. 7.6, we can write:

$$\langle e^{-i\vec{k}\cdot(\vec{r}_i-\vec{r}_j)}\rangle = \frac{1}{N}\int d^3\vec{r}\, e^{-i\vec{k}\cdot\vec{r}}\, \rho[h_{ij}(\vec{r})+1], \tag{7.8}$$

It is worth to notice that the pair correlation function $h_{ij}(\vec{r})$ decay to zero at a finite distance if the particles i and j are disconnected [63]. We consider the thermodynamic limit where $N \to \infty$ and $L \to \infty$ leaving the density ρ constant and analyze the behavior of the integral in Eq. 7.8. The first term, the Fourier transform of the correlation function $h_{ij}(\vec{r})$ multiplied by ρ, is finite when $L \to \infty$ since $h_{ij}(\vec{r})$ decays to zero at a finite distance. The second term, the Fourier transform of ρ, is not larger in modulus than $8\rho/|k_x k_y k_z|$, and again remains finite when $L \to \infty$. As a consequence, the integral in Eq. 7.8 remains finite for any finite fixed $\vec{k}$, so that the l.h.s. of Eq. 7.8 is of order $O(1/N)$.

As the disconnected pairs are at most of order N^2, the second term in Eq. 7.4 is also of order $O(1/N)$ and can be neglected in the thermodynamic limit. As a consequence, $\chi_{as}(k,\phi) \equiv \lim_{N\to\infty}\lim_{t\to\infty}\chi_4(k,t)$ is given by

$$\chi_{as}(k,\phi) = \lim_{N\to\infty}\frac{1}{N}\sum_{i,j=1}^{N}\left[\gamma_{ij}\left|\langle e^{-i\vec{k}\cdot(\vec{r}_i-\vec{r}_j)}\rangle\right|^2\right] \tag{7.9}$$

where only connected particles contribute. For $\phi < \phi_c$, clusters will have at most a linear size of order ξ, so that the relative distance $|\vec{r}_i - \vec{r}_j|$ of connected particles will be $|\vec{r}_i - \vec{r}_j| \leq \xi$. Therefore, for $|\vec{k}| \ll \xi^{-1}$ the exponent $\vec{k}\cdot(\vec{r}_i - \vec{r}_j)$ will tend to zero. Hence for $\gamma_{ij} = 1$, i.e. connected particles, we have that $\langle e^{-i\vec{k}\cdot(\vec{r}_i-\vec{r}_j)}\rangle$ tends towards 1 and

$$\lim_{k\to 0}\chi_{as}(k,\phi) = \chi \tag{7.10}$$

where $\chi = \sum_{i,j}\gamma_{ij}$ is the mean cluster size [18], introduced in Sect. 1.1.

In Fig. 7.2 $\chi_{as}(k_{min},\phi)$ calculated in the simulations is plotted as a function of $(\phi_c - \phi)$ together with the mean cluster size χ independently evaluated. We find a good agreement between χ and $\chi_{as}(k_{min},\phi)$. We observe that, as the percolation threshold is approached from below, $\chi_{as}(k_{min},\phi)$ displays a power law behavior. The exponent, within the numerical accuracy, is in very good agreement with the value of the exponent γ for the mean cluster size.

Our results open the way to a new method to measure critical exponents in irreversible gels, in particular we suggest to measure the mean cluster size by means of scattering experiments, as the dynamical susceptibility $\chi_4(k,t)$ is related to the fluctuations of the scattered intensity in scattering experiments. In

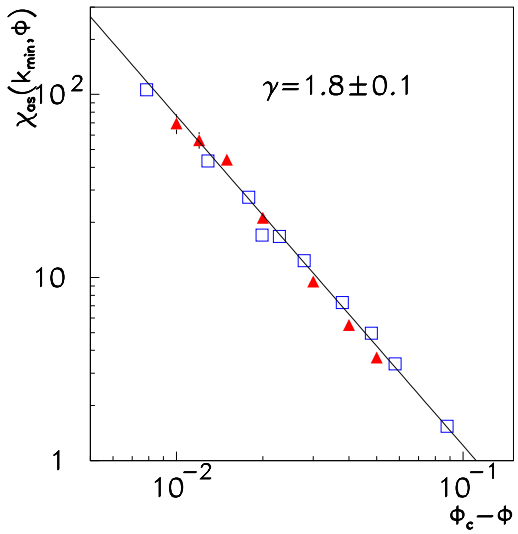

Figure 7.2: Asymptotic values of the susceptibility (full triangles), $\chi_{as}(k_{min},\phi)$ and mean cluster size (open squares) as a function of $(\phi_c-\phi)$, with $\phi_c=0.10$. The data are fitted by the power law $(\phi_c-\phi)^{-\gamma}$ with $\gamma=1.8\pm0.1$.

usual approaches (Sect. 1.4) the sample needs to be dissolved in a known quantity of solvent in such a way that each cluster is separated from the others and then the mean cluster size is measured by light scattering measurements. Beyond gelation threshold, finite clusters, which are trapped into the holes of the gel, must be extracted from the gel phase, but such separation is very difficult to achieve experimentally as clusters tend to break during this process [20]. Hence in the existing procedures the sample has to be manipulated in order to extract information on the cluster size distribution. On the contrary, the method proposed on the basis of our results relates percolation quantities to directly observable quantities, with no need to treat the sample.

In conclusion, our results lead to a correspondence between $\chi_{as}(k_{min},\phi)$, a quantity defined starting from dynamics fluctuations, and the mean cluster size χ, a purely percolative quantity.

7.2 Analogy with the percolation correlation function

In the previous section we have analyzed, for the first time in gelling systems, the asymptotic behavior of the dynamical susceptibility, obtaining a close relation between dynamics fluctuations and a percolative quantity. Pushing further this

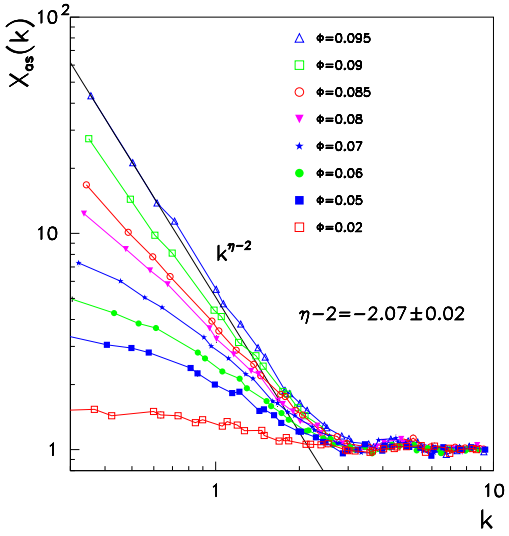

Figure 7.3: Asymptotic values of the susceptibility, $\chi_{as}(k, \phi_c)$ as a function of the wave vector k. At ϕ_c the data are fitted with a power law (full line) $\sim k^{-2.07}$, in agreement with the exponent $\eta - 2$ of random percolation.

correspondence, we investigate the analogy between the behavior of $\chi_{as}(k, \phi)$ versus the wave vector and the Fourier transform of the percolation correlation function $g(r)$ [18]. The function $g(r)$, known also as pair connectivity function, gives the probability that, given a particle in the origin, a particle in r belongs to the same cluster. The percolation correlation function decays following a power law behavior for $r \ll \xi$, with an exponential cutoff:

$$g(r) = \frac{e^{-r/\xi}}{r^{d-2+\eta}}. \tag{7.11}$$

Hence its Fourier transform has the following power law behavior:

$$\int e^{i\vec{k}\cdot\vec{r}} \frac{e^{-r/\xi}}{r^{d-2+\eta}} d^d\vec{r} \sim k^{\eta-2}. \tag{7.12}$$

In Fig. 7.3 we plot $\chi_{as}(k, \phi)$ as a function of the wave vector k for different ϕ approaching ϕ_c. At the percolation threshold and for low wave vectors, $\chi_{as}(k, \phi_c)$ follows a scaling behavior as a function of k, with an exponent -2.07 ± 0.02, consistent, within the numerical accuracy, with the prediction $\eta - 2$ of random percolation [18]. This result indicates again that the dynamic susceptibility is strongly affected by the critical properties of the percolation transition. It shows that if one varies the wave vector k, and $2\pi/k > \sigma$ where σ is the particle diameter, sufficiently close to the percolation threshold the measure of the dynamic

susceptibility is able to detect the self-similarity of the structure of the system due to the percolation transition. Finally it suggests that at the percolation threshold the asymptotic value of the dynamic susceptibility at low k has the same scaling behavior as the Fourier transform of the percolation correlation function [18]. Since to vary the wave vector corresponds to vary the length scale used to probe the dynamics of the system, $\chi_{as}(k,\phi)$ is expected to be a function of the rescaled variable $k(\phi_c-\phi)^{-\nu}$ and we can perform a standard finite size analysis.

Moreover, close to ϕ_c the plateau value $\chi_{as}(k,\phi) \sim (\phi_c-\phi)^{-\gamma}$ for $k=0$, hence for finite small k we can write $\chi_{as}(k,\phi) \sim (\phi_c-\phi)^{-\gamma} g(k\xi)$, where $\xi = A(\phi_c-\phi)^{-\nu}$ is the connectedness length, and $g(z)$ has the following behavior:

$$g(z) = \begin{cases} \text{constant} & z \ll 1 \\ z^{-\gamma/\nu} & z \gg 1 \end{cases} \tag{7.13}$$

Writing $\chi_{as}(k,\phi) = k^{-\gamma/\nu} k^{\gamma/\nu} (\phi_c-\phi)^{-\gamma} g(k\xi)$, we finally obtain:

$$\chi_{as}(k,\phi) = k^{\eta-2} f(k\xi) \tag{7.14}$$

where we have used the relation $\eta - 2 = -\gamma/\nu$ [18] and we have defined the function $f(k\xi)$:

$$f(k\xi) = (k)^{\gamma/\nu}(\phi_c-\phi)^{-\gamma} g(k\xi) = A^{-\gamma/\nu}(k\xi)^{\gamma/\nu} g(k\xi) \tag{7.15}$$

using $(\phi_c - \phi) = (\xi A)^{-1/\nu}$. Therefore we plot $\chi_{as}(k,\phi)k^{2-\eta}$ as a function of the rescaled variable $k(\phi_c-\phi)^{-\nu}$ in Fig. 7.4. The data support our scenario. A good collapse onto a unique master curve is obtained at low wave vectors and sufficiently close to the percolation threshold. As ϕ grows towards ϕ_c, the collapse of the data is obtained over a wider interval of values of the rescaled variable $k^{-1/\nu}(\phi_c-\phi)$. All these results coherently show how in the present system the dynamical correlated domains, signalled by the dynamical susceptibility in Fig. 7.1, are indeed static and coincide with the clusters of particles connected by bonds whose correlation length is the connectedness length ξ, diverging at the percolation threshold. A similar behavior is observed in a dilute spin glass model [96] with quenched interactions, where the heterogeneities have a static nature and the asymptotic value of the dynamical susceptibility coincides with the static non-linear susceptibility diverging at the spin glass transition threshold. Interestingly enough, in the same model, by introducing interactions with a finite lifetime, there is no divergence of the static susceptibility and one recovers the behavior of the dynamic susceptibility which is typical of supercooled liquids. We suggest therefore that also in our case glassy like dynamical properties should appear by introducing a finite bond lifetime. This idea is also corroborated by the results obtained via Monte Carlo simulations of a lattice model for gelling system where the relaxation functions were studied in both cases of permanent bonds and finite lifetime bonds [94]. The case of bonds with a finite lifetime is more relevant to other gelation phenomena, as in the case of colloidal gelation, where there is no chemical bonding [97, 98].

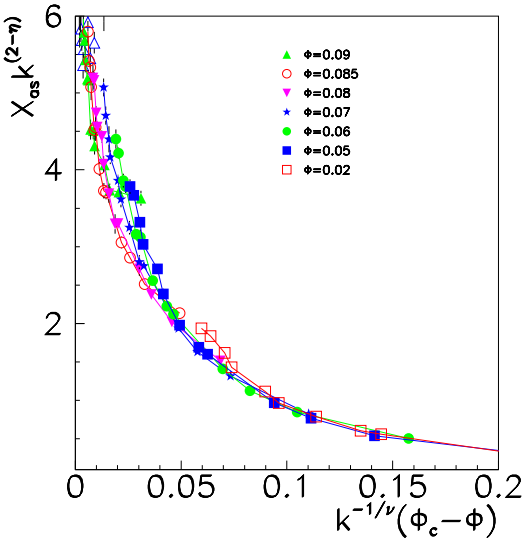

Figure 7.4: Scaling plot showing $\chi_{as}(k,\phi)k^{2-\eta}$ as a function of $k^{-1/\nu}(\phi_c - \phi)$.

7.3 Heterogeneities and quenched disorder

Our investigations indicate that heterogeneities in irreversible gels have a static nature, due to the presence of permanent clusters of bonded particles. Bonds between particles may be treated as quenched variables, which cause quenched disorder.

The dynamical susceptibility, which we analyze for the first time in a model for irreversible gels, is usually used to investigate the presence of heterogeneities in glasses and spin glasses. Structural glasses are generally characterized by annealed interactions, so that disorder is self-organizing. As a consequence, in such systems dynamical heterogeneity has a different nature and the dynamical susceptibility has a different behavior from the one we observe in our model. Indeed, we note that the presence of quenched interaction strongly influences the dynamical susceptibility, as it has been observed also in spin glasses.

Let us consider a dilute spin glass model with quenched interactions [99], in which the dynamical susceptibility has been investigated [96].

The hamiltonian of the model is:

$$-\beta H = J \sum_{\langle ij \rangle} (\epsilon_{ij} S_i S_j - 1) n_i n_j + \mu \sum_i n_i, \tag{7.16}$$

where $S_i = \pm 1$ are Ising spins, $n_i = 0, 1$ are occupation variables, and $\epsilon_{ij} = \pm 1$ are ferromagnetic and antiferromagnetic interactions between nearest neighbor

spins. The variables ϵ_{ij} may be quenched variables randomly distributed with equal probability or annealed variables evolving in time.

In the limit $\mu \to \infty$ all sites are occupied, i.e. $n_i \equiv 1$, and the model reproduces the Ising spin glass. In the limit $J \to \infty$ the model describes a frustrated lattice gas with properties recalling those of a "frustrated" liquid. In fact the first term of hamiltonian in Eq. 7.16 implies that two nearest neighbor sites can be freely occupied only if their spin variables satisfy the interaction, that is if $\epsilon_{ij} S_i S_j = 1$, otherwise they feel a strong repulsion. To make the connection with a liquid, we note that the internal degree of freedom S_i may represent for example internal orientation of a particle with non symmetric shape. Two particles can be nearest neighbors only if the relative orientation is appropriate, otherwise they have to move apart. Since in a frustrated loop the spins cannot satisfy all interactions, in this model particle configurations in which a frustrated loop is fully occupied are not allowed. The frustrated loops in the model are the same of the spin glass model and correspond in the liquid to those loops which, due to geometrical hindrance, cannot be fully occupied by the particles.

In this lattice model the dynamical susceptibility is defined as follows:

$$\chi_{SG}(t) = N \left[\langle q(t)^2 \rangle - \langle q(t) \rangle^2 \right], \tag{7.17}$$

where

$$q(t) = \frac{1}{N} \sum_i S_i(t') n_i(t') S_i(t+t') n_i(t+t'). \tag{7.18}$$

The square brackets $[\ldots]$ indicates the average over the disorder, the triangular brackets $\langle \ldots \rangle$ stands for the thermal average over a fixed disorder configuration.

The dynamical susceptibility of the dilute spin glass with quenched interaction [96], reported in Fig. 7.5, behaves in a similar manner to the susceptibility in irreversible gels obtained in our simulations, plotted in Fig. 7.1. It is a monotonic function increasing in time, which tends to a plateau value. The asymptotic value $\chi(\infty)$ corresponds to the static susceptibility, and therefore has a divergence at the critical threshold $\phi_c \simeq 0.62$. This behavior is a consequence of quenched disorder: the heterogeneities have a static nature, due to the presence of permanent interactions. The analogy between dilute spin glass model with quenched interactions and irreversible gels suggests a possible common description of the involved transitions. Furthermore, we stress the analogy between the dynamical susceptibility defined in Eq. 7.17 and the irreversible gel dynamical susceptibility defined in Eq. 7.2 according to which the order parameter $q(t)$ of the spin glass transition may be put in correspondence with the self intermediate scattering function $\Phi_s(k,t)$.

In the annealed version of the dilute spin glass model, where the interactions ϵ_{ij} in Eq. 7.16 are annealed dynamical variables evolving in time, the dynamical susceptibility of Eq. 7.17 has a non-monotonic behavior. In Fig. 7.6 the dynamical susceptibility of the annealed dilute spin glass is reported: it has the same

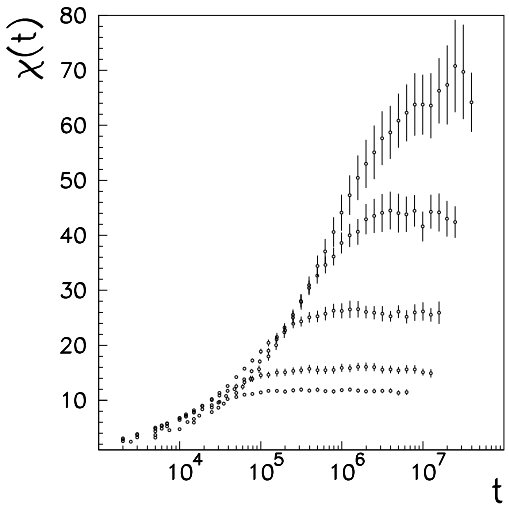

Figure 7.5: Dynamical susceptibility for a dilute spin glass system of size $L = 16$ and densities $\phi = 0.58, 0.59, 0.60, 0.61, 0.62$ [96].

behavior of a Lennard-Jones binary mixture [100], presenting a maximum $\chi(t^*)$ that seems to diverge together with the time of the maximum t^* as the density grows. The non-monotonic behavior of the dynamical susceptibility in these systems may be due to the annealed nature of disorder, which is self-organizing. We expect that in physical gels, where there are not quenched interactions between particles, we recover the behavior of annealed dilute spin glass models, which resembles the one of structural glasses. This in fact found in experimental investigations of colloidal suspension forming colloidal gels [101]. Further investigations on physical gels are required to clarify this issue.

7.4 Conclusion

We have presented for the first time a study of the dynamical susceptibility calculated from the fluctuations of the self-intermediate scattering function in a chemical gel. This quantity is a monotonically increasing function of time. For the lowest wave vector its asymptotic value diverges at the gelation transition as the mean cluster size. We have argued that this finding can be generally expected to hold in a sufficiently large system, at a low wave vector k such that $2\pi/k > \xi$, ξ being the linear size of the largest cluster. This result is supported by the scaling behavior of the asymptotic value of the dynamical susceptibility as function of the wave vector and of the distance from the percolation threshold. Interestingly enough, these results allow to connect a structural feature of the gelling solution,

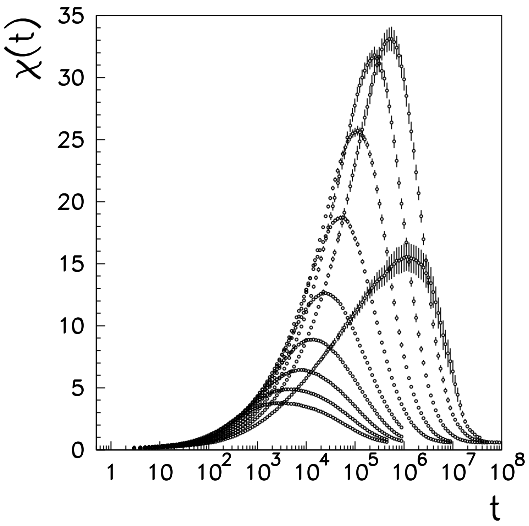

Figure 7.6: Dynamical susceptibility for the annealed version of the dilute spin glass model, for a system of size $L = 16$ and densities ϕ ranging from $\phi = 0.52$ to $\phi = 0.61$ with step $\delta\phi = 0.01$ [96].

i.e. the mean cluster size, whose critical behavior signals the percolation transition, to a dynamical quantity which is measurable in light scattering experiments [102].

Due to the static nature of heterogeneities we find a behavior very different from the one observed in glassy systems where the divergence of the peak of the dynamical susceptibility is interpreted as related to a divergence of a dynamical correlation length, which can not relate to any static correlation length. In the present case no peak is present: the observed behavior of the dynamical susceptibility is similar to that observed in a dilute spin glass model with quenched interactions [96], suggesting a possible common description of the involved phase transitions. Moreover, the results obtained in the dilute spin glass model with annealed interactions suggest that, in the investigation of physical gels one should consider bonds with finite lifetime [94, 97] and should recover a behavior more similar to structural glassy systems.

Conclusions

In this thesis we have studied the gelation transition from different points of view. We have introduced and investigated three different models in order to stress and deeper comprehend relations between structural and dynamical properties of gelling systems. We have first introduced two models investigated by means of Monte Carlo simulations on lattice, in order to describe two specific processes of gelation and degradation. Later we have introduced a general model for irreversible gelation, investigated by means of molecular dynamics simulations in order to describe the gelation transition in the framework of transitions toward a disordered solid state involving critical slowing down of dynamics.

Our lattice model introduced to study the kinetics of bond formation between gelatin chains and reactant agents, describes and clarifies the principal mechanisms involved in bond formation. By means of Monte Carlo simulations, we have investigated the crucial role of two typical time scales in the kinetics. Our results reproduce well the experimental data and indicate that the two time scales detected in experiments correspond to the average time of forming single bonds reactant-chain and bridges chain-chain via cross-linkers. These two time scales are related to the characteristic times of diffusion of free reactants and reactants which have already formed one bond. Their ratio controls the kinetics of the bond formation. In fact, variations of the concentration, the cross-linker reactivity and the pH strongly affect this ratio and therefore the kinetics of the gelation process. Our findings also show that the probability p_b to form a bridge between two active sites allows to finely tune the kinetics of the reaction via the ratio of the two characteristic times. A variation of p_b in our interpretation corresponds to a variation of the free energy barrier to overcome in order to form the bond, or to different orientations of bonds vectors; hence the variation of p_b corresponds to change the reactant agent in the gelatin solution. In conclusion, our simple model allows to analyze in detail the kinetics of bond formation and provides a good description of chemical gelation of gelatin chains. It represents therefore a useful tool to investigate rheological behavior of gelatin solutions and the relation between the kinetics and the gel structure. The viscoelastic response of the system obtained at the end of the reaction between gelatin chains and cross-linkers, is actually under investigation.

The degradation process due to the action of enzymes which catalyze the hy-

drolysis of bonds between gelatin chains in the extracellular matrix has been also investigated by means of Monte Carlo simulations of a lattice model. The reverse sol-gel transition has been studied using the percolation theory. Our results show that, for low density of enzymes, our model belongs to a universality class different from random percolation. The change in the critical exponents is due lo long range correlations between bonds. If the density of enzymes is sufficiently high, the correlation disappears and there is a crossover to random percolation universality class. Our results on the viscoelastic response approaching the transition threshold stimulated further experimental measurements. Preliminary results on the elastic response are in good agreement with our predictions. Our simple lattice model provides a good description of the degradation process, as it captures the main features of real systems.

Finally, to complete our study of gelation phenomena, we have presented a molecular dynamics study of a chemical gelling system and investigated its structural and dynamical properties. Due to the formation of permanent bonds, the system undergoes a gelation transition in correspondence with the percolation threshold. We have shown that the percolation transition belongs to the random percolation universality class, and the correlation functions in the sol phase and at the transition threshold reproduce the experimental results. We have analyzed the viscoelastic response of the system, obtaining that the critical behavior of the elastic modulus is governed by the exponent $f = d\nu \simeq 2.6$, where d is the Euclidean dimension of the embedding space and $\nu \simeq 0.88$ is the critical exponent which characterizes the divergence of the connectedness length in random percolation. We expect that for colloidal gels at the critical point, where the system should belong to the Ising universality class with $\nu \simeq 0.6$, one obtain $f \sim 1.8$, which coincides with de Gennes predictions. The elastic response at the critical point is actually under investigations.
For the first time we have presented a study of the dynamical susceptibility in a chemical gel, defined as the fluctuations of the self intermediate scattering function. We have observed that the susceptibility increases in time until it reaches a plateau. This asymptotic value diverges approaching the gelation threshold following a power law with the same critical exponent of the mean cluster size. By analytical investigation, we have demonstrated that the asymptotic value of the susceptibility corresponds to the mean cluster size. Our results suggest that the percolation critical exponent γ in the sol-gel transition could be measured directly via the fluctuations of the self intermediate scattering functions, without the manipulation of the sample needed in usual methods. The observed behavior of the susceptibility in our model for irreversible gelation is very different from the non-monotonic behavior observed in structural glasses. In these systems, the susceptibility grows in time until it reaches a maximum and then decays to zero, due to self-organizing nature of disorder. When the glass transition is approached in the supercooled regime there is no significantly growing static correlation length. In spite of this, a dynamical correlation length, which is related to the size of cor-

related domains and diverges approaching the transition threshold, is observed. Our findings suggest that one key difference between irreversible gelation due to chemical bonds and supercooled liquids close to the glass transition is that in irreversible gelation the heterogeneities have a static nature, due to the presence of permanent clusters of molecules. These clusters, on the other hand, affect the dynamics and as a consequence the dynamic transition coincides with the static transition, characterized by the divergence of a static correlation length, i.e. the linear size of the clusters. The behavior of the dynamical susceptibility of our model is similar to the one observed in a spin glass model with quenched interactions, suggesting a possible common description of the phase transition involved. In fact, also in this case the dynamic transition is connected to the divergence of a static length. In physical gels, where the clusters are not permanent due to finite bond lifetime, we expect that the dynamical susceptibility behavior is analogous to the one of glass forming liquids. This is in fact found in experimental investigations of colloidal suspension, forming colloidal gels, and in some MD simulations. Interestingly enough, also in some spin glass models, by introducing interactions with finite lifetime, there is no divergence of the static susceptibility and one recovers the behavior of the dynamic susceptibility which is typical of supercooled liquids. Further information on gelling systems, both irreversible and reversible gels, may be obtained investigating the case of physical gels, where the bonds between particles have a finite lifetime.

Appendix A

Fractal dimensions and static structure factor

The static structure factor of an aggregating system, defined as the Fourier transform of the density correlation function, may be directly related to the intensity of the scattered light in a scattering experiment. In particular, the fractal dimension of fractal aggregates may be measured by light scattering experiments. In the followings, we recall the basic properties of fractal objects and discuss about the method generally used to measure fractal dimension of aggregates.

A.1 Fractal geometry

Fractal objects are scale invariant systems, whose volume scales with the linear size L following a power law with an exponent D lower that the Euclidean d dimension of the space in which it lives. The volume $V(L)$ may be measured by covering the fractal with d-dimensional boxes or spheres of linear dimension l with $l \ll L$, therefore $V(L) = N(L, l)$, where $N(L, l)$ is the number of such spheres. The exponent D is defined through the scaling of $N(L, l)$ as a function of decreasing L: for mathematical fractals $N(L, l)$ diverges as $L \to \infty$ following a power law behavior characterized by a non integer exponent:

$$N(L, l) \propto L^D \tag{A.1}$$

where

$$D = \lim_{L \to \infty} \frac{\ln N(L, l)}{\ln L}. \tag{A.2}$$

For fractals having a finite size and infinitely small ramifications, when the size of the covering balls $l \to 0$, $N(L, l) \propto l^{-D}$ with

$$D = \lim_{l \to 0} \frac{\ln N(L, l)}{\ln(1/l)}. \tag{A.3}$$

We note that the above definitions for non-fractals objects give a value of D which coincide with the Euclidean dimensions d of the embedding space.

A.2 Experimental method

When measuring the fractal dimensions of growing structures, the given definitions of D usually cannot be applied. Hence, quantities related to the fractal dimensions have to be measured. The most widely applied methods divide into four categories [103], namely

1. digital image processing of two-dimensional pictures,
2. scattering experiments,
3. covering the structures with monolayers,
4. direct measurement of dimensional-dependent physical properties including measurements of current, electromagnetic power dissipation and frequency dependence of impedance.

Scattering experiments provide a powerful method for the determination of fractal dimension of microscopic structures. Most of the fractal structures studied experimentally are made of small particles whose size exceeds the spatial resolution typical in small angle X-ray or neutron scattering measurements. Hence, it is useful to separate the scattered intensity into two factors:

$$I(k) = \rho_0 P(k) \left[1 + S(k)\right], \tag{A.4}$$

where ρ_0 is the average density of the sample, $P(k)$ is a form factor and $S(k)$ is the interparticle structure factor. For $kr_0 \ll 1$, where r_0 is the radius of particles, the form factor is approximately constant.
The structure factor is defined as the Fourier transform of the density-density correlation function $g(r)$ [63], defined as

$$g(r) = \frac{1}{V} \sum_{\mathbf{r}'} \rho(\mathbf{r} + \mathbf{r}')\rho(\mathbf{r}'). \tag{A.5}$$

It can be shown that for fractal objects of gyration radius R, $g(r) \propto r^{D-d} f(r/R)$, where $f(x) \simeq$ constant for $x \ll 1$ and $f(x) \ll 1$ for $x \gg 1$. The scale invariance of the fractal clusters ensures that the cutoff of the function $f(x)$ only depends on the ratio r/R. It follows that for an isotropic fractal system

$$S(k) = 4\pi \int_0^\infty g(r) r^2 \frac{\sin(kr)}{kr} dr \sim k^{-D} \int_0^\infty z^{D-1} f(z/kR) \sin z dz, \tag{A.6}$$

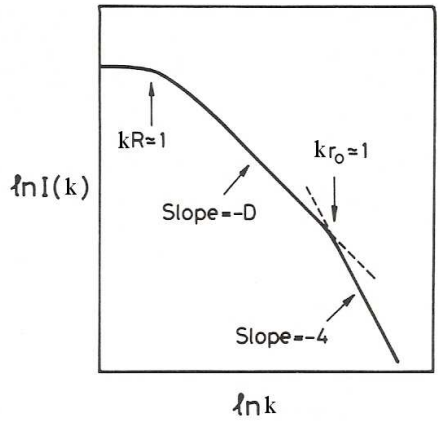

Figure A.1: Schematic representation of scattering curve showing the three main regimes which can be observed for an ensamble of fractal aggregates [103].

where we have changed the integration variable $r = z/k$. Since $f(x)$ is approximately constant up to large values of z, the integral only weakly depends on k and we can conclude that $I(k) \simeq S(k) \sim k^{-D}$ for $1/R \ll k \ll 1/r_0$.

In conclusion, in scattering experiments, three regimes may be distinguished, as it is schematically shown in Fig. A.1:

- $1/r_0 \ll k \ll 1/b$
  where b is the intermolecular distance. In this case the form factor $P(k) \sim k^{-4}$ (Porod's law), and the scattered intensity $I(k)$ follows the same behavior.

- $1/R \ll k \ll 1/r_0$
  In this regime the scattered intensity decay as k^{-D}, hence the fractal dimension can be determined from the slope of $\ln I(k)$ vs $\ln k$.

- $k \leq 1/R$
  In this limit the fractal object behaves as a single particle and the fractal dimension D may be measured measuring the weigh average mass M_w and the weigh average radius R.

A.3 An ensamble of polydisperse aggregates

In real experiments a polydisperse ensamble of aggregates is considered, as aggregation processes involve cluster size distributions with finite width. The scattered light intensity gives an effective structure factor for the ensamble, which may be

written as follows [104]:

$$S_{eff}(k) = \frac{\int s^2 n_s S[kR_g(s)]ds}{\int s^2 n_s ds}, \tag{A.7}$$

where n_s is the number of clusters per unit volume with s monomers per cluster, and $S[kR_g(s)]$ is the single aggregate structure factor. Let us consider the power law regimes:

$$\begin{aligned} S(k) &\simeq 1, \quad k \ll 1/R_g \\ &\simeq (kR_g)^{-D}, \quad k \gg 1/R_g. \end{aligned} \tag{A.8}$$

Then we define the i-th moment of the size distribution as

$$M_i = \int s^i n_s ds =< s^i > . \tag{A.9}$$

Hence, using $s = k_0(R_g/a)^D$, where a is the monomer diameter and k_0 a proportionality constant, we can write $R_g = (s/k_0)^{1/D}a$. Substituting this expression in Eq. A.9 and calculating the integral in Eq. A.7, we obtain

$$S_{eff}(k) \simeq 1, \quad k \ll 1/R_g \tag{A.10}$$

$$\simeq \frac{M_1}{M_2} k_0 (ka)^{-D}, \quad k \gg 1/R_g. \tag{A.11}$$

Since experiments deal with an ensamble of different sized aggregates, we require $S(k)$ as a function of $k\langle R_g\rangle$, where $\langle R_g\rangle$ is the average of gyration radius. Hence we introduce the z-average of the gyration radius

$$R_{g,z}^2 = \frac{\int s^2 R_g^2(s) n_s ds}{\int s^2 n_s ds}, \tag{A.12}$$

which may be written as [104]

$$R_{g,z}^2 = a^2 k_0^{2/D} \frac{M_{2+2/D}}{M_2}. \tag{A.13}$$

Then, using Eq. A.13 we can write a in terms of $R_{g,z}^2$ and substituting on a^{-D} in Eq. A.11, we obtain:

$$S_{eff}(k) \simeq 1, \quad k \ll 1/R_g \tag{A.14}$$

$$\simeq \frac{M_1}{M_2} k_0 (\frac{M_{2+2/D}}{M_2})^{D/2} (kR_{g,z})^{-D}, \quad k \gg 1/R_g. \tag{A.15}$$

It is worth to notice that the coefficient of the power law is modified by the polydispersity of the ensamble, but does not affect the power law decay of the structure factor versus the wave vector. Nevertheless, if this factor strongly

deviates from unity, using the single cluster structure factor on scattering data could yield erroneous results. Finally we remark that the relation between the structure factor and the intensity of scattered light is valid under the assumption of no internal multiple scattering. Hence, when fractal dimensions are $D \geq 2$ and multiple scattering may abolish the field coming from the interior scatters, measurement results have to be analyzed with some caution.

Furthermore, we observe that the power law behavior considered in Eq. A.15 does not take into account the possibility of M_i to scale with the wave number k. In fact, let us consider a polydisperse sample characterized by the distribution $n_s = s^{-\tau} h(\epsilon s^{\sigma})$, which is typical of percolating systems [18], where $\epsilon = p - p_c$ measures the distance from the transition threshold p_c. The exponents τ and σ are related to the critical exponent β of the order parameter and to γ of the mean cluster size [18]:

$$\begin{aligned} \beta &= (\tau - 2)/\sigma \\ -\gamma &= (\tau - 3)/\sigma. \end{aligned} \tag{A.16}$$

The total scattered intensity from a polydisperse fractal sample is expressed as an integration over the size distribution of the static structure factor $S(k)$ [105]. The density-density correlation function $g(r)$ be written as

$$g(r) = \frac{f(r/s^{1/D})}{r^{d-D}}, \tag{A.17}$$

hence the total structure factor can be written as follows:

$$S_{tot}(k) = \frac{\int s^2 n_s S(k) ds}{\int s^2 n_s ds} = \frac{1}{M_2} \int s^2 s^{-\tau} h(\epsilon s^{\sigma}) ds \int e^{i\vec{k}\cdot\vec{r}} f(r/s^{1/D}) r^{D-d} d^d r. \tag{A.18}$$

The scattered intensity $I(k)$ is proportional to the structure factor: $I_{tot}(k) = B\rho_0 v M_2 S_{tot}(k)$, where B is a constant depending on the experimental apparatus, ρ_0 is the average density of the sample and v is the scattering volume. At the gel point, where $\epsilon = 0$, using Eq. A.18 we obtain

$$I(k) \sim k^{-D(3-\tau)}, \tag{A.19}$$

which, using Eq. A.16 and the relation $D = d - \beta/\nu$, can be rewritten as $I(k) \sim k^{d-2D}$.

In conclusion, the power law behavior of the static structure factor may be strongly influenced by the polydispersity of the sample. Although it is well known that for a single fractal object the static structure factor behaves as k^{-D} as it is shown in Fig. A.1, for a polydisperse sample is not obvious that the same result should be still valid.

Appendix B

Computer simulations

In the last years computer simulations have revested a fundamental role in the investigation of complex systems. They let measure a wide class of properties, ranging from local to macroscopic quantities, providing a direct comparison between model results and experiments. In this section we describe two different simulation techniques: Monte Carlo simulation method and molecular dynamics technique.

B.1 Monte Carlo simulations

The Monte Carlo method [106] results to be very useful when studying systems whose motion equation are complicated and difficult to be solved. By means of Monte Carlo simulations, the probability distribution which defines the ensamble of system states is directly sampled introducing an "effective" dynamics.

The thermal average of an observable $A(\mathbf{x})$, where $\mathbf{x}$ is a vector in phase space describing the considered degrees of freedom, is defined as:

$$\langle A(\mathbf{x})\rangle = \frac{1}{Z}\int \exp\left[-\mathcal{H}(\mathbf{x})/k_BT\right] A(\mathbf{x})d\mathbf{x}, \tag{B.1}$$

where

$$Z = \int \exp\left[\mathcal{H}(\mathbf{x})/k_BT\right] d\mathbf{x} \tag{B.2}$$

is the partition function, and $\mathcal{H}(\mathbf{x})$ is the Hamiltonian of the model. The normalized Boltzmann factor $P(\mathbf{x}) = \exp\left[\mathcal{H}(\mathbf{x})/k_BT\right]/Z$ plays the role of a probability density, representing the statistical weight with which the configuration $\mathbf{x}$ occurs in thermal equilibrium. Within the Monte Carlo method, the exact Eq. B.1 is approximated with the sum over a subset of phase space points $\{\mathbf{x}_1, \mathbf{x}_2, ..., \mathbf{x}_M\}$, which are used as statistical sample. Clearly, the discrete sum

$$\overline{A(\mathbf{x})} = \frac{\sum_{l=1}^{M} \exp\left[-\mathcal{H}(\mathbf{x}_l)/k_BT\right] A(\mathbf{x}_l)}{\sum_{l=1}^{M} \exp\left[-\mathcal{H}(\mathbf{x}_l)/k_BT\right]} \tag{B.3}$$

must approximate Eq. B.1 in the limit $M \to \infty$. It can be shown that $\overline{A} =< A > +O(N^{-1/2})$ [107].

The dynamics arising from Monte Carlo simulation moves along the discrete set of phase space variables $\{\mathbf{x}_1, \mathbf{x}_2, ..., \mathbf{x}_M\}$: it takes place in discrete time steps, each $\mathbf{x}_i$ univocally determines the probability distribution of the successive state, and such probability does not depend on time explicitly. Metropolis et al. [108] advanced the idea to choose the successive states $\{\mathbf{x}_l\}$ building a Markov process, where each state $\mathbf{x}_{i+1}$ is constructed from the previous $\mathbf{x}_i$ via a suitable transition probability $W(\mathbf{x}_i \to \mathbf{x}_{i+1})$. They pointed out that it is possible to choose the transition probability W such that in the limit $M \to \infty$ the distribution function $P(\mathbf{x}_l)$ generated by this Markov process tends towards the desired equilibrium distribution $P_{eq}(\mathbf{x}_l)$:

$$P_{eq}(\mathbf{x}_l) = \frac{1}{Z} \exp\left(-\frac{\mathcal{H}(\mathbf{x}_l)}{k_B T}\right). \tag{B.4}$$

To achieve this issue, it is sufficient to impose the principle of detailed balance:

$$P_{eq}(\mathbf{x}_l) W(\mathbf{x}_l \to \mathbf{x}_{l'}) = P_{eq}(\mathbf{x}_{l'}) W(\mathbf{x}_{l'} \to \mathbf{x}_l). \tag{B.5}$$

Using Eq. B.4 and Eq. B.5 we obtain:

$$\frac{W(\mathbf{x}_l \to \mathbf{x}_{l'})}{W(\mathbf{x}_{l'} \to \mathbf{x}_l)} = \exp\left(-\frac{\delta\mathcal{H}}{k_B T}\right), \tag{B.6}$$

where $\delta\mathcal{H} = \mathcal{H}(\mathbf{x}_{l'}) - \mathcal{H}(\mathbf{x}_l)$ is the energy variation. The latter equation does not fix the transition probability uniquely, and some arbitrariness in the explicit choice of W remains. One of the most common used expression of the transition probability is the following:

$$W(\mathbf{x}_l \to \mathbf{x}_{l'}) = \begin{cases} \exp\left(-\delta\mathcal{H}/k_B T\right)/\tau_s & \text{if } \delta\mathcal{H} > 0 \\ 1/\tau_s & \text{otherwise} \end{cases}$$

where τ_s is an arbitrary factor, representing the unit of Monte Carlo time. Hence W is the transition probability per unit time [106].

B.2 Bond fluctuation dynamics

Here we describe an algorithm that may be used to analyze the dynamical properties of polymers. Lattice algorithms [109] generally used to describe polymer dynamics according the Rouse model [55] have several disadvantages: standard algorithms do not allow for simulations of branched polymers, furthermore serious difficulties arise in simulations of very dense systems, as these algorithms are not ergodic.

In the bond fluctuation dynamics, each polymer consists of N monomers. We note that in a Monte Carlo simulation one monomers represents a Kuhn's

segment, i.e. an orientation independent segment of the polymer. Monomers are implemented in a cubic lattice (square lattice in $d = 2$) with unit lattice spacing: each monomer occupies a unit cell and two occupied cells cannot have any site in common (self avoiding walk condition). Linked monomers are bonded by a segment of length l, which in $d = 3$ must be smaller than or equal to $\sqrt{10}$. Hence, in $d = 3$ the permitted bond lengths are $l = 2, \sqrt{5}, \sqrt{6}, 3, \sqrt{10}$; $l = \sqrt{8}$ must be excluded, to preserve ergodicity [8]. The condition on bond lengths prevents bond cuts. At each step, a monomer is randomly chosen and a move of one lattice unit is selected in one of the six (four in $d = 2$) lattice directions. If the move complies with the self avoiding walk condition and the bond length restrictions it is accepted, otherwise it is rejected. Hence, the bond fluctuation dynamics algorithm is a lattice algorithm consisting of single beads moves. The dynamics resulting from this algorithm is realistic, in the sense that it reproduces the Rouse dynamics. In addition it may be used to simulate branched polymers and it is ergodic. As a consequence, this algorithm solves the problems of the other lattice algorithms for polymer simulations [109].

B.3 Slithering-snake algorithm

The dynamics of polymer chains may be simulated using the slithering snake algorithm [84]. This algorithm implies moving the head of a chain one lattice spacing in a lattice direction, with all other elements of the chain moving forward along the chain contour. Possible moves of the head of one unit along the lattice directions are selected at random. If the move complies the bond fluctuation dynamics rules, it is accepted, otherwise the old configuration is retained and the head is interchanged with the tail. The snake move along the existing backbone of a chain is equivalent to removing an end monomer and connecting it to the other end of the chain, leaving the lattice positions of the middle monomers unchanged. Such a move corresponds to a global move of the chain, differently from the standard bond fluctuation dynamics move, which is a local one. It has been verified by Mattioni and coworkers [84] that, independently of the chain length, global move acceptance rate is higher than local move acceptance rate for volume fraction $\phi \leq 0.5$, where ϕ is defined as the ratio between the number of present monomers and the maximum possible one.

B.4 Molecular dynamics simulations

In molecular dynamics simulations, equations of motion are solved. This method provides a deterministic description of time evolution of the system under investigation: once fixed the initial conditions, the time evolution is univocally determined. Different algorithms may be used to solve the equations of motion.

In our study we have used the velocity-Verlet algorithm, with the thermostat of Nosé-Hoover, in order to keep the temperature constant.

B.4.1 The velocity-Verlet algorithm

The velocity-Verlet algorithm [92] calculates the new coordinates and velocities at time $t + \delta t$, using the positions, the velocities and the accelerations at time t, proceeding in two steps. At first it calculates the positions at time $t + \delta t$ and the velocities at time $t + \delta t/2$ using the velocities and the accelerations at time t, and then it determines the accelerations at time $t + \delta t$ in order to calculate the velocities at $t + \delta t$. Hence during the first step

$$\begin{aligned} \mathbf{r}(t+\delta t) &= \mathbf{r}(t) + \mathbf{v}(t)\delta t + \frac{1}{2}\mathbf{a}(t)\delta t^2 \\ \mathbf{v}(t+\delta t/2) &= \mathbf{v}(t) + \frac{1}{2}\mathbf{a}(t)\delta t \end{aligned} \tag{B.7}$$

and during the second one

$$\mathbf{v}(t+\delta t) = \mathbf{v}(t+\delta t/2) + \frac{1}{2}\mathbf{a}(t+\delta t)\delta t. \tag{B.8}$$

Using this algorithm, the equations of motion are solved in the (NVE)-ensamble. If the temperature T has to be kept constant, i.e. the ensamble to be considered is the NVT we have to introduce a thermostat. The algorithm to be used is the velocity-Verlet algorithm with thermostat [91]. A new variable s, representing the thermal piston, is introduced with mass Q and as a consequence, in the Hamiltonian an additional term appears, which is proportional to Q:

$$\mathcal{H} = \frac{m\mathbf{v}^2}{2} + V(\mathbf{r}) + \frac{Q}{2}\left(\frac{\dot{s}}{s}\right)^2 + (1+f)k_B T \log s \tag{B.9}$$

where m is the mass of the particle, $V(\mathbf{r})$ is the potential energy and $f = 3N$ is the number of degrees of freedom (N being the number of particles). To obtain the dynamical evolution of the system, we have to solve the following equations:

$$\begin{aligned} \mathbf{a} &= \frac{1}{m}\mathbf{F} - \frac{\dot{s}}{s}\mathbf{v} \\ \ddot{s} &= \frac{\dot{s}^2}{s} + \frac{s}{Q}\left[m\mathbf{v}^2 - (1+f)k_B T\right]. \end{aligned} \tag{B.10}$$

During the first step, the algorithm calculates the quantities in Eq. B.7, in addition to $s(t+\delta t)$ and $\dot{s}(t+\delta t/2)$ using $\dot{s}(t)$ and $\ddot{s}(t)$. During the second step, the algorithm calculates the forces $F(t+\delta t)$ and solves the following equations:

$$\mathbf{v}(t+\delta t) = \mathbf{v}(t+\delta t/2) + \frac{1}{2}\mathbf{a}(t+\delta t)\delta t \tag{B.11}$$

$$
\begin{aligned}
\mathbf{a}(t+\delta t) &= \frac{1}{m}\mathbf{F}(t+\delta t) - \mathbf{v}(t+\delta t)\frac{\dot{s}(t+\delta t)}{\ddot{s}(t+\delta t)} \\
\dot{s}(t+\delta t) &= \dot{s}(t+\delta t/2) + \frac{1}{2}\ddot{s}(t+\delta t)\delta t \\
\ddot{s}(t+\delta t) &= \frac{\dot{s}(t+\delta t)^2}{s(t+\delta t)} + \frac{\dot{s}(t+\delta t)}{Q}\left[m\mathbf{v}(t+\delta t)^2 - (1+f)k_BT\right].
\end{aligned}
$$

When initializing the simulations, we fix the total momentum to be zero. The thermal piston is fixed to $s = 1$ with zero velocity $\dot{s} = 0$. The particle velocities are initially extracted from a gaussian distribution with variance equal to k_BT/m for each direction. The mean value $< m\mathbf{v}^2 >= 3NK_BT$, where $< ... >$ indicates the temporal average, with fluctuations that depend on Q. If the mass Q increases, the amplitude of fluctuations decreases, but their characteristic time $\pi\sqrt{2Q/fk_BT}$ increases. The hamiltonian $\mathcal{H}$ is a constant of motion.

Bibliography

[1] R. S. Whitney, W. Burchard *Makromol. Chem.* **181**, 869 (1980).

[2] M. Schmidt, W. Burchard *Macromolecules* **14**, 370 (1981).

[3] J. E. Martin, J. Wilcoxon, D. Adolf *Phys. Rev. A* **36**, 1803 (1987).

[4] S. Z. Ren, C. M. Sorensen *Phys. Rev. Lett.* **70**, 1727 (1993); F. Ikkai, M. Shibayama *Phys. Rev. Lett.* **82**, 4946 (1999).

[5] P. M. Goldbart, H. E. Castillo, A. Zippelius *Adv. Phys.* **45**, 393 (1996); C. Wald, P. M. Goldbart, A. Zippelius *cond-mat/0509694*.

[6] C. Joly-Duhamel, D. Hellio, M. Djabourov, *Langmuir* **18**, 7208 (2002).

[7] D. Hellio-Serughetti, M. Djabourov, *Langmuir* **22**, 8516 (2006).

[8] I. Carmesin, K. Kremer, *Macromolecules* **21**, 2819 (1988); I. Carmesin, K. Kremer, *J. Phys. (Paris)* **51**, 915 (1990); H.P. Deutsch, K. Binder, *J. Chem. Phys.* **94**, 2294 (1991).

[9] T. Abete, E. Del Gado, D. Hellio-Serughetti, L. de Arcangelis, M. Djabourov and A. Coniglio, *J. Chem. Phys.* **125**, 174903 (2006).

[10] H. Berry, J. Pelta, D. Lairez, V. Larreta-Garde, *Biochim. et Biophys. Acta* **1524**, 110 (2000).

[11] G.C. Fadda, D. Lairez, B. Arrio, J.P. Carton, V. Larreta-Garde, *Biophys. J.* **85**, 2808 (2003).

[12] P. G. de Gennes, J. Phys. (France) Lett. **37**, L-1 (1976).

[13] P. G. de Gennes, C. R. Acad. Sci. Paris B **286**, 131 (1978).

[14] G. S. Grest and K. Kremer, Phys. Rev. A **33**, 3628 (1986); K. Kremer, G. S. Grest, J. Chem. Phys. **92**, 5057 (1990).

[15] S. Franz, C. Donati, G. Parisi and S. C. Glotzer, *Philos. Mag. B* **79**, 1827 (1999). C. Donati, S. Franz, S. C. Glotzer and G. Parisi, *J. Non-cryst. Solids* **307**, 215 (2002).

[16] P.G. de Gennes, *Scaling Concepts in Polimer Physics*, Cornell University Press, Ithaca (1993).

[17] P. J. Flory, *Principles of Polymer Chemistry*, Cornell University Press, Ithaca (1971).

[18] D. Stauffer and A. Aharony, *Introduction to Percolation Theory*, Taylor & Francis (1992).

[19] D. Stauffer, *Physica A* **106**, 177 (1981).

[20] D. Stauffer, A. Coniglio, M. Adam, *Adv. in Pol. Sci.* **14**, 103 (1982).

[21] H. E. Stanley, *Introduction to Phase Transition and Critical Phenomena*, Oxford University Press (1971).

[22] H. J. Herrmann, D. Stauffer, D. P. Landau, *J. Phys. A: Math. Gen.* **16**, 1221 (1983).

[23] F. Y. Wu, *Rev. Mod. Phys.* **54**, 235 (1982).

[24] P. W. Kasteleyn, C. M. Fortuin, *J. Phys. Soc. Japan Suppl.* **26**, 11 (1969).

[25] M. Daoud, A. Coniglio, *J. Phys. A: Math. Gen.* **14**, L301 (1981).

[26] D. R. Bland, *The Theory of Viscoelasticity*, Pergamon Press, Belfast (1960).

[27] M. Adam, D. lairez, M. Karpasas, M. Gottlieb, *Macromolecules* **30**, 5920 (1997).

[28] C. P. Lusignan, T. H. Mourey, J. C. Wilson, R. H. Colby, *Phys. Rev. E* **52**, 6271 (1995).

[29] R. H. Colby, J. R. Gillmore, M. Rubistein, *Phys. Rev. E* **48**, 3712 (1993); C. P. Lusignan, T. H. Mourey, J. C. Wilson, R. H. Colby, *Phys. Rev. E* **60**, 5657 (1999).

[30] D. Lairez, M. Adam, J. R. Emery, D. Durand, *Progr. Coll. Polym. Sci.* **90**, 37 (1992).

[31] T. Nicolai, H. Randrianantoandro, F. Prochazka, D. Durand, *Macromolecules* **30**, 5897 (1997).

[32] G. Champetier, *Chimie Macromoleculaire* Vol. **2**, Hermann, Paris.

[33] W. Burchard, K. Kajiwara, M. Gordon, J Kálal, J. W. Kennedy, *Macromolecules* **6**, 642 (1973).

[34] A. D. Dinsmore, D. A. Weitz, *J. Phys.: Condens. Matter* **14**, 7581 (2002).

[35] P. N. Segré, V. Prasad, A. B. Schofield, D. A. Weitz, *Phys. Rev. Lett.* **86**, 6042 (2001).

[36] V. Trappe, V. Prasad, L. Cipelletti, P. N. Segré, D. A. Weitz, *Nature* **411**, 772 (2001).

[37] F. Mallamace, P. Gambadauro, N. Micali, P. Tartaglia, C. Liao, S. H. Chen, *Phys. Rev. Lett.* **84**, 5431 (2000).

[38] E. Donth, *The Glass Transition*, Springer-Verlag, Berlin (2001).

[39] F. Sciortino, *Nature Materials, News and Views* **1**, 145 (2002).

[40] T. A. Witten, L. M. Sander, *Phys. Rev. Lett.* **47**, 1400 (1981).

[41] R. Jullien, M. kolb, *J. Phys. A: Math. Gen.* **17**, L639 (1984); W. D. Brown, R. C. Ball, *J. Phys. A: Math. Gen.* **18**, L517 (1985).

[42] M. Y. Lin, H. M. Lindsay, D. A. Weitz, R. C. Ball, R. Klein, P. Meakin, *Phys. Rev. A* **41**, 2005 (1990).

[43] M. Carpineti, F. Ferri, M. Giglio, E. Paganini, U. Perini, *Phys. Rev. A* **42**, 7347 (1990); M. Carpineti, M. Giglio, *Phys. Rev. Lett.* **68**, 3327 (1992).

[44] M. Lattuda, H. Wu, M. Morbidelli, *Phys. Rev. E* **64**, 061404 (2001).

[45] M. Djabourov, J. Leblond, P. Papon, *J. Phys.* (Paris) **49**, 33 (1988); G. C. Fadda, D. Lairez, J. Pelta, *Phys. Rev. E* **63**, 061405 (2001).

[46] M. Djabourov, *Contemp. Phys.* **29**, 273 (1988).

[47] F. Devreux, J. P. Boilot, F. Chaput, L. Malier, *Phys. Rev. E* **47**, 2689 (1993).

[48] M. A. Axelos, M. Kolb, *Phys. Rev. Lett.* **64**, 1457 (1990).

[49] M. Takahashi, K. Yokoyama, T. Masuda, T. Takigawa, *J. Chem. Phys.* **101**, 798 (1994).

[50] R. H. Colby, B. K. Coltrain, J. M. Salva, S. M. Melopolder, *Fractal Aspects of Materials: Disordered Systems*, edited by A. J. Hurd, D. A. Weitz, B. B. Mandelbrot, Materials Research Society, Pittsburgh, PA (1987).

[51] J. E. Martin, D. Adolf, J. P. Wilcoxon, *Phys. Rev. Lett.* **61**, 2620 (1988).

[52] M. Tokita, K. Hikichi, *Phys. Rev. A* **35**, 4329 (1987).

[53] M. Adam, M. Delsanti, D. Durand, *Macromolecules* **18**, 2285 (1985); M. Adam, M. Delsanti, D. Durand, G. Hild, J. Munch, *Pure Appl. Chem.* **53**, 1489 (1981).

[54] I. Bodnár, J. K. G. Dhont, *Phys. Rev. Lett.* **77**, 5304 (1996); A. J. Liu, S. R. Nagel, *Nature* **396**, 21 (1998).

[55] P. E. Rouse, *J. Chem. Phys.* **21**, 1272 (1953).

[56] K. Dusek, W. Prins, *Adv. Polym. Sci.* **6**, 1 (1969).

[57] S. Feng, P. Sen, *Phys. Rev. Lett.* **52**, 216 (1984); Y. Kantor, I. Webman, *Phys. Rev. Lett.* **52**, 1891 (1984).

[58] M. Born, K. Huang, *Dynamical Theory of Crystal Lattices*, Oxford University Press, Oxford (1954).

[59] J. Kertesz, *J. Phys. A* **16**, L471 (1983).

[60] M. Plischke, D. C. vernon, B. Joós, Z. Zhou, *Phys. Rev. E* **60**, 3129 (1999); M. Plischke, B. Joós, *Phys. Rev. Lett.* **80**, 4907 (1998).

[61] X. Xing, S. Mukhopadhyay, P. M. Goldbart, *Phys. Rev. Lett.* **93**, 225701 (2004).

[62] L. van Hove, *Phys. Rev. B* **95**, 249 (1954).

[63] J. P. Hansen, I. R. McDonald, *Theory of Simple Liquids*, Academic Press Inc., London (1976).

[64] F. Mezei, W. Knaak, *Phys. Rev. Lett.* **58**, 571 (1987).

[65] L.D. Landau and E.M. Lifshitz, *Fluid Mechanics*, Pergamon Press (1963).

[66] L.P. Kadanoff and P.C. Martin, Ann. Phys. **24**, 419 (1963).

[67] J. E. Martin, J. P. Wilcoxon, *Phys. Rev. Lett.* **61**, 373 (1988).

[68] M. Adam, M. Delsanti, J. P. Munch, *Phys. Rev. Lett.* **61**, 706 (1988).

[69] J. E. Martin, J. P. Wilcoxon, J. Odinek, *Phys. Rev. A* **43**, 858 (1991).

[70] P. Lang, W. Burchard, *Macromolecules* **24**, 815 (1991).

[71] E. del Gado, L. de Arcangelis, A. Coniglio, *Phys. Rev. E* **65**, 041803 (2002); E. Del Gado, L. de Arcangelis, A. Coniglio, J. Phys. A **31**, 1902 (1998)

[72] T. Abete, A. de Candia, E. Del Gado, A. Fierro, A. Coniglio, cond-mat/0607815.

[73] M. Djabourov, J. P. Lechaire, F. Gaill, *Biorheology* **30**, 191 (1993).

[74] D. Hellio Serughetti *Les Gels physique et chimiques de gelatine: structure et rheologie*, PhD Thesys, Universite Paris VI (2003).

[75] P. L. Privalov, *Advances in Protein Chemistry* **35**, 1 (1982).

[76] I. Pezron, T. Herning, M. Djabourov, J. Leblond, *Physical Networks*, Elsevier Applied Science, London (1990), S. B. Ross-Murphy and W. Burchard Eds.

[77] G. Champetier, L. Monnerie, *Introduction à la Chimie Macromoléculaire*, Masson et Cie Editeurs (1969).

[78] D. Vernon, M. Plischke, Phys. Rev. E **63**, 031505 (2001)

[79] B. E. Eichinger, *Computational and Theoretical Polymer Science* **10 (1)**, 83 (2000); D. Rigby, B. E. Eichinger, *Polymer International* **44**, 311 (1997)

[80] H.S. Ma, R. Jullien and G.W. Scherer, *Phys. Rev. E* **65**, 041403 (2002); A. Hasmy, R. Jullien and R. Botet, *Phys. Rev. Lett.* **75**, 3777 (1995); R. Jullien and A. Hasmy, *Phys. Rev. Lett.* **75** 2454 (1995).

[81] M. Rotterau, J.C. Gimel, T. Nicolai and D. Durand, *Eur. Phys. J. E* **15**, 133 (2004); *ibidem* **15**, 141 (2004).

[82] M. Doi, S. F. Edwards, *The Theory of Polymer Dynamics*, Clarendon Press, Oxford (1988).

[83] I. Pezron, M. Djabourov, J. Leblond, *Polymer* **32**, 3201 (1991).

[84] L. Mattioni, J. P. Wittmer, J. Baschnagel, J. L. Barrat, E. Luijten, *Eur. Phys. J. E* **10**, 369 (2003); F. T. Wall, J. C. Chin, F. Mandel, *Macromolecules* **66**, 3143 (1977).

[85] R. F. T. Stepto, J. I. Cail, D. J. R. Taylor, *Materials Research Innovations* **7 (1)**, 4 Springer (2003).

[86] T. Abete, A. de Candia, D. Lairez, A. Coniglio, *Phys. Rev. Lett.* **93**, 228301 (2004).

[87] P. Manneville, L. de Seze, *Numerical Methods in the Study of Critical Phenomena*, eds. I. Della Dora, J. Demongeot, B. Lacolle (Springer, Berlin, 1981); H.J. Herrmann, D.P. Landau, and D. Stauffer, *Phys. Rev. Lett.* **49**, 412 (1982).

[88] M. Suzuki, *Prog. Theor. Phys* **51**, 1992 (1974).

[89] A. Weinrib and B.I. Halperin, *Phys. Rev. B* **27**, 413 (1983); A. Weinrib, *Phys. Rev. B* **29**, 387 (1984).

[90] H.R. Warner, *Ind. Eng. Chem. Fundam.* **11**, 379 (1972).

[91] S. Nosé, *J. Chem. Phys.* **81**, 511 (1984); W. G. Hoover, *Phys. Rev. A* **31**, 1695 (1985); D. C. Rapaport, pagg. 146-156.

[92] M. P. Allen, D. J. Tildesley *Computer Simulation of Liquids*, Oxford Press (2000).

[93] M. Rotterau, J. C. Gimel, T. Nicolai, D. Durand, *Eur. Phys. J. E* **11**, 61 (2003).

[94] E. Del Gado, L. de Arcangelis, A. Coniglio, *Eur. Phys. J. E* **2**, 352 (2000); E. Del Gado, A. Fierro, L. de Arcangelis, A. Coniglio, *Phys. Rev. E* **69**, 051103 (2004).

[95] C. Toninelli, G. Biroli and D.S. Fisher *Phys. Rev. Lett.* **96**, 035702 (2006); J.P. Bouchaud and G. Biroli, *Phys. Rev. B***72**, 064204 (2005).

[96] A. Fierro, A. de Candia, A. Coniglio, *Phys. Rev. E* **62**, 7715 (2000).

[97] E. Del Gado, A. Fierro, L. de Arcangelis and A. Coniglio *Europhys. Lett.***63**, 1 (2003); A. Coniglio, L. de Arcangelis, E. Del Gado, A. Fierro and N. Sator, *J. Phys.: Condens. Matter* **16**, S4831 (2004).

[98] A. de Candia, E. Del Gado, A. Fierro, N. Sator, and A. Coniglio, *Physica A* 358, 239-248 (2005).

[99] A. Coniglio, "Frustration and connectivity in glass forming systems and granular materials", in *Proc. Int. School on the Physics of Complex Systems "Enrico Fermi" CXXXIV course* (Varenna 1996), F. Mallamace and H.E. Stanley Eds., p.491; M. Nicodemi and A. Coniglio, *J. Phys. A Lett.* **30**, L187 (1996); A. Coniglio, A. de Candia, A. Fierro and M. Nicodemi, *J. Phys.: Condens. Matter.* **11**, A167 (1999); F. Ricci-Tersenghi, D. A. Stariolo and J. Arenzon, *Phys. Rev. Lett.* **84**, 4473 (2000); M. H. Vainstein, D. A. Stariolo and J. J. Arenzon, *J. Phys. A-Math. Gen.* **36** (43), 10907 (2003).

[100] C. Donati, S. Franz, G. parisi, S.C. Glotzer, cond-mat/9905433.

[101] L. Cipelletti and L. Ramos, *J. Phys.: Condensed Matter* **17**, R253 (2005); A. Duri, H. Bissig, V. Trappe, L. Cipelletti, *Phys. Rev. E* **72**, 051401 (2005); A Duri and L. Cipelletti, *cond-mat/0606051* to appear on *Europhys. Lett.*.

[102] W. van Megen, T. C. Mortensen, S. R. Williams and J. Muller, *Phys. Rev. E* **58**, 6073 (1998).

[103] T. Vicsek, *Fractal growth phenomena*, World Scientific Publishing, Singapore (1989).

[104] C. M. Sorensen, *Aerosol Science and Technology* **35**, 648 (2001).

[105] J. E. Martin, B. J. Ackerson, *Phys. Rev. A* **31**, 1180 (1985).

[106] K. Binder, D. W. Hermann, *Monte Carlo Simulation in Statistical Physics*, Springer-Verlag, Berlin (1988).

[107] L. Peliti, *Appunti di Meccanica Statistica*, Bollati Boringhieri, Torino (2003).

[108] N. Metropolis, A. W. Rosenbluth, M. N. Rosenbluth, A. H. Teller, E. Teller, *J. Chem. Phys.* **21**, 1087 (1953).

[109] K. Kremer, K. Binder, A. Baumgärtner, *J. Phys. A* **71**, 2541 (1982); K. Kremer, *Macromolecules* **16**, 1632 (1983); J. P. Downey, C. C. Crabb, J. Kovac, *Macromolecules* **19**, 2202 (1986).